ABSTRACT

AUTOMATIC DETECTION OF QT AND RELATED INTERVALS

by
Divya Gowdar

The objective of this thesis is divided into two main sections: The first section comprises of the development of the algorithm for the detection of the Q wave, T_{max} and the T_{end} to measure the intervals such as QT, QT corrected (QTc), RT, QT_{max} and RT_{max} respectively. The second section deals with the analysis of different variabilities including heart rate variability (HRV), QT, QTc, RT, QT_{max} and RT_{max}.

Using the R wave points as reference points, the Q wave was detected by using the Differential Threshold Method (DTH). The T_{max} was detected by using a search window on the derived signal of ECG starting from the R peak. The T_{end} was detected by two different procedures. The first procedure was a combination of two different methods: the Least Squares Method (LSI) and the Threshold Method (TH) and the second procedure was based on the Differential Threshold Method (DTH). Once the points were detected, the relationship between the heart rate variability (HRV) and corrected QT variability along with other variabilities was studied in this research.

The algorithm was validated on ten patients of five minute data segment of paced breathing at 6 breaths per minute and 12 breaths per minute respectively. The algorithm for the detection of the Q wave, T_{max} and the T_{end} produced an overall success of 99.16% according to automatic verification of accuracy detection and 96.4% based on manual inspection. In this study, the duration of the QT interval was in the range of 450 to 500 milliseconds, which indicated normal duration of ventricular repolarization. The variability plots indicated similarity between HR variability and QT corrected variability.

AUTOMATIC DETECTION OF QT AND RELATED INTERVALS

by
Divya Gowdar

A Thesis
Submitted to the Faculty of
New Jersey Institute of Technology
in Partial Fulfillment of the Requirements for the Degree of
Master of Science in Biomedical Engineering

Department of Biomedical Engineering

May 2006

APPROVAL PAGE

AUTOMATIC DETECTION OF QT AND RELATED INTERVALS

Divya Gowdar

Dr. Ronald Rockland, Thesis Advisor — Date
Associate Professor of Engineering Technology, NJIT
Associate Professor of Biomedical Engineering, NJIT

Dr. Stanley Reisman, Committee Member — Date
Professor of Biomedical Engineering, NJIT

Dr. Joel Schesser, Committee Member — Date
Special Lecturer in Biomedical Engineering, NJIT

BIOGRAPHICAL SKETCH

Author: Divya Gowdar

Degree: Master of Science

Date: May 2006

Undergraduate and Graduate Education:

- Master of Science in Biomedical Engineering,
  New Jersey Institute of Technology, Newark, NJ, 2006

- Bachelor of Science in Instrumentation Technology,
  Bapuji Institute of Engineering and Technology, Karnataka, India, 2003

Major: Biomedical Engineering

To my parents, Ashok Kumar and Sujatha Ashok Kumar,

for their unconditional love and support all throughout my life.

ACKNOWLEDGMENT

I would like to express my deepest gratitude to Dr. Ronald Rockland, my advisor, for providing his valuable insights, suggestions and resources for my research. He is a person with incredible patience and knowledge, and I thank him for always listening to my problems and heeding to it. His expertise and suggestions at the right time made my research an enjoyable and rewarding experience. I would also like to acknowledge and express my appreciation to Dr. Stanley Reisman and Dr. Joel Schesser, who gladly agreed to be my committee members and took time and effort to review this work.

I would like to thank my colleagues at Honors College, NJIT, for allowing me time off to do this work. I also want to thank Biomedical Department, Signal Processing Laboratory, for providing me with lab facilities. Special thanks to Diane Donnelly, whose suggestion helped me out of a dilemma. I would also like to thank the libraries at NJIT and UMDNJ, Newark, NJ, for assisting me with all the materials required to complete this research.

Special thanks to my friends, Abhishek and Kibrom, who helped me with the MATLAB programming. How can I forget to thank my friend Mohan, for getting me coffee every night, to keep the midnight oil burning. If it would not have been their support and help, I wouldn't have completed this research.

Last, but not least, a bolstering source of confidence and love, my family. I know they always want me to have an independent and positive outlook, no matter where I am. Dad and Mom!! Thanks for all your prayers and love. It kept me going.

TABLE OF CONTENTS

Chapter **Page**

TABLE OF CONTENTS
(Continued)

Chapter **Page**

TABLE OF CONTENTS
(Continued)

Chapter **Page**

LIST OF TABLES

Table **Page**

LIST OF FIGURES

Figure **Page**

LIST OF FIGURES
(Continued)

Figure **Page**

LIST OF FIGURES
(Continued)

Figure **Page**

LIST OF FIGURES
(Continued)

Figure **Page**

CHAPTER 1

BACKGROUND

1.1 Introduction

Cardiovascular diseases are the primary cause of death in the adult population. Half of cardiac deaths occur as sudden death. An abnormal QT interval prolongation can be associated with serious ventricular arrhythmias and sudden death. Thus, QT interval measurement assumes great importance in diagnostic ECG and several methods are proposed in the literature to implement QT interval measurement [4].

Accurate measurement of the QT interval is very important from a clinical perspective. There are various issues involved in the measurement of the QT interval especially regarding the end of the T wave and different morphological pattern of T-U complexes. The other issue is significant spontaneous variability in the QT interval, resulting in spurious QT prolongation and unnecessary concern.

The QT interval relies on the identification of the end of the T wave, which may be visually assessed differently according to the experience and training of the cardiologist. The use of a computer algorithm helps to detect more consistently the location of the end of the T wave [11] [30]. However, computers may fail to identify this location correctly if the shape of the T wave is abnormal (low amplitude biphasic T wave) requiring visual checking of the automatic measurements.

The ability to define QT interval prolongation reliably is important because of its association with ventricular abnormalities. The QT interval prolongation is hampered by the fact that the QT interval is not constant and highly dependent on the preceding cardiac cycles and therefore on the heart rate.

The objective of this thesis is to accurately detect the points Q wave, T_{max} and the T_{end} on the electrocardiogram to measure the QT and other related intervals including QTc, RT_{max}, QT_{max}, and RT interval. This thesis also examines the relationship between the heart rate variability and QT corrected variability.

To detect the Q wave, differential threshold method (DTH) was used. This method was based on running a search window on the differentiated ECG signal to detect the maximum and minimum derivative points at the onset of the QRS complex. A certain percentage of threshold level is created to detect the Q wave. The point T_{max} is detected based on the window method.

The end of the T wave is the most difficult point to detect because of its varying morphologies. In this study, two different procedures were used to detect the end of the T wave. The first procedure involved a combination of two methods: the Least Squares Method (LSI) and the Threshold Method (TH). This procedure had a potential problem of early detection of the T_{end} and therefore a second procedure with the Differential Threshold Method (DTH) was used to detect the T_{end}.

In order to study the variabilities of different intervals, power spectrum of various intervals was calculated using Fast Fourier Transform (FFT). Before performing the FFT, the average of all the corresponding beat intervals were calculated. The variability plots of different intervals were quantitatively analyzed by measuring the amount of power in the LF and HF regions.

1.2 The Heart: Electrophysiology

The heart is a small hollow muscular pump about the size of a closed fist, but able to pump approximately 5-6 liters (1.5 gallons) of blood per minute. The Human heart is divided into four chambers. The top two chambers are called atria and two lower ones are called ventricles (Figure 1.1). The atrium functions as a weak primer pump for the ventricle, helping the ventricle to move the blood. The ventricle supplies the force that is required to push the blood out through the pulmonary circulation.

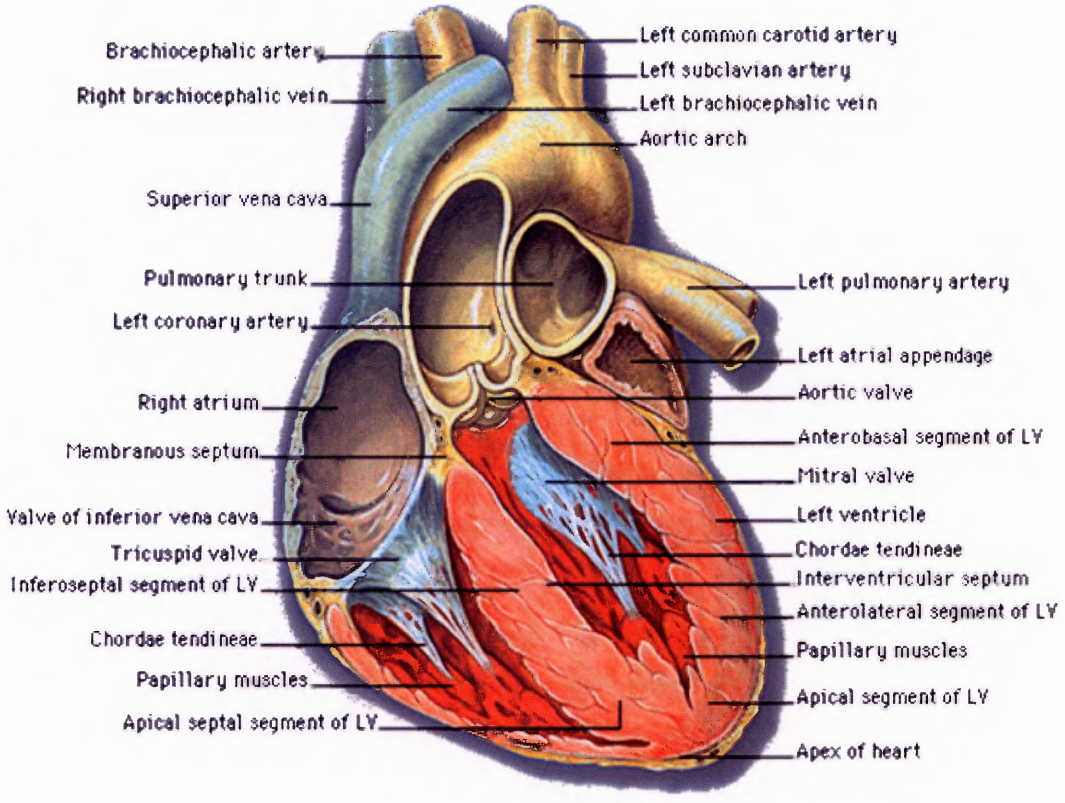

(**Reference.** http://www.corante.com/mooreslore/archives/images/heart_anatomy.gif)

Figure 1.1 Anatomy of the heart.

The heart is composed of three major types of cardiac muscle: atrial muscle, ventricular muscle and specialized excitatory and conductive muscle fibers. The myocardium (cardiac muscle) is a specialized form of muscle consisting of individual cells joined by electrical connections [2]. The contraction of each cell is produced by a rise in intracellular calcium concentration leading to spontaneous depolarization and as each cell is electrically connected to its neighbor, contraction of one cell leads to a wave of depolarization and contraction across the myocardium.

1.2.1 Cardiovascular System

The cardiovascular system transports essential substances such as oxygen and nutrients between various tissues and organs. It also helps to transport and eliminate waste products. The arteries, veins and capillaries together with blood form a sophisticated network of the cardiovascular system. The blood vessels of the cardiovascular system are divided into two main pathways [1]. The blood vessels in the pulmonary circulation system carry blood from the heart to the lungs and then back to the heart. The blood vessels in the systemic circulation system carry blood from the heart to the different parts of the body and then back to the heart. Figure 1.2 shows the anatomy of the cardiovascular system.

Blood enters the heart on the right side through two main veins: the Superior vena cava and the Inferior vena cava. The blood fills the right atrium. In addition to the two veins, the coronary sinus also empties blood into the right atrium. When the right atrium is full it contracts and forces blood through the tricuspid valve into the right ventricle, which then contracts to pump the blood into the pulmonary circulation system.

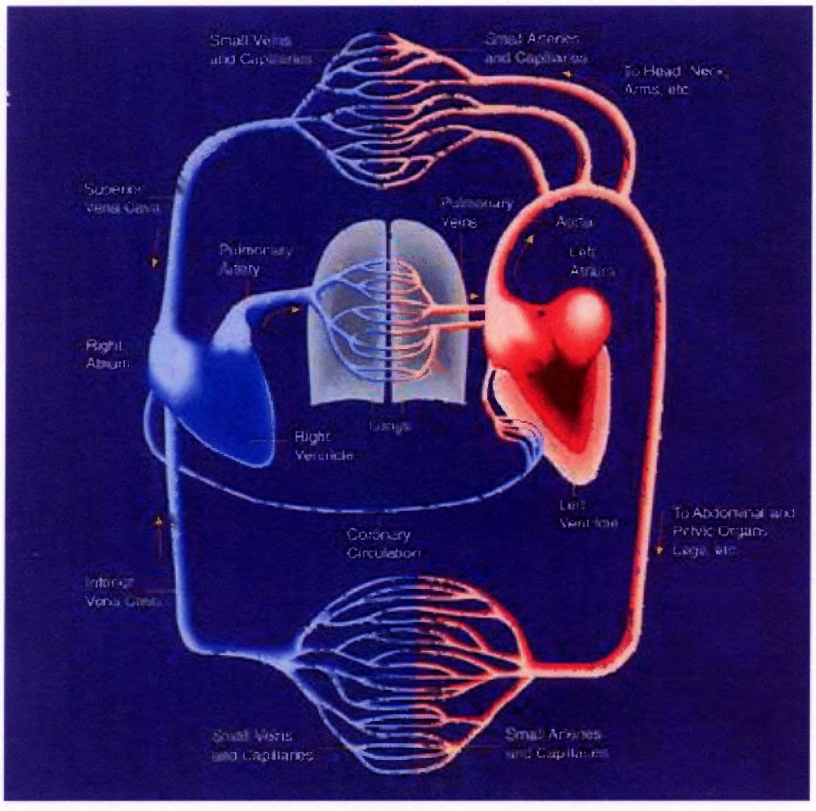

(**Reference.** http://images.google.com/imgres?imgurl=http://www.niaaa.nih.gov)

Figure 1.2 Cardiovascular system.

When ventricular pressure exceeds atrial pressure, the tricuspid valve closes, and the high ventricular pressure forces the pulmonary artery to open. The blood is forced through the pulmonary artery, which divides into the lungs where exchange of gas takes place. The pulmonary artery divides into many smaller arteries, which become arterioles that supply blood to the alveolar capillaries. In the alveoli of the lungs, the red blood cells are recharged with oxygen by giving up their carbon dioxide [1]. The Lung mass is divided into capillaries which feed into tiny veins. These veins combine to form larger veins which return oxygenated blood to heart via the pulmonary vein.

The blood enters the left atrium from the pulmonary vein and from there it is pumped through the mitral valve into the left ventricle, by contraction of the atrial muscles. When the left ventricle muscles contract, the pressure produced by the contraction of the ventricles forces the mitral valve to close and the high pressure of the ventricles causes the aortic valve to open, which causes the blood to flow through systemic circuit to different parts of the body.

1.3 Conductive System of the Heart

Figure 1.3 shows the conductive system of the heart that controls cardiac contractions. This figure shows the Sinoatrial (SA) node, where the normal rhythmical impulse is generated. The Internodal pathways conduct the impulse from the SA node to the Atrioventricular (AV) node, where the impulse from the atria is delayed before passing into the ventricles. The AV bundle then conducts the impulse from the atria into the ventricles through the left and right bundle branches [2]. The bundle branches then bifurcate into the Purkinje fibers, which conduct the cardiac impulse to all parts of the ventricles.

1.3.1 Sinus Node

The Sinus Node is a small, flattened, ellipsoidal strip of specialized muscle about 3 millimeters wide and is located in the superior wall of the right atrium. The sinus fibers directly connect to the atrial fibers, so that any action potential that begins in the sinus node spreads immediately into the atria.

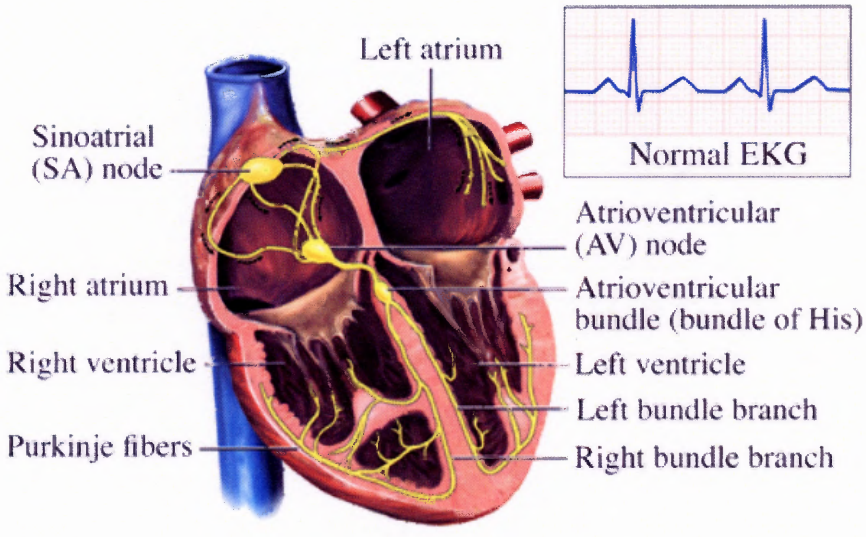

(**Reference.** http://images.google.com/imgres?imgurl=http://images.webmd.com/images/hw/)

Figure 1.3 Conduction system of the heart.

The potential of the sinus fiber has a resting membrane potential of -55 to -60 millivolts when compared to ventricular muscle which is -85 to -90 millivolts. The cause of this negativity is that the cell membranes of the sinus fibers are naturally leaky to sodium ions. It is because of this reason that the sinus node is self- excitatory. There are three types of channels which causes the change in voltages of the action potential: (1) fast sodium channels (2) slow calcium-sodium channels and (3) potassium channels.

1.3.2 Internodal Pathways

The ends of the sinus nodal fibers fuse with the surrounding atrial muscle fibers and action potentials originating in the sinus node travel outward into these fibers. There are three small bundles called anterior, middle and posterior internodal pathways through which the action potentials are spread into the entire atrial muscle and finally reach the AV node.

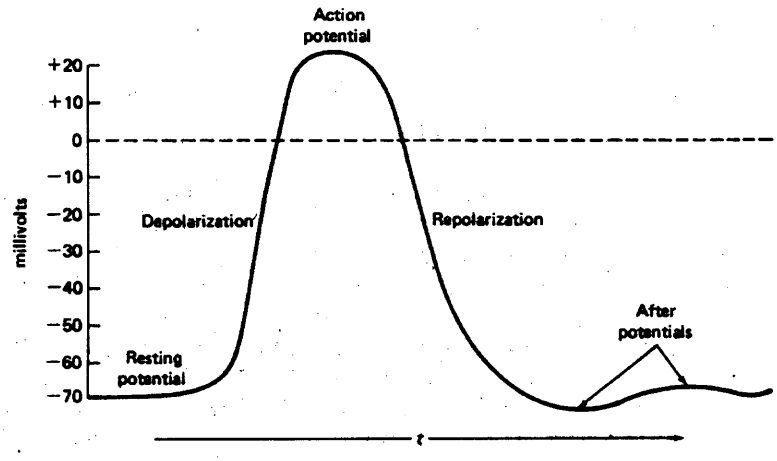

Figure 1.4 Waveform of action potential.

1.3.3 AV node and AV left and right bundle

The conduction system is organized so that the cardiac impulse will not travel from the atria into the ventricles too rapidly; this delay allows time for the atria to empty their contents into the ventricles before ventricular contraction begins. The AV node is located in the posterior septal wall of the right atrium immediately behind the opening of the coronary sinus. It is primarily the AV node and its adjacent conductive fibers that delay this transmission of the cardiac impulse from the atria into the ventricles.

After a delay of about 90 milliseconds in the AV node, the impulse travels through the penetrating portion of the AV bundle passing through left and right bundle branches making its way into the ventricles.

1.3.4 Purkinje System

The Purkinje fibers lead from the AV node through the AV bundle into the ventricles. They are very large fibers, even larger than ventricular fibers, and transmit the action potentials at a velocity of 1.5 to 4.0 m/sec. This velocity is 6 times larger than the normal cardiac muscle fiber conduction rate. This rapid transmission of action potentials by the Purkinje fibers is believed to be caused by the high level of permeability of the gap

junctions at the intercalated discs that connect between two cardiac cells. Therefore, the ions are transmitted easily from one cell to another cell at a faster rate. Once the impulse reaches the end of the Purkinje system, the action potential is transmitted through the entire ventricle mass by the ventricle muscle fibers themselves.

1.4 Electrocardiogram (ECG)

The Electrocardiograph (ECG) is a clinically useful tool that shows the electrical activity within the heart, simply by placing electrodes at various points on the body surface. The ECG is composed of a P wave, a QRS complex and a T wave as shown in figure 1.5.

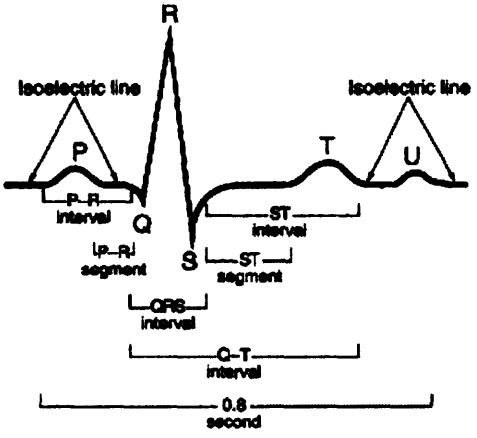

Figure 1.5 Electrocardiogram

The P wave is caused by electrical potentials generated as the atria depolarize before contraction. The QRS complex is generated by action potentials when the ventricles depolarize before contraction. Therefore, both P wave and QRS complex are depolarization waves. The T wave is caused by the ventricular repolarization as the ventricles start to recover from the state of depolarization and this wave is known as the repolarization wave.

During depolarization, the normal negative potential inside the fiber is lost and the membrane potential reverses; that is, it becomes slightly positive inside and negative outside. This happens when the fast sodium channels are open for few 10,000ths of a second and the positive sodium ions leak into the cell fiber, which increases the potential from -70 to -85 millivolts (resting membrane potential) to a positive potential. Once the positive potential peak is reached, the action potential reverses again and the potassium channels open from which positive ions start leaking to the extracellular fiber and the action potential voltage starts decreasing. This wave gives rise to the repolarization wave.

Before the contraction can occur, depolarization must spread through the muscle to initiate the chemical process of contraction. Therefore, the P wave occurs at the beginning of contraction of the atria and the QRS wave occurs at the beginning of contraction of the ventricles.

The repolarization of the ventricles begins after a few milliseconds of depolarization wave, that is, about 150 to 350 milliseconds. Thus, the process of repolarization extends over a long period. For this reason, the T wave in the normal ECG is a prolonged wave.

The atria repolarize about 150 to 200 seconds after the P wave. This occurs at the instant when the QRS complex is being recorded in the ECG. Thus, the atrial repolarization wave is usually obscured by the larger QRS complex and is seldom observed in the normal ECG.

1.4.1 Electrographic Leads

The Electrocardiogram (ECG) is measured using 12 standard leads. They are:

- Three Bipolar limb leads (lead I, lead II and lead III)
- Three Augmented leads (aVF, aVR and aVL)
- Six Precordial or Chest leads (V1 through V6)

1.4.1.1 Bipolar limb leads. The term "bipolar" here means that the ECG is recorded from two electrodes on the surface of the body and a reference electrode on the right leg. In working with the ECG from these three bipolar leads, Einthoven postulated that the heart is near the center of the equilateral triangle, the apexes of which are right and left shoulder and the crotch [3]. Therefore, the points of this triangle represent the electrode positions for the placement of the three limb leads as shown in the fig 1.6. Einthoven showed that the instantaneous voltage measured from any one of the limb lead positions is equal to the algebraic sum of the other two, or the vector sum of all the three limb leads is equal to zero. A slightly different measurement is made at each of the limb leads with respect to the indifferent electrode, which is assumed to represent an average of the potentials of the three limb leads. This average can be approximated to a central terminal connected to each of the three limb electrodes through equal resistances. A unipolar measurement made from any one of these three limb leads to an indifferent electrode is designated as VL, VR and VF.

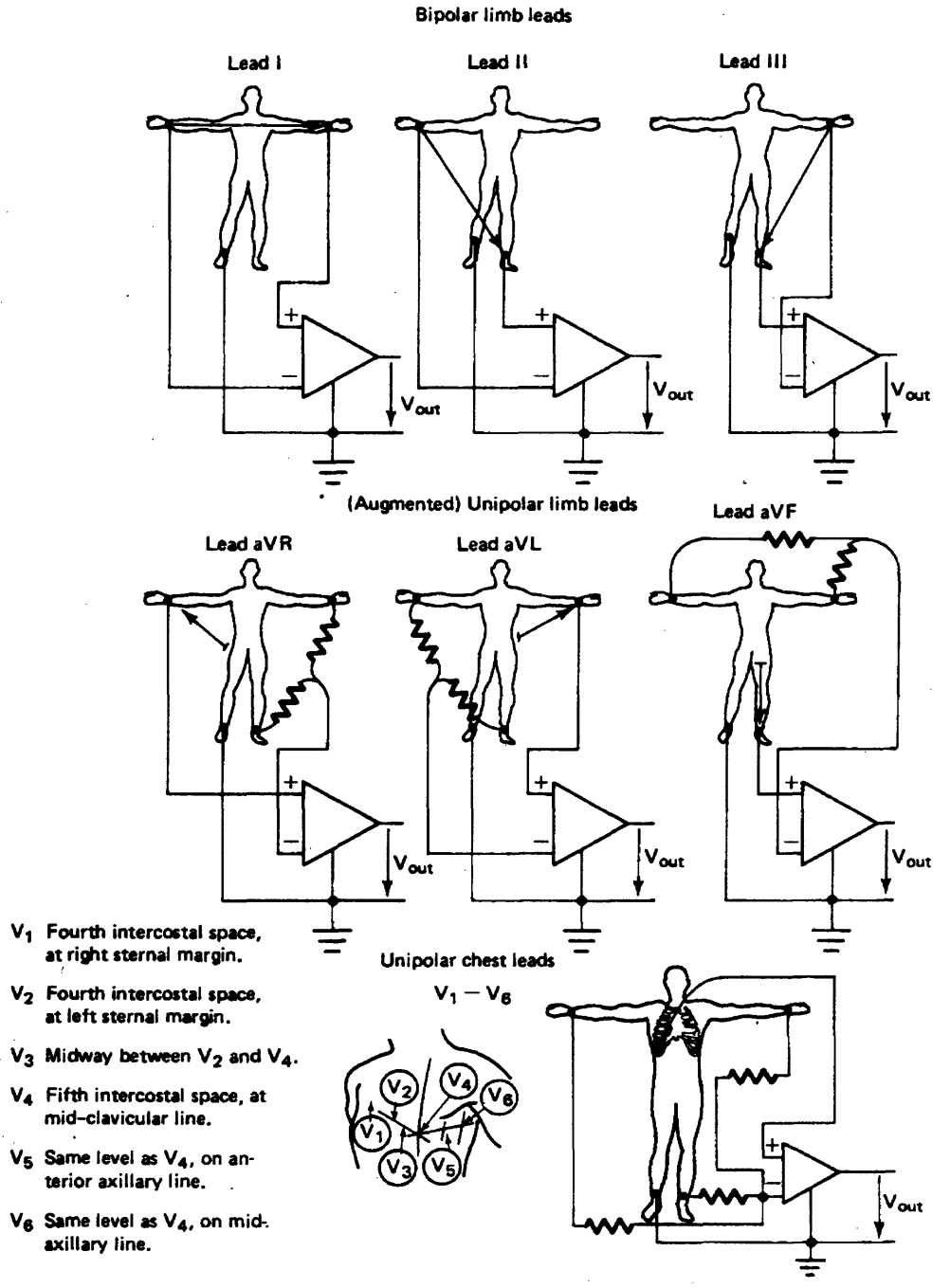

(**Reference**. L. Cromwell, F. Weibell, E. Pfeiffer, "Biomedical Instrumentation and Measurements", Prentice Hall, 1996.)

Figure 1.6 ECG lead configurations

1.4.1.2 Augmented leads. Because of the loading effect of the resistance network required to provide the central terminal, the ECG potentials measured at the three limb leads with respect to the central terminal are inconveniently small. To offset this difficulty, it was found that by disconnecting the measuring electrode from the network, the measured voltage can be increased by 50%. Unipolar leads obtained in this manner are called augmented unipolar limb leads, which are designated AVL, AVR and AVF.

1.4.1.3 Six Chest leads. The bipolar limb leads and the augmented unipolar limb leads are essentially limited to measurements in the frontal plane. While the precordial leads do include some effect of the third dimension, they do not provide a true representation of the electrical activity in the saggital (front-to-back) direction.

Therefore, a single chest electrode is used as an exploratory electrode which is sequentially placed on each of the six predesignated points on the chest to give a picture of the saggital view. These chest positions are called the precordial unipolar leads, which are designated V1 through V6.

1.5 Physiological Background

The QT interval is measured as the time interval between the onset of the QRS complex and the end of the T wave, the end of the T wave being the time at which repolarization is completed and the T wave voltage amplitude returns to the baseline [13] [11]. The QT interval is thus a measure of the duration of the ventricular depolarization and repolarization.

Accurate measurement of the QT interval is very important from a clinical screening perspective. Expert manual measurement is both imprecise and imperfectly reproducible, yet it is used as the reference standard to assess the accuracy of current

automatic computer algorithms, which thus produce reproducible but incorrect measurements of the QT interval [4]. The relationship between different cellular action potentials and the QT interval recorded at the body surface is very complex and thus it is difficult to measure the end of the T wave with precision [7].

First, there is inherent precision in identifying the end of the T wave because of incomplete understanding of the recovery process and its projection on the body surface. Second, significant variation both in onset of QRS complex and the end of the T wave among some ECG leads provides different QT values depending on the leads selected for measurement [12]. Third, technical factors like paper speed and sensitivity influence QT measurements with higher paper speed leading to shorter interval values and higher sensitivity resulting in QT prolongation [13].

1.5.1 QT and Corrected QT Interval (QTc)

There are various issues involved in the measurement of the QT interval especially regarding the end of the T wave and the different morphological pattern of T-U complexes. The other issue is significant spontaneous variability in the QT interval, resulting in spurious QT prolongation and unnecessary concern.

The QT interval relies on the identification of the end of the T wave, which may be visually assessed differently according to the experience and training of the cardiologist. The use of a computer algorithm helps to detect more consistently the location of the end of the T wave [11] [30]. However, computers may fail to identify this location correctly if the shape of the T wave is abnormal (low amplitude biphasic T wave) requiring visual checking of the automatic measurements.

The ability to define QT interval prolongation reliably is important because of its association with ventricular abnormalities. The QT interval prolongation is hampered by the fact that the QT interval is not constant and highly dependent on the preceding cardiac cycles and therefore on the heart rate. The QT interval varies not only with the heart rate, but also with many factors, including gender and because of diurnal variability, time of the day. To correct for the inconstancy of dependence of the QT interval on preceding R-to-R changes, a rate-normalized or corrected QT interval (QTc) is used [28].

The object of QTc is to normalize the QT interval to the value that it would have had if the heart rate were 60 beats/min, that is QTc=QT when RR interval is equal to one second. One of the first, and still most widely used, QT correction formulas was developed by Bazett. In Bazett's formula QTc is defined as the QT interval divided by the square root of the of its preceding R to R time interval. It is given by:

$$QTc = \frac{QT}{\sqrt{RR}} \tag{1.1}$$

RR is the duration between the two consecutive R waves which occurs during ventricular depolarization. The QT correction formula was derived by defining QT interval equals to QTc when RR=1 sec, and solving for the resulting expression. Because the Bazett's formula tends to be inaccurate by overcorrecting and undercorrecting QT interval at high and low ends of the range of heart rates, many other empirical formulas have been developed. However, there is no agreement as to which is the best method for QT correction, and Bazett's formula remains the best known and most widely accepted method for rate normalization of QT interval [15].

Table 1 Range of QT corrected interval in individuals

Rating	QTc in msec	
	Adult males	Adult females
Normal	<430	<450
Borderline	430-450	450-470
Prolonged	>450	>470

1.5.2 Long QT syndrome

The QT interval as well as the corrected QT interval are important in the diagnosis of long QT syndrome (LQTS). Long QT syndrome is a cardiac ion channel disease that leads to lethal ventricular arrhythmias [16]. In individuals who have long QT syndrome, the time required for ventricular repolarization is prolonged. This creates a problem because it makes the heartbeat electrically unstable and especially vulnerable to the arrhythmias like Torsades de Pointes (polymorphic ventricular tachycardia that occurs due to prolonged QTc interval) and ventricular fibrillation [17]. If the heart falls into any of these rhythms death can occur within only a few minutes. Long QT syndrome is characterized by prolongation of QT interval and thus, QT interval is a significant clinical tool in assessing life threatening arrhythmias.

In people with long QT syndrome, as the heart recharges, the small channels in the heart cells do not open and close properly to let the particles move at the correct times. Researchers are still not certain how these channels are connected to the dangerous heart rhythms associated with long QT syndrome, but it is known that the defective channels make the heart's electrical system unstable as it recharges. When the heart is unstable, it can enter into a problematic heart rhythm and cause the heart to pump blood inefficiently.

1.6 QT Variability and QT Dispersion

The electrographic QT interval represents a measure of ventricular repolarization. Lability in the repolarization process would be expected to manifest as beat-to-beat oscillations in the QT interval [4]. Temporal lability in ventricular repolarization is a marker for, and is mechanistically related to, increased risk of malignant arrhythmias [12]. QT measurement is highly dependent on waveform morphology near the end of the T wave. Erroneous measurements are likely in the setting of signal artifacts or noise, even if the noise is low in amplitude. Since the T wave is low in amplitude, locating the time of its peak and terminus is easily corrupted by artifacts that often cannot be distinguished from the true waveform [11].

It is known that the QT interval is controlled by a neural regulatory system in the same way as heart rate (HR) and the variation in the duration of the QT interval is the same way as heart rate varies during time [6]. While this kind of variation is the normal part of the regulation of the cardiac system, it has been argued that abnormal variation in the repolarization duration could be a marker for a group of severe cardiac diseases such as ventricular arrhythmias. It has also been argued that the QT variability could yield such additional information which can not be observed from HR variability [15].

A single global QT interval measurement from the 12 lead electrocardiogram has been the standard measure, but recently there has been a great interest in the distribution of the QT intervals, at given instant of time, across the 12 lead electrocardiogram leads [13]. This is called QT dispersion.

The QT dispersion is defined as the difference between maximum QT interval and minimum QT interval [18]. It was originally proposed as an index of the spatial

dispersion of ventricular recovery times. The QT interval duration varies between leads on the standard ECG. These interlead differences, called QT interval dispersion was proposed as an index of the spatial dispersion of the ventricular recovery times [19]. This measurement was an attempt to distinguish between a myocardium that is homogeneous from a myocardium that displays inhomogeneity, which is accompanied by increased dispersion of the ventricular recovery times and prolongation of repolarization.

The initial concept that QT dispersion is an index of inhomogeneity was supported by the link between the dispersion of ventricular recovery times and the genesis of arrhythmias [21]. It was believed that the standard 12-lead ECG contained information about regional ventricular repolarization; thus, when increased QT dispersion was seen in cardiac diseases, it was assumed that this increased QT dispersion was a direct reflection of the heterogeneous ventricular recovery times [22][31].

1.7 RT_{max} interval

The long QT syndrome (LQTS) is characterized by exercise or stress-induced syncope or sudden death associated with a prolonged corrected QT interval (QTc). Because of the difficulty in measuring the QT interval at rapid heart rates and the subjective nature of the measurement of the beginning of the Q wave and end of the T wave, the RT_{max} interval was measured. It was defined as the interval from the peak of the R wave to the peak of the T wave [14].

Recent studies have shown that both the RT_{max} interval and the QT interval are prolonged in patients with LQTS and these intervals also correlated well in normal subjects during paced breathing. Thus, RT_{max} interval can be used as a surrogate of the QT interval, the accepted measurement to quantify repolarization [14]. However, the

abnormal configuration of repolarization in LQTS patients often makes the precise end of the T wave difficult to determine. This problem is further hampered by fusion of the T and P waves at higher rates. The use of the RT_{max} interval facilitates the development of automated technology to measure and quantify the duration of repolarization. The use of the peaks of the R and T waves minimizes the potential for observer bias in the manual acquisition of data.

CHAPTER 2

ALGORITHMS FOR QT INTERVAL MEASUREMENT

2.1 Current Methods

In the study of ventricular activity, it is important that the QT interval is measured correctly. Therefore, an algorithm to accurately detect QRS complex beginning points and T wave end points is of great importance to compute QT intervals.

Several methods for automatic electrocardiogram T wave detection and QT interval assessment have been developed [9] [8] [6]. While beginning of the QRS complex can be measured with good accuracy due to its higher frequency content, the T wave end presents greater difficulties. Currently the algorithms can be divided into two categories, namely, threshold based algorithms and algorithms based on intersection of slope and an isoelectric line [4].

In the threshold method, the threshold can be derived from a certain percentage of the T peak or the derivative of the T peak, and the intersection is based on the threshold level with the T wave. The slope methods are based on the intersection of the maximum T wave slope after the T wave peak with an isoelectric line in the TP segment. Several methods for the measurement of the end and, peak of the T wave are reviewed and compared in this chapter. Measurement methods compared here include:

2.1.1 Threshold Method (TH): The point at which the T wave intersects a threshold level.

2.1.2 Derivative Threshold (DTH): The point at which the derivative of the T wave intersects a threshold.

2.1.3 Slope Intercept (SI): The intersection of the maximum slope of T the wave and the isoelectric line.

2.1.4 Least squares Intercept (LSI): The intersection of a line fitted by least squares at the maximum slope of the T wave and an isoelectric line.

2.1.5 T Wave Area (TA): The total area of the T wave is considered and threshold is fixed at 90% of the total area. Wherever the threshold intersects with the baseline, the point is detected as the T wave end.

2.1.6 Wavelet Detection Method (WD): This method decomposes a signal into its components based on different scales. The detection of QRS beginning, T peak and T_{end} is based on the maximum absolute method and zero crossings of the mother wavelet transform at characteristic scales.

2.1.7 Principal Component Analysis (PCA) of T wave: The PCA method takes the total morphology of the T wave into consideration. The T wave is decomposed into principal component matrices. This matrix is used to define S/F ratio, which is the ratio of second component to the first component multiplied by 100. This ratio determines the size and shape of the T wave and based on that it provides an estimate of T wave complexity.

2.1.1 Threshold Method (TH)

This method aims at determining the end of the T wave by considering the point at which the threshold level intersects with the T wave as shown in fig 2.1. The threshold level is based on 5-20% of the maximum T peak [9]. For this technique, the T wave amplitude and threshold level were calculated relative to an isoelectric level to allow for any baseline offsets [23].

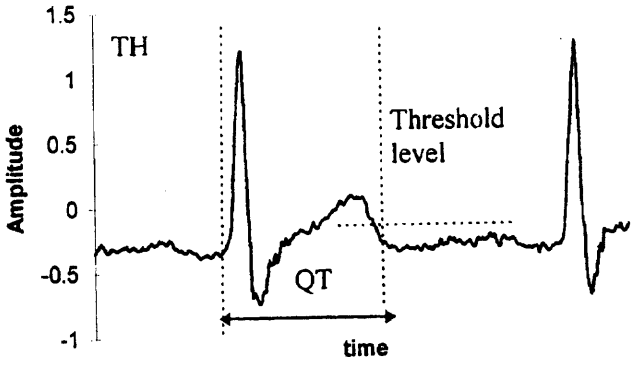

(**Reference.** Z. Sahinoglu, "Analysis of Multi lead QT Dispersion by means of an Algorithm implemented in LabVIEW", *NJIT MS Thesis*, January 1998.)

Figure 2.1 T wave end detection with threshold method (TH)

2.1.2 Differential Threshold Method (DTH)

Fig 2.2 shows the Differential Threshold Method (DTH) to detect the T wave end. In this method, a search window is defined to find the maximum and minimum point between the limits of the window which is located after the QRS complex. Then, the amplitude of the maximum or minimum is used to set the threshold level [6] [9]. Thereafter, the threshold crossing point is detected in the same way as in the threshold method [23].

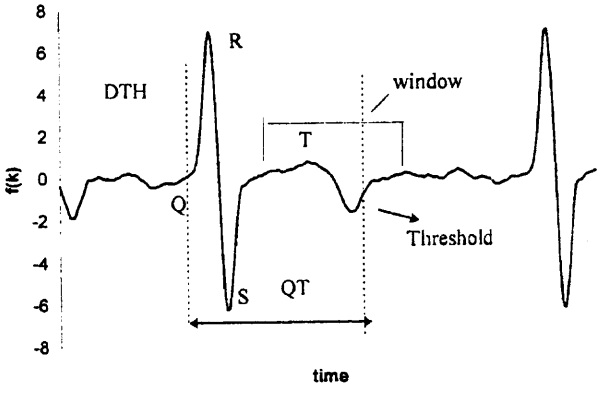

(**Reference.** Z. Sahinoglu, "Analysis of Multi lead QT Dispersion by means of an Algorithm implemented in LabVIEW", *NJIT MS Thesis*, January 1998.)

Figure 2.2 Differential threshold method (DTH) to detect T wave end.

2.1.3 Slope Intercept (SI)

In this technique, the end of the T wave is defined as the intercept of an isoelectric level and a line tangential to the point of maximum T wave slope. The SI method is illustrated in the fig 2.3 [20].

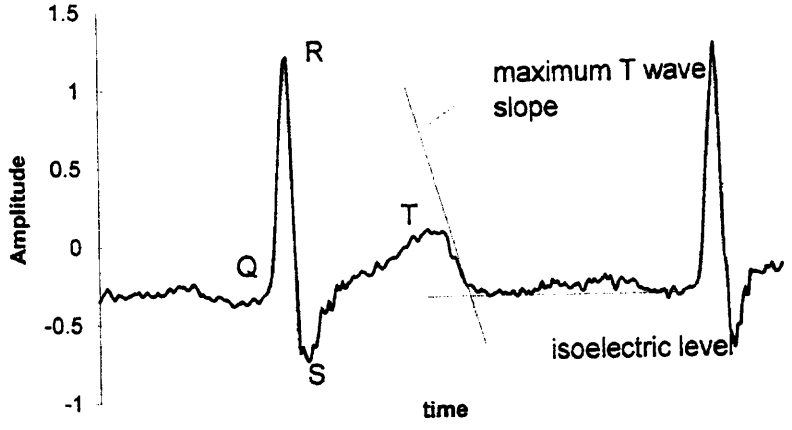

(**Reference.** Z. Sahinoglu, "Analysis of Multi lead QT Dispersion by means of an Algorithm implemented in LabVIEW", *NJIT MS Thesis*, January 1998.)

Figure 2.3 Slope intercept (SI) technique

2.1.4 Least squares Intercept (LSI) Method

This method is the interception of a least squared fitted line with the isoelectric line which is then detected as T wave end. The least squares fitted line is a straight line of y=mx+b which is determined based on the data points around the maximum slope point (MSP) after the T peak is reached [4] [6]. The fit line is drawn based on the criteria that the sum of squares of deviations of all points from MSP is minimal or ideally zero. The least squares method is shown in the fig 2.4 [20].

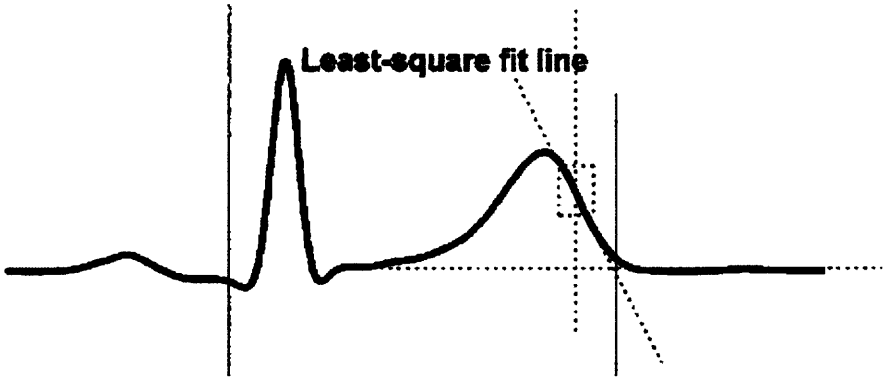

(**Reference.** Q. Xue, S. Reddy, "Algorithms for Computerized QT Analysis", *Journal of Electrocardiology*, Vol. 30 Suppl)

Figure 2.4 Least squares intercept (LSI) to detect T_{end}.

2.2 Comparison of Different Methods

According to the literature, different QT measurement techniques produced results which were influenced, to varying degrees, by filtering and other variables [9]. This is relevant for the inter-comparison of studies using different techniques and to assess the influence of lead selection, electrocardiogram filtering, and threshold levels.

Across the different filter parameter combinations, the technique threshold (TH) demonstrated the largest intra-technique range of mean and standard deviation (SD) QT difference values [11]. These variations with relatively small changes in filtering and algorithm parameters together with the high values of SD make the technique threshold (TH) unreliable.

The QT interval measured with good quality and normal electrocardiograms revealed that the technique Derivative Threshold (DTH), Slope Intercept (SI), and Least squares Intercept (LSI) produce consistent results over most filter/parameter combinations but with an underestimate of the QT interval in SI method [9]. Even with these techniques, however, it should be noted that the effect of filtering has a critical influence on their performance. The absence of 40 Hz high cut off frequency in filtering resulted in failed measurements in SI and LSI methods respectively. The failure ratio for TH and DTH measurements remained zero for almost all filter settings.

The QT interval measured using automatic techniques differ considerably and these differences encountered were much greater than manual measurement. The application of the TH method for QT interval measurement performed particularly poorly [4]. Furthermore, the non-uniform distribution of automatic QT difference across different electrocardiogram leads means higher dispersion values for automatically determined QT intervals.

The slope based methods in general have better reproducibility than other methods of T wave end determination [25]. There are two reasons why slope based algorithms have better reproducibility than threshold-based algorithms:

- The maximum slope point (MSP) of the T wave is more stable, or more reproducible than the T wave amplitude from which the threshold level is determined.
- The straight line corresponding to the maximum slope is better than the original curve for obtaining a stable point of intersection with a horizontal line.

A similar reason can explain why a higher threshold can improve reproducibility, since the horizontal threshold line intersects with more stable portion of the T wave. The

LSI method achieved better reproducibility than simple slope method [6], mainly because of more stable fitting line due to more sample points.

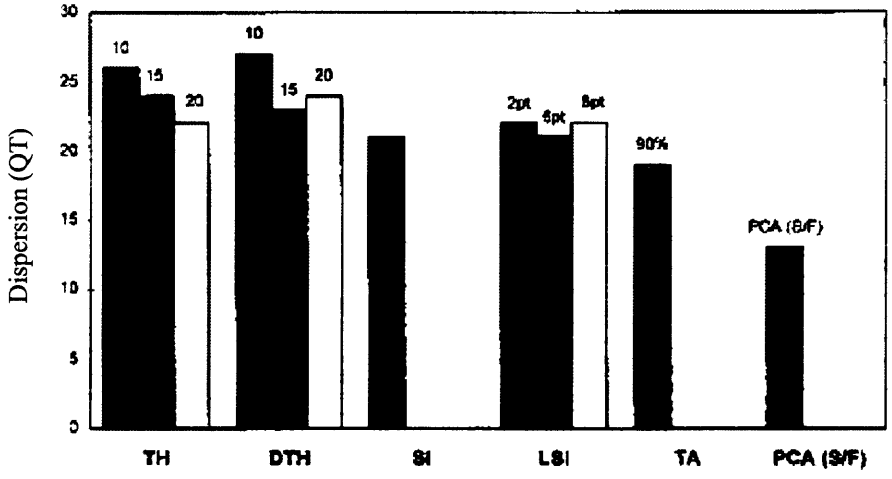

(**Reference.** Q. Xue, S. Reddy, "Algorithms for Computerized QT Analysis", *Journal of Electrocardiology*, Vol. 30 Suppl.)

Figure 2.5 Comparison of average QT interval dispersion by different algorithms.

As shown in fig 2.5, the first three bars are threshold algorithms with 10, 15, and 20% of the maximum amplitude of the T peak, considered as threshold level for detecting the T_{end}. The second bars are Derived Threshold (DTH) algorithms with same threshold levels as in the Threshold (TH) method.

The third and fourth are the slope generated algorithms. The least squares fit algorithm has 2, 6 and 8 sample points for the fitting lines. The QT interval dispersion among the three bars of the least squares method (LSI) is much less when compared to bars in the TH and DTH methods. From fig 2.5, it is clear that the threshold based algorithms have larger QT dispersion values than slope algorithms and thus, making slope methods more reproducible.

CHAPTER 3

METHODS

3.1 Getting Proper Data

The first step of the QT algorithm was to provide the proper inputs and obtain the sampling frequency for the inputted data. The algorithm was validated using five ECG data sets. The data sets were obtained from the NJIT, Signal Processing Laboratory resources. These data sets were 5 minute segments of paced breathing at 12 breaths per minute. The ECG segments chosen for this algorithm were all clean and noise free. The dataset were sampled at 250 samples/sec. The input data was in the text format and was read into LabVIEW 7.0 Software.

3.2 The Algorithm

The algorithm was divided into four main categories:

3.2.1 Filtering and Differentiation Process

3.2.2 R wave Detection

3.2.3 Q wave Detection

3.2.4 T_{max} and T_{end} Detection

3.2.1 Filtering and Differentiation Process

The frequency range of an ECG is in between 0.1 Hz to 100 Hz. The ECG contains various types of noise of different frequencies: low frequency noise (<0.03 Hz) due to electrode movement and respiration, that causes baseline wander in ECG signal, EMG noise which has a wide frequency range (1-5000Hz) and 60 Hz power line

interference. Thus, to effectively remove these noise effects and enhance the signal, a filtering process was required. A high pass filter with a cutoff frequency can be set anywhere between 0.05-0.5 Hz to remove the baseline wander [9]. To reduce the noise in the T wave, a low pass filter can be applied to the original ECG signals. Usually, a lower cutoff frequency was used for the T wave complex than for the QRS complex because spectral analysis of ECG reveals that the frequency of the T wave was below 15-20 Hz and the QRS complex has frequencies in the range of 15-40 Hz [4]. The combination of high pass low and pass filters can be implemented by a Bandpass filter. The algorithm that was developed uses a digital Butterworth Bandpass filter with high and low cutoff frequencies of 0.5 Hz and 40 Hz respectively. The baseline wandering was reduced in the filtered signal due to the removal of low frequency components and the signal now has improved signal-to-noise ratio. This Bandpass filter uses an order 2. The maximum delay, in samples, used in creating each output sample is called the order of the filter or, the number of previous inputs used to calculate the current output. The order of 2 would be a compromise between getting a sharp cutoff at the transition band and delay in processing the signal.

After the filtering procedure, the electrocardiogram was passed through a differentiator. The differentiation process enhances slopes and peaks in the signal making the detection process easier. The block diagram of filtering and differentiation of the ECG is shown in figure 3.1 and its implementation in LabVIEW is shown in figure 3.2.

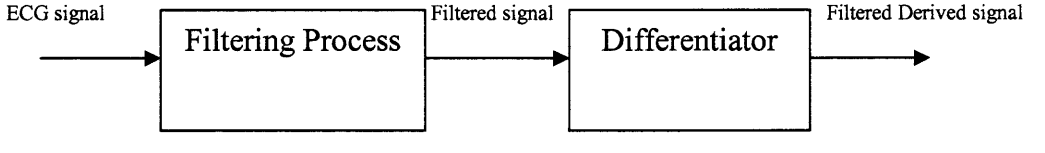

Figure 3.1 Block diagram of filtering and differentiation process

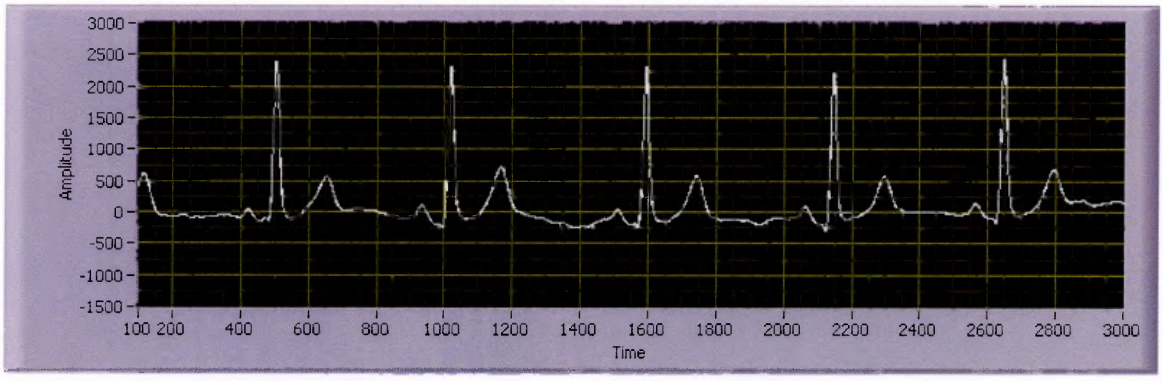

Figure 3.2 (a) Original ECG

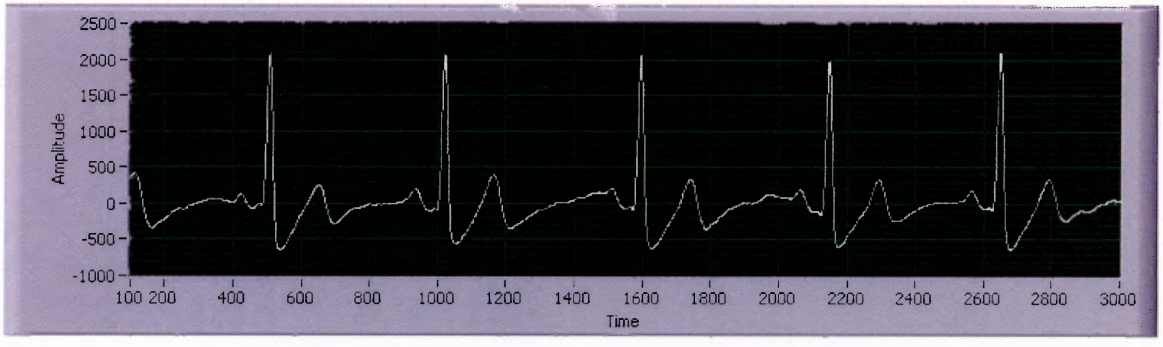

Figure 3.2 (b) Filtered ECG

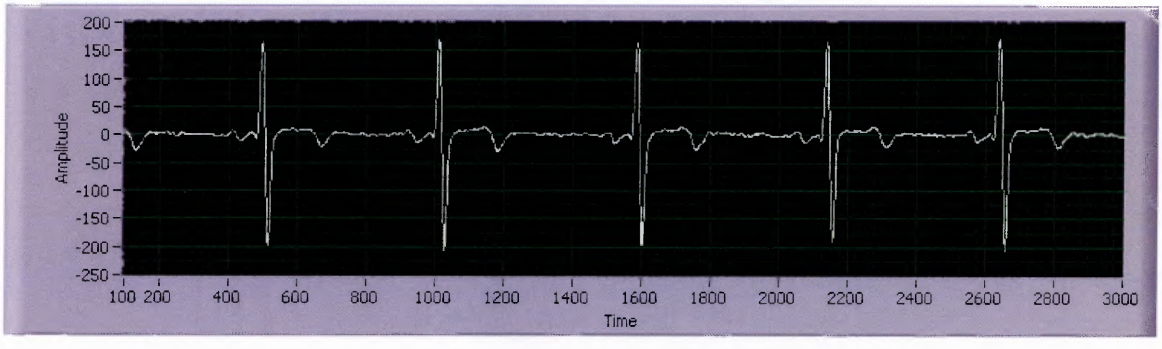

Figure 3.2 (c) Filtered derived ECG

Figure 3.2 Screen shots of original, filtered and filtered derived ECG

3.2.2 R wave Detection

The R wave points were used as reference points to detect Q wave, T_{max} and T_{end} respectively. The R peak was detected using an existing R wave detector [27]. The R wave array indices were stored in a file by running the R detector program on various ECG datasets. The R wave array was inputted into the QT detector and, these points were used as reference points to detect Q wave, T_{max} and T_{end} respectively. The R peaks displayed on ECG dataset is shown in figure 3.3.

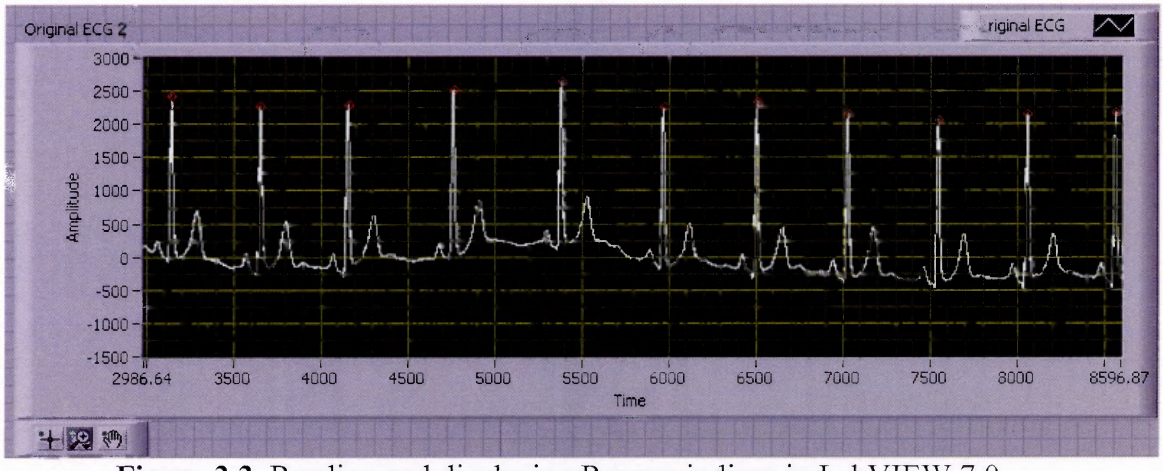

Figure 3.3 Reading and displaying R wave indices in LabVIEW 7.0

3.2.3 Q wave Detection

In order to detect the onset of the QRS waveform, the R peaks were used as reference points, as described earlier. The QRS onset is defined as the beginning of the Q wave. The Q wave detection process was comprised of three different steps:

- Detection of maximum positive and minimum negative derivative points
- Decision of morphology of Q wave
- Q wave detection

3.2.3.1 Detection of Maximum Positive and Minimum Negative Derivative Points

A search window was run on the differentiated signal of ECG to detect the maximum positive and minimum negative points. According to the literature, QRS complex is approximately 90 to 150 milliseconds wide [28]. Thus the length of the window starting from the R wave could be set up to a length of 80 msec. The length of the window was approximately 60-70 msec. The length of the window was defined by taking the number of points equivalent to ((60*sampling frequency)/1000), where the sampling frequency fs = 250 samples/sec and thus, the length of the window depends on the sampling frequency. In this search window, the maximum value and the minimum value was searched and displayed on the ECG differentiated signal in figure 3.4.

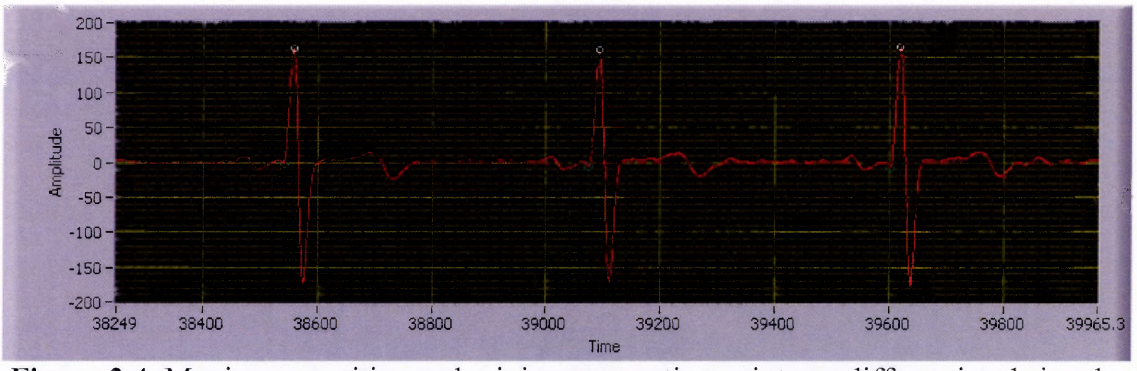

Figure 3.4 Maximum positive and minimum negative points on differentiated signal

3.2.3.2 Decision of Morphology of Q wave. There were two types of Q wave at the beginning of the QRS onset. This algorithm has the robustness to detect the morphology of the Q wave and then, implement the corresponding detection steps. The two different types of morphology of Q wave are:

- Q with negative wave
- Q without negative wave

3.2.3.2.i Q with Negative wave. To decide the type of the Q wave, maximum and minimum points were considered. The peak maximum point derivative was used to set percentage level with which, the minimum negative point was compared. About 10% of the maximum point in the derived signal was compared with the minimum negative point. If 10% of the maximum point was less than the minimum point, then the program can conclude that there was a negative wave present at the beginning of the QRS complex based on the values of two points and, correspondingly apply the detection process.

3.2.3.2.ii Q without Negative wave. The same percentage level was used to compare both the minimum and maximum derivative points. If 10% of the maximum point was greater than the minimum negative point, then the QRS onset does not have a negative wave and the detection process for this type of Q wave is applied.

3.2.3.3 Q wave Detection

Depending on the morphology of the Q wave, the corresponding detection process was applied. Since there were two types of Q waves, two different detection processes was applied based on the differential threshold method (DTH):

3.2.3.3.i Q wave detection with negative wave

3.2.3.3.ii Q wave detection without negative wave

3.2.3.3.i Q wave Detection with Negative wave. This detection process was based on the differential threshold method. The minimum negative point was considered for creating the threshold level. The threshold level was set as 10 % of the minimum negative point. The same window was used which was created in the previous section, for

generating points less than this threshold level. Therefore, an array of all the points less than this threshold value within this window was generated. The first point in this array was considered as the Q wave and the corresponding index in the ECG was read and displayed. The example of a Q negative wave is shown in figure 3.6 (b). However, in this algorithm, none of the datasets used for validation had negative Q wave. But the algorithm was able to distinguish between the ECG with negative Q wave and the one without it.

3.2.3.3. ii Q wave Detection without Negative wave. This detection process was very similar to the one with a negative Q wave except for the threshold level. The threshold level was set as 10% of the maximum positive derivative point on the differentiated ECG signal. Then, an array of points which are less than this threshold level was generated within the search window. The first point within this array was detected as Q wave and this point was correspondingly displayed on the ECG signal. The detection process for Q wave is shown in figure 3.5 and its implementation in LabVIEW is shown in figure 3.6.

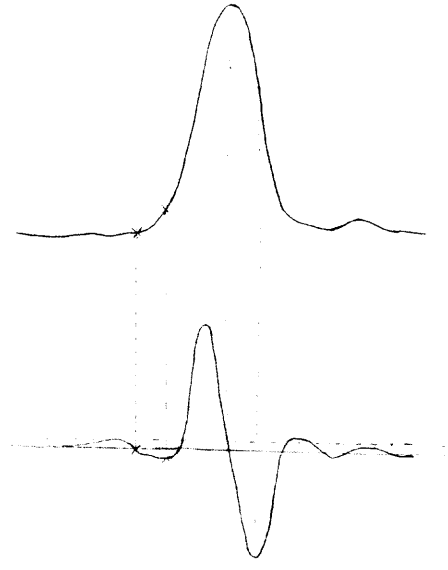

Figure 3.5 Q wave detection using differential threshold method (DTH).

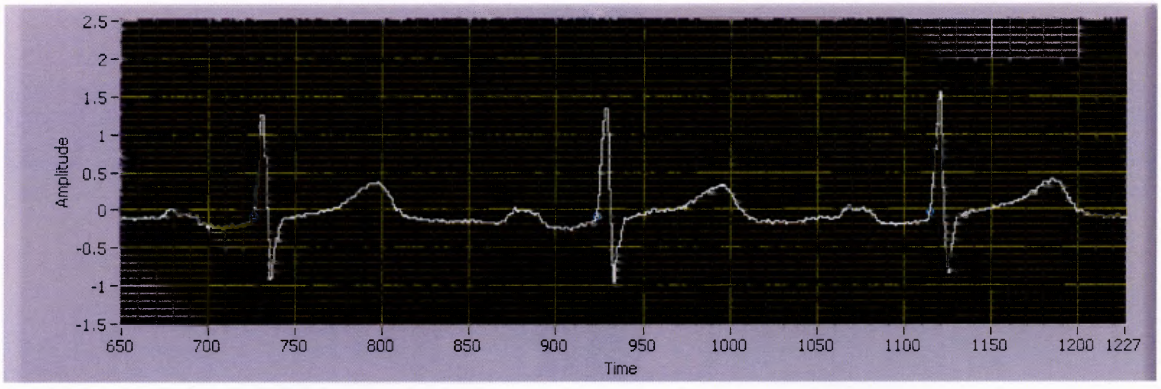

Figure 3.6 (a) Detection of Q wave without negative wave

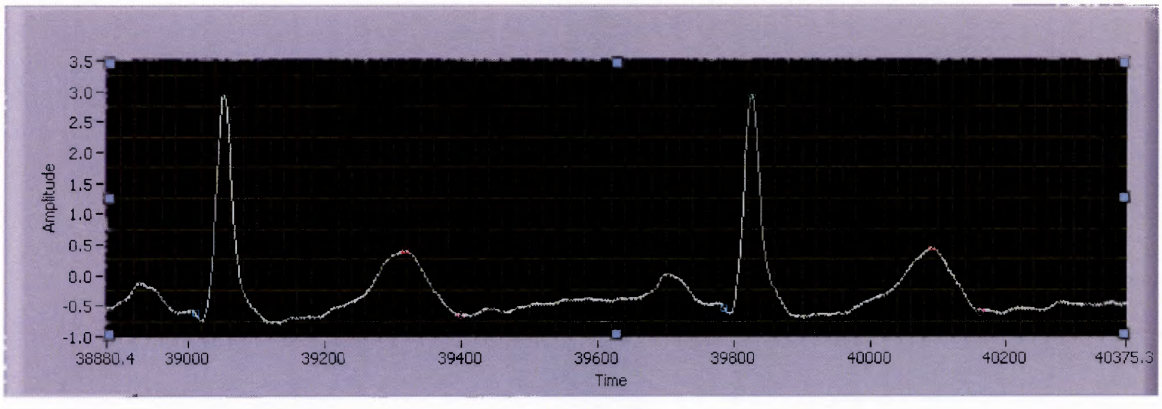

Figure 3.6 (b) Detection of Q wave with negative wave

3.2.4 T_{max} and T_{end} Detection

The T wave operations include T_{max} detection and T_{end} detection. The T_{max} detection was based on the window method. Starting with the R peak in the original ECG signal, a search window was set. A refractory period of about 60 milliseconds was set starting from the R peak so that no other maximum point other than T_{max} is detected. The length of the window was approximately 250 milliseconds based on the literature of the RT interval [31] [14]. In this window, the maximum value was searched and displayed on original ECG. This point was detected as T_{max}.

The T_{end} detection was based on the combination of two different methods: the Threshold method (TH) and the Least squares Intercept (LSI) method. The least squares method was based on generating a slope or "best-fit line" starting at T_{max} on the T wave. This best-fit line was based on the least squares solution and the detailed explanation of least squares method is given in appendix A. The least squares method generates a straight best-fit line, which is better than the original curve that intersects with the isoelectric line to obtain the T wave end [6]. Due to 60 Hz noise interference from the power line and low frequency noise from electrode movements, there exists baseline wandering which makes the detection of the T wave end difficult. Thus, the threshold method facilitates this detection because; the straight line threshold was intersecting with a more stable portion of the T wave than fluctuating and wandering baseline. Thus, higher threshold values were selected.

Starting from the T_{max}, a search window was used to generate the subset of the array for which the best-fit line has to be drawn. To draw the best-fit line, an array of points on X-axis and Y-axis were required. The best fit line is in the form of Y=mX+b, where m is the slope and b is the intercept.

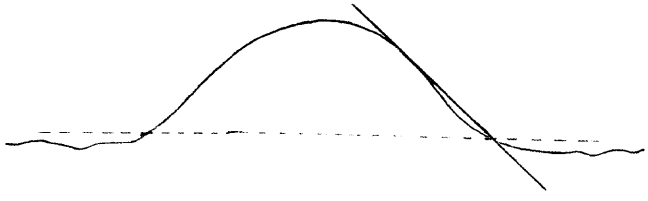

Figure 3.7 T_{end} detection based on least squares method (LSI).

To get the X-axis points, an array of points from 0 to maximum index in the ECG signal was generated. From this array, the X points of the best-fit line were extracted by taking a subset of the array starting at T_{max} and going for a length of about 75 milliseconds. To generate the Y-axis points of the best-fit line, an array was generated from the ECG signal array starting at the T_{max} point (value) and, going for a length of about 75 milliseconds. To draw the slope on the T wave, the size of the X array and Y array has to be the same at all times. Once the arrays were generated, they are fed into the linear fit block available in LabVIEW 7.0 to draw the slope starting at T_{max}.

The next step was to find the intersection point of the best fit line with the threshold. To define the threshold level, 5% of the T_{max} amplitude was considered [25]. The point of intersection of the slope generated with the threshold level was detected as T_{end} and the corresponding point was read on the ECG signal as shown in figure 3.8 (a).

3.2.4.1 Potential Problems of this Method. The process of validation was carried out by testing this algorithm on several data sets. To understand the potential problem of this algorithm exactly, this algorithm was run on two different data sets as shown in the figure 3.8 (a) and 3.8 (b) respectively.

The intersection of the best fit line drawn around the region of slope of the T wave with constant threshold level was considered as the T_{end}. Figure 3.8 (a) shows a normal ECG data set where the constant threshold level was set just above the 'zero line'. Since the most part of the T wave was above the 'zero line', the intersection of slope and threshold was at a point where it can detect the exact T_{end}.

Figure 3.8 (b) is another example of a normal ECG data set. Since half of the T wave is below the 'zero line', an intersection of the slope and threshold will be somewhere in the middle of the T wave, since threshold level is kept at a constant level above zero. Therefore, the intersection results in the detection of a wrong T_{end}. The problem was due to the fixed threshold level. To address this problem, a more easy and accurate method was developed based on the differential threshold method.

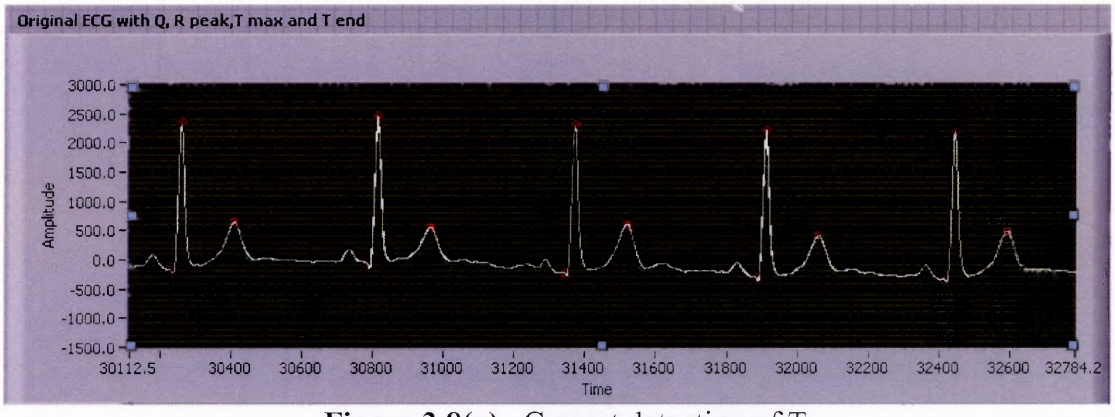

Figure 3.8(a) Correct detection of T_{end}

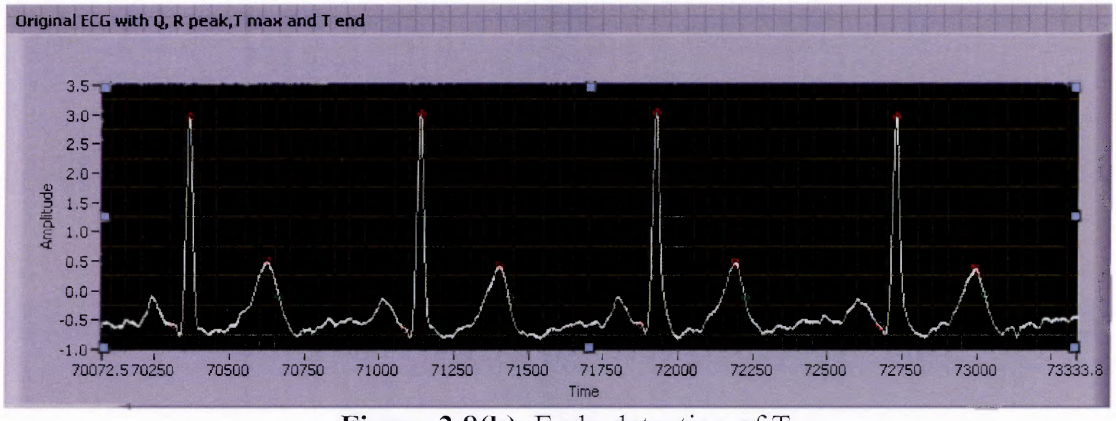

Figure 3.8(b) Early detection of T_{end}

Figure 3.8 Correct and early detection of T_{end}

3.2.5 T_{end} Detection Based on Differential Threshold Method (DTH)

Two different types of T waves were defined according to the locations of the maximum and minimum points between the limits of the window. However, the algorithm failed to decide on the morphology of the T wave, but applied the detection process correctly on T positive.

Starting from the R peak, a refractory period of 60 milliseconds was created. This point was taken as start of the search window to find the maximum and minimum T wave points in the derived signal. The length of the window was approximately 200 to 250 milliseconds, depending on the sampling rate of the ECG signal, which in this study is 250 samples/sec. The length of the window was defined by the taking number of points equivalent to ((250*sampling frequency)/1000). In this search window, the maximum and minimum points were detected.

The minimum negative point was now compared with the maximum positive point, in the derived signal, to find the earlier point in terms of occurrence. If the maximum positive point occurs before the minimum negative point, then the T wave was considered as positive T wave. If the minimum negative point occurs earlier than the maximum positive point, then the T wave was considered as T negative.

In case of T positive, the threshold level was set as 10% of the maximum amplitude of the T peak in the derived signal of the ECG. Using the same window which was created in this section, all the points in this window were compared with the threshold level. The points which are less than the threshold level were put in an array and the first point in this array was considered as T wave end. The detection process for T_{end} is shown in figure 3.9.

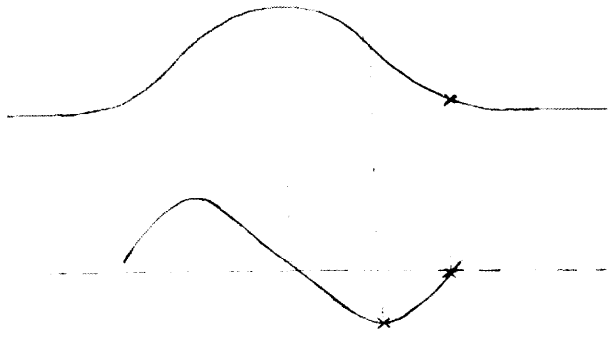

Figure 3.9 T_{end} detection based on differential threshold method (DTH).

3.3 Interval Measurements

For this study, various intervals were measured including QT, QTc, RT_{max}, QT_{max}, RR, and RT interval. The software used is LabVIEW 7.0 Express, which allows creating a separate array for each detected point. The four different arrays created were R, T_{max}, Q and T_{end} array.

The QT interval is defined as the interval from the beginning of the Q wave to the end of the T wave. The QT interval has some dependence on the heart rate variability and it is presumed to follow the preceding RR interval [26]. The QT interval was corrected for preceding R-to-R interval using Bazett's formula and the corresponding interval was called QT corrected (QTc). The Bazett's formula is given by:

$$QTc = \frac{QT}{\sqrt{RR}} \tag{3.1}$$

Where RR= R peak-to-peak interval in seconds.

Since the measurement of the QT interval variability should be independent of the heart rate variability, this formula reduces the influence due to heart rate changes on QT interval. The RT_{max} interval is defined as the interval from R peak to T_{max} or T peak. The interval from the beginning of the Q wave to the peak of the T wave is called the QT_{max} interval. The peak of the R wave to the end of the T wave is measured as the RT interval. The RR interval is measured from R peak-to-peak which is also called inter beat interval (IBI).

All these intervals were in the array form which is then converted into text file format. The text format of the array was read into the MATLAB for plotting. The intervals RT, RT_{max}, QT_{max}, QT, and QTc in milliseconds were plotted against the length of the ECG signal. Since the length of the ECG signal was considered for five minutes, the intervals were plotted for 350 to 400 seconds. When comparing signals, all the signals must be of the same length in order to make the comparison convenient. The vertical scales of all the intervals were fixed so that the analysis becomes easy.

3.4 Obtaining IIBI and Power Spectrum

The Inter beat interval (IBI) represents difference between two consecutive R wave peaks in the ECG signal. The purpose of calculating the power spectrum was to study the amount of influence of the sympathetic and parasympathetic branches of the Autonomic Nervous System (ANS) on the QT interval and compare it with different variabilities like RT variability (RTV), RT_{max} variability ($RT_{max}V$), QT_{max} variability ($QT_{max}V$), QTc variability (QTcV) and heart rate variability (HRV).

In order to obtain IBI samples suitable for frequency analysis and comparison, interpolation was required. In this research, backward interpolation was used to obtain

interpolated inter beat interval (IIBI), as it is the most simplest and accurate method. The IIBI of various intervals was then found by using the IIBI creator in LabVIEW. The IIBI creator gives the IIBI array for a 5 minute signal. The corresponding beat-to-beat intervals of QT, QTc, QT_{max}, RT_{max}, RT and RR were stored in an array format. These arrays were then read into the MATLAB for power spectral analysis.

3.4.1 IIBI Creator

In order to perform the variability analysis it was important to have equally spaced samples in the signal. The IBI samples were not equally spaced and a transformation was performed by interpolating points according to a desired sampling rate. Figure 3.10 shows the steps involved in constructing an IBI and IIBI signal. In, figure 3.10 (d), the pulse wave of figure 3.10 (c) is interpolated to produce a wave with equally spaced samples. This type of interpolation is called Backward Step Interpolation, where the height of the wave in a time interval is kept constant at the value of the length of the previous time interval. Figure 3.10 (d) is called an interpolated interbeat interval (IIBI).

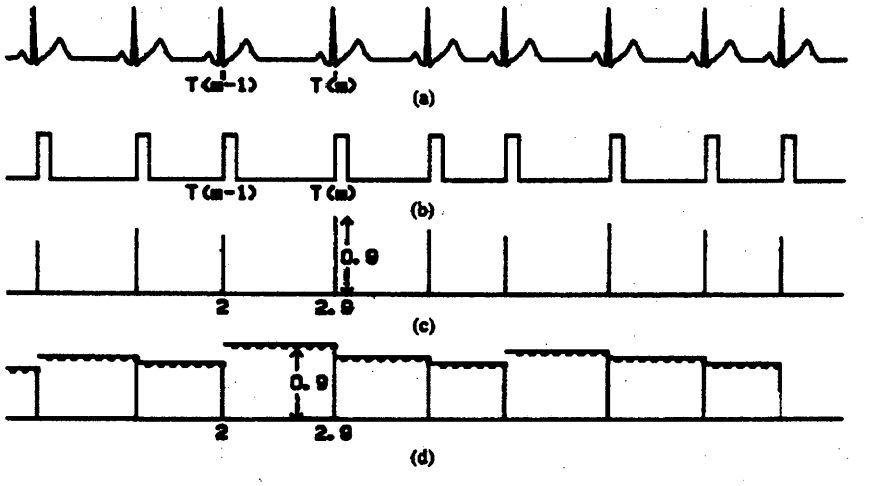

(**Reference.** Dr. Reisman S. lecture notes, ECE 667, 1999)

Figure 3.10 Steps to create an interpolated interbeat signal (IIBI)

Generally, the sampling rate chosen was the same as the one for sampling the ECG signal, but for too long and complex datasets, it was time consuming to interpolate data at such a high sampling rate. It would be adequate to choose a sampling frequency as low as 5 to 10 Hz, as the highest frequency of interest would not be more than 0.7 Hz.

3.4.2 Power Spectral Analysis

The spectral analysis of the ECG signal was based on the Fourier transform. The Fourier transform was a method to determine the frequency content of a time domain signal. The Fourier transform converts the time domain signal *x (t)* into the frequency domain signal *X (f)*. It is defined by the following equation:

$$X(f) = \int_{-\infty}^{+\infty} x(t).e^{-j\omega t}dt \qquad (3.2)$$

Where $\omega = 2\pi f$, t is time, f is frequency, *x(t)* is the time domain signal and *X(f)* is the frequency domain signal, representing a spectral density function with magnitudes and phases of the frequency content of *x(t)*. The Fourier transform can be applied to non periodic signals and therefore, can be viewed as a Fourier series of a periodic function whose period goes to infinity. Since the Fourier series relates the magnitudes and phases of a periodic signal at a specified frequency, called the spectrum, the Fourier transform becomes a spectral density which represents the contribution of any given frequency to the signal. The power spectrum density S_{xx} (f) is defined as:

$$S_{xx}(f) = X^*(f)X(f) = |X(f)|^2 \qquad (3.3)$$

where $X^*(f)$ is the complex conjugate of the Fourier transform $X(f)$. The Fourier transform analysis of the ECG assumes that the input signal is a stationary signal. In general, physiological signals are non stationary. However, for the purpose of paced breathing, the ECG signals were assumed stationary. This assumption was based on the fact that there are a limited number of influences affecting the autonomic nervous system during rest.

Before calculating the power spectrum of the IIBI signals, a zero averaged IBI was generated. The average of the IBI was subtracted from each value of the IBI array to get the zero averaged IBI. The purpose of doing this was to eliminate the DC component which would otherwise result in a high frequency component close to zero in the power spectrum. The IIBI's of all the intervals were calculated using the zero averaged IBI. The power spectrum of various intervals including IIBI (RR interval), IQTcI (QT corrected), IQTI (QT interval), IRTI (RT interval), $IQT_{max}I$ (QT_{max} interval) and $IRT_{max}I$ (RT_{max} interval) were found out and the variabilities of all these intervals were compared and analyzed with respect to each other. Once the power spectrum was calculated, the next step was to quantify the amount of energy contained in different frequency bands of the power spectrum.

Spectral analysis of heart rate variability (HRV) usually reveals three peaks in the following bands: very low frequency (VLF; 0-0.04 Hz), low frequency (LF; 0.04-0.15 Hz), and high frequency (HF; 0.15-0.4 Hz). The VLF is related to thermoregulatory mechanisms. The LF region is mainly influenced by the activity of both the parasympathetic and sympathetic parts of the autonomic nervous system and is related to baroreceptor mechanisms (blood pressure control system). The HF region is an indicator

of parasympathetic activity and is mainly related to respiratory sinus arrhythmia (RSA) and a predominant peak usually occurs in the power spectrum at the respiration frequency. The power in the LF and HF regions were calculated for each of the above mentioned intervals and the plots of all the interval variabilities were analyzed quantitatively and qualitatively. Before the analysis, the spectrum was windowed using a Hanning Window. The purpose of doing a windowing function on the power spectrum was to remove all the high frequency components at the beginning and end of the spectra. The advantage of using a Hanning window was the reduction in the size of the side lobe height at the expense of an increase in the main lobe width. Reduction of the side lobes height was more important than the main lobe width. The Hanning window is the most commonly used window.

CHAPTER 4

RESULTS AND DISCUSSIONS

The accuracy of the QT detection algorithm was verified by testing it on ten ECG data sets obtained from the NJIT, Signal Processing Laboratory. These data sets involved five minute segment of patients who were paced breathing at 6 breaths per minute and 12 breaths per minute respectively. The different parameters for which the algorithm was tested included QT interval, QT corrected, QT_{max}, RT_{max}, R-to-R, and RT interval. The intervals were plotted with respect to time of the ECG signal for each patient. The data sets with 12 breaths per minute were used to study variability analysis in which, QT variability was compared with heart rate variability and QT corrected variability.

Table 2 shows five different intervals measured for three data sets, each sampled at 500 samples/sec. The data set paced and cbirecg1 were 3 minute and 5 minute segments of paced breathing at 12 breaths per minute. These intervals are the result of the first method used in this algorithm, which is, a combination of LSI and Threshold (TH) method. This method had a potential problem of early detection of the T_{end}, and to compensate for this problem, the differential threshold method was used to detect the T_{end}

Table 2 Five different intervals measured for three subjects using LSI method

Subjects	**QT_{max} msec**	**RT_{max} msec**	**RR msec**	**QT msec**	**RT msec**
Paced	181	148	530	217	184
Non-paced	321	266	809	348	298
Cbirecg1	321	257	519	356	300

The result of detection of all four points on two data sets using LSI method is shown in the figure 4.1 and 4.2 respectively.

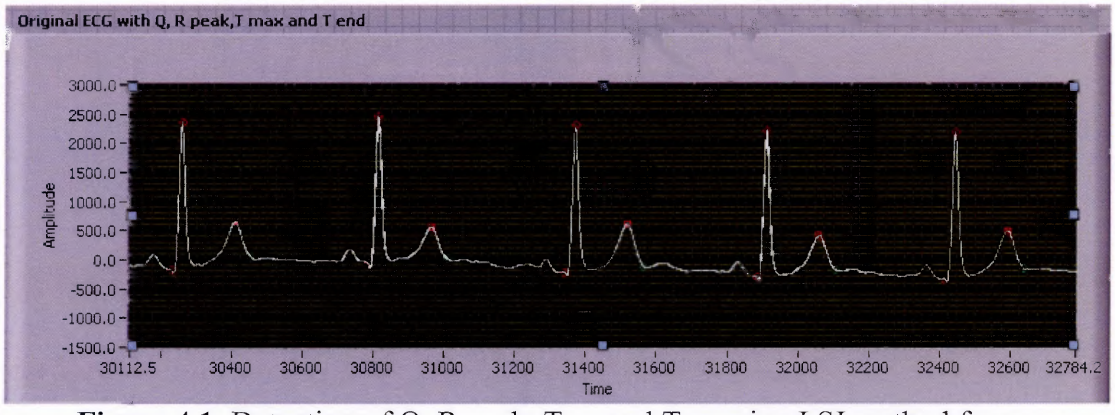

Figure 4.1 Detection of Q, R peak, T_{max} and T_{end} using LSI method for non-paced data set

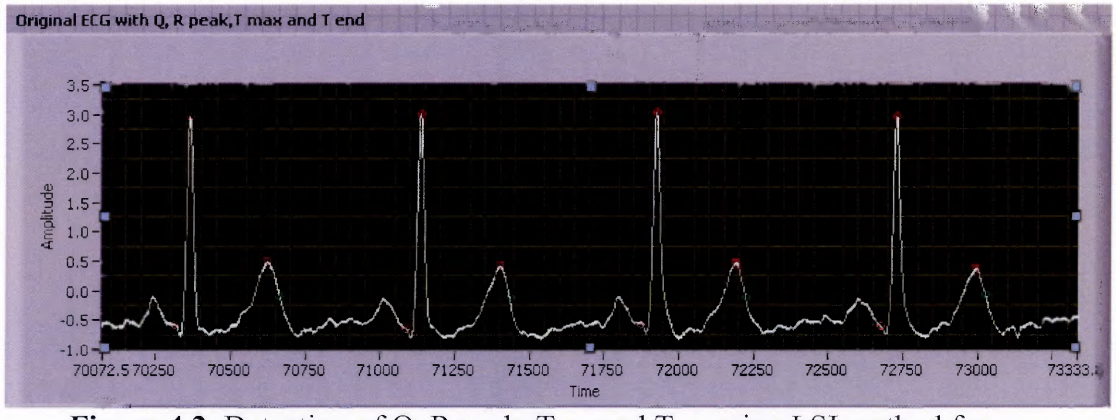

Figure 4.2 Detection of Q, R peak, T_{max} and T_{end} using LSI method for cbirecg1 data set

The intervals detected with the differential threshold method (DTH) for data sets at 6 breaths per minute and 12 breaths per minute is shown in table 3 and table 4 respectively. For each subject, six different intervals were measured. The average (mean) and standard deviation for each of these intervals were calculated for each data set. Figure 4.3 shows the screen shot of all the four points detected at correct positions for the data set stress20040825a respectively.

Table 3 Average interval measurements for subjects with 6 breaths per minute paced breathing (intervals in ms)

Subject	RR	QT	QTc	QTmax	RTmax	RT
20040413b	721±31	417±15	491±24	299±7	236±6	356±15
20040414a	827±112	496±78	504±34	331±48	270±48	435±78
20040414b	1098±95	528±23	551±118	402±19	341±18	467±22
20040415b	778±25	433±23	491±27	324±13	263±13	372±23
20040415c	827±34	461±6	508±12	353±15	292±14	400±6

Note: All the intervals are mean intervals and in milliseconds.

Table 4 Average interval measurements for subjects with 12 breaths per minute paced breathing (intervals in ms)

Subject	RR	QT	QTc	QTmax	RTmax	RT
20040406a	978±90	515±57	524±84	366±50	305±49	454±57
20040407c	791±49	433±11	489±54	325±11	264±11	372±11
stress20040311c	971±58	461±14	469±22	347±6	286±6	401±14
stress20040825a	806±35	446±15	498±19	344±11	285±10	388±15
stress20040830b	890±76	461±10	463±19	304±13	247±13	359±11

Note: All the intervals are mean intervals and in milliseconds.

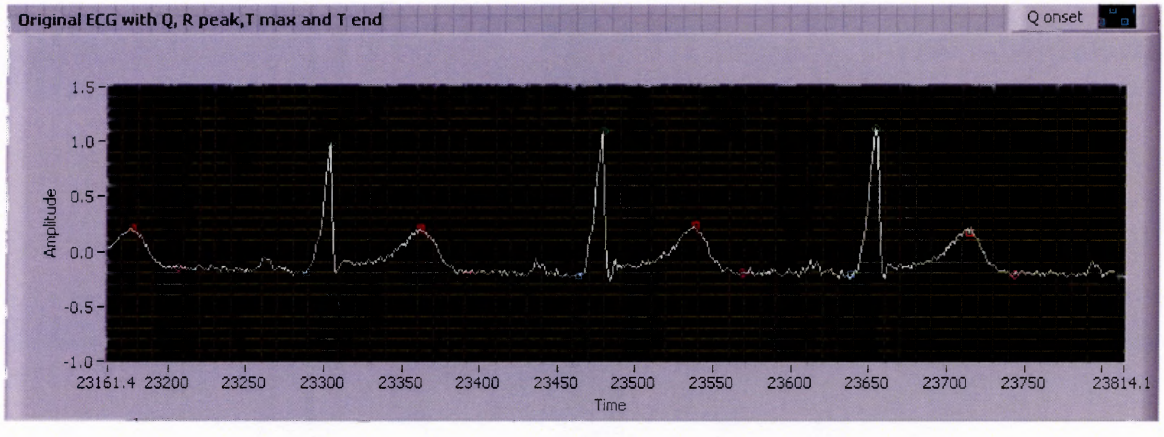

Figure 4.3 Detection of Q, R peak, T_{max} and T_{end} in stress20040825a data set.

In the data set stress20040825a, the total number of R beats in ECG was 372. The accuracy of detection of different points including Q, T_{max} and T_{end} was verified, both using the program generated in LabVIEW as well by visual inspection. The R peak detection was 100% accurate based on the calculations performed using both the methods. The RR interval for the entire ECG was stored in an array. The average or mean value of the RR interval was compared with each R-to-R interval in this array. If there was any large deviation from this average value, the program considers the detected point as the wrong one and stores it in an array. The percentage success was then calculated based on the total number of points in ECG and the number of wrong detections. All the detected points on ECG were then visually examined to check if they were at the right positions. The wrong detection was based on the positions of the points in original ECG. If the T_{end} occurred farther than 20 msec than its usual position, then the point was detected as wrong T_{end} detection. A similar procedure was adopted to find the accuracy of Q wave and T_{max} as well.

The number of accurately detected Q, T_{max} and T_{end} points and the percentage success of these points, using both methods is shown in table 5 and table 6 respectively. Figure 4.4 shows the wrong detection of Q, T_{max} and T_{end} in Stress20040825a data set. On an average, the algorithm produced 99.16% success results according to program and 96.4% success based on visual inspection.

Table 5 Percentage success of detection using LabVIEW program in different patients

PATIENT	Q POINTS			T_{max} POINTS			T_{end} POINTS		
	Total points	Points detected	% success	Total points	Points detected	% success	Total points	Points detected	% success
20040406a	307	305	99.3	307	292	95	307	292	95
20040407c	379	378	99.7	379	378	99.7	379	377	99.4
Stress20040311c	309	308	99.6	309	309	100	309	305	98.7
Stress20040825a	372	371	99.7	372	372	100	372	371	99.7
Stress20040830b	375	375	100	375	374	99.7	375	375	100
Total	1742	1737	99.7	1742	1726	99.08	1742	1720	98.7

Table 6 Percentage success of detection by visual inspection in different patients

PATIENT	Q POINTS			T_{max} POINTS			T_{end} POINTS		
	Total points	Points detected	% success	Total points	Points detected	% success	Total points	Points detected	% success
20040406a	307	298	97.0	307	288	93.8	307	261	85.0
20040407c	379	370	97.6	379	373	98.4	379	369	97.3
Stress20040311c	309	301	97.4	309	305	98.7	309	302	98.3
Stress20040825a	372	364	97.8	372	353	94.8	372	357	95.9
Stress20040830b	375	370	98.6	375	361	96.5	375	370	98.6
20040413b	333	332	99.6	333	331	99.3	333	330	99
20040414a	290	283	97.5	290	278	95.8	290	260	89.6
20040414b	205	204	99.5	205	203	99	205	200	97.5
20040415b	308	298	96.7	308	308	100	308	300	97.4
20040415c	290	289	99.6	290	289	99.6	290	289	99.6
Total	3168	3109	98.1	3168	3089	97.5	3168	3038	95.8

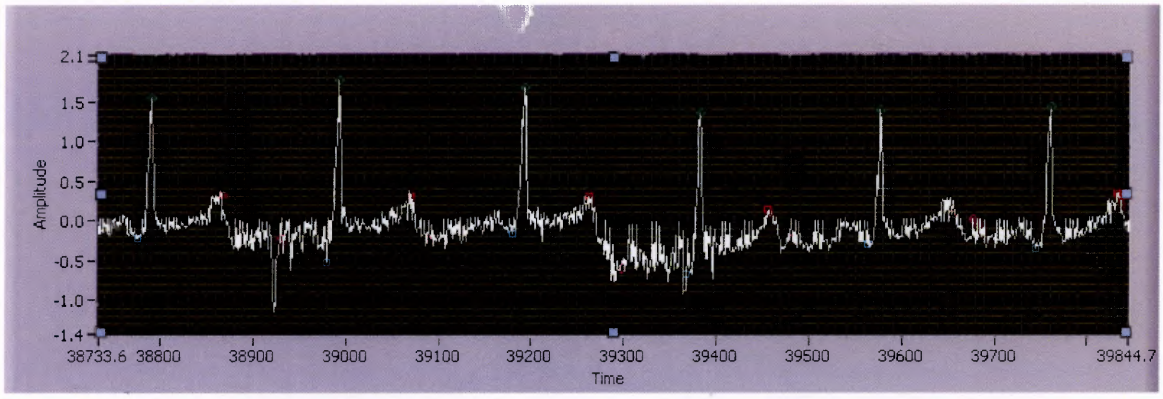

Figure 4.4 (a) Wrong detection of Q wave in stress20040825a data set.

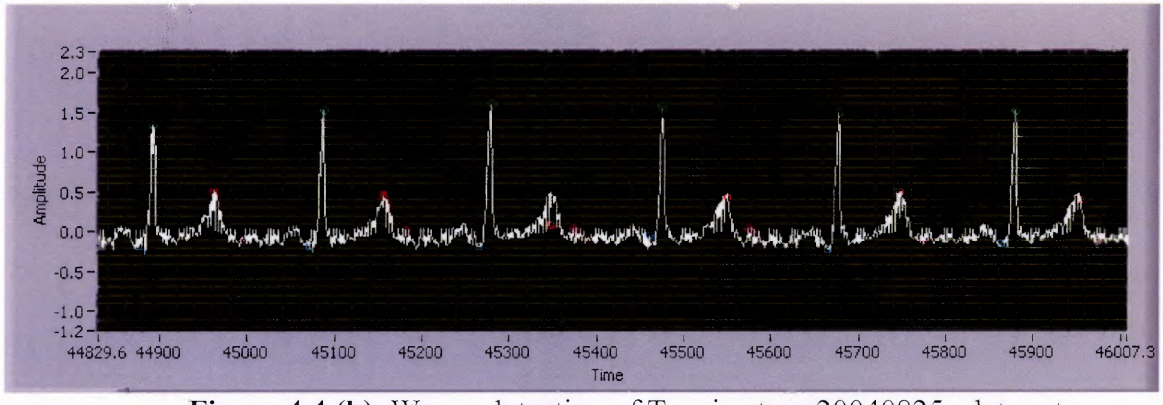

Figure 4.4 (b) Wrong detection of T_{max} in stress20040825a data set.

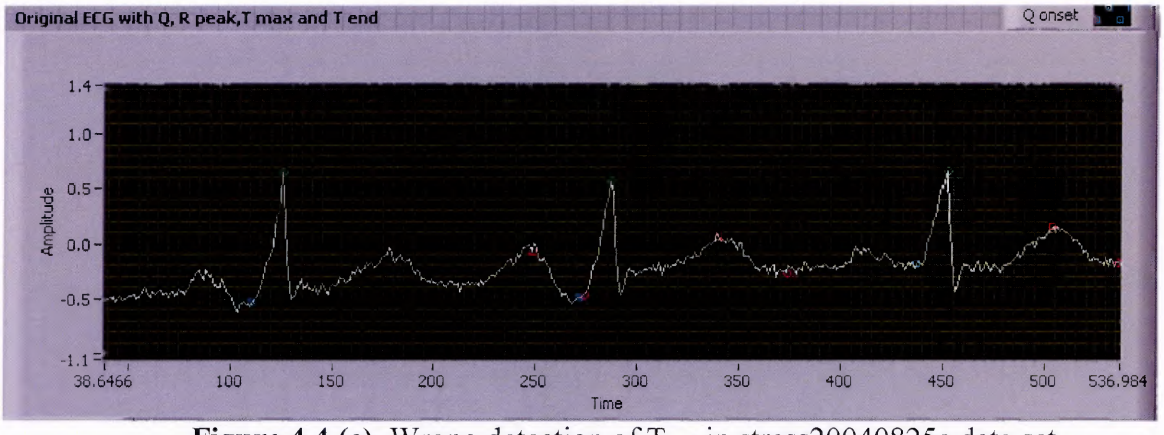

Figure 4.4 (c) Wrong detection of T_{end} in stress20040825a data set.

Figure 4.4 Wrong detection of points Q, T_{max} and T_{end} in stress20040825a data set

4.1 Interval and Variability Plot Analysis

The inter beat interval (IBI) of various intervals RR, QT corrected (QTc), QT, RT, QT_{max} and RT_{max} were calculated and are named IBI, QTcI, QTI, RTI, $QT_{max}I$ and, $RT_{max}I$ respectively. The inter beat interval of all the intervals were plotted against the length of the ECG signal for each patient. There were six IBI plots for six different intervals for five different data sets. The interval plots for one of the data sets stress200400825a is shown in figure 4.5.

For all the IBI interval plots, the time axis and the interval axis are fixed so as to make the analysis easy. By comparing all the intervals, the QT corrected interval appears to have the largest interval as shown in figure 4.5 (b). The variation in the interval of IBI, QTmaxI, and $RT_{max}I$ interval is small as seen in figure 4.5 (a), 4.5 (e), and 4.5 (f) respectively. In 4.5 (c) and 4.5 (d), there is a peak at 200 msec indicating a wrong detection of point. One interesting thing to note about these interval plots is the similarity between them. The QTI and RTI plots look similar, however with an increase in QT interval. Similarly, $QT_{max}I$ and $RT_{max}I$ also look similar with QT_{max} interval being greater than RT_{max} interval.

The IBI was used to calculate the interpolated beat-to-beat interval of all the intervals. The interpolated beat-to-beat interval of RR, QTc, QT, RT, QT_{max} and RT_{max} were named IIBI, IQTcI, IQTI, IRTI, $IQT_{max}I$ and $IRT_{max}I$ respectively. The interpolated beat-to-beat intervals of all the intervals were run through the FFT program to calculate the power spectrum. The variability plots of various intervals are shown in figure 4.6 for stress20040825a data set.

The heart rate variability (HRV) shown in figure 4.6 (a) shows a spike at frequency 0.2 Hz implying, that the paced breathing was done at 12 breaths per minute which was true for this patient and the HF region has few reduced amplitude peaks. The HF region is thought to be primarily due to parasympathetic activity.

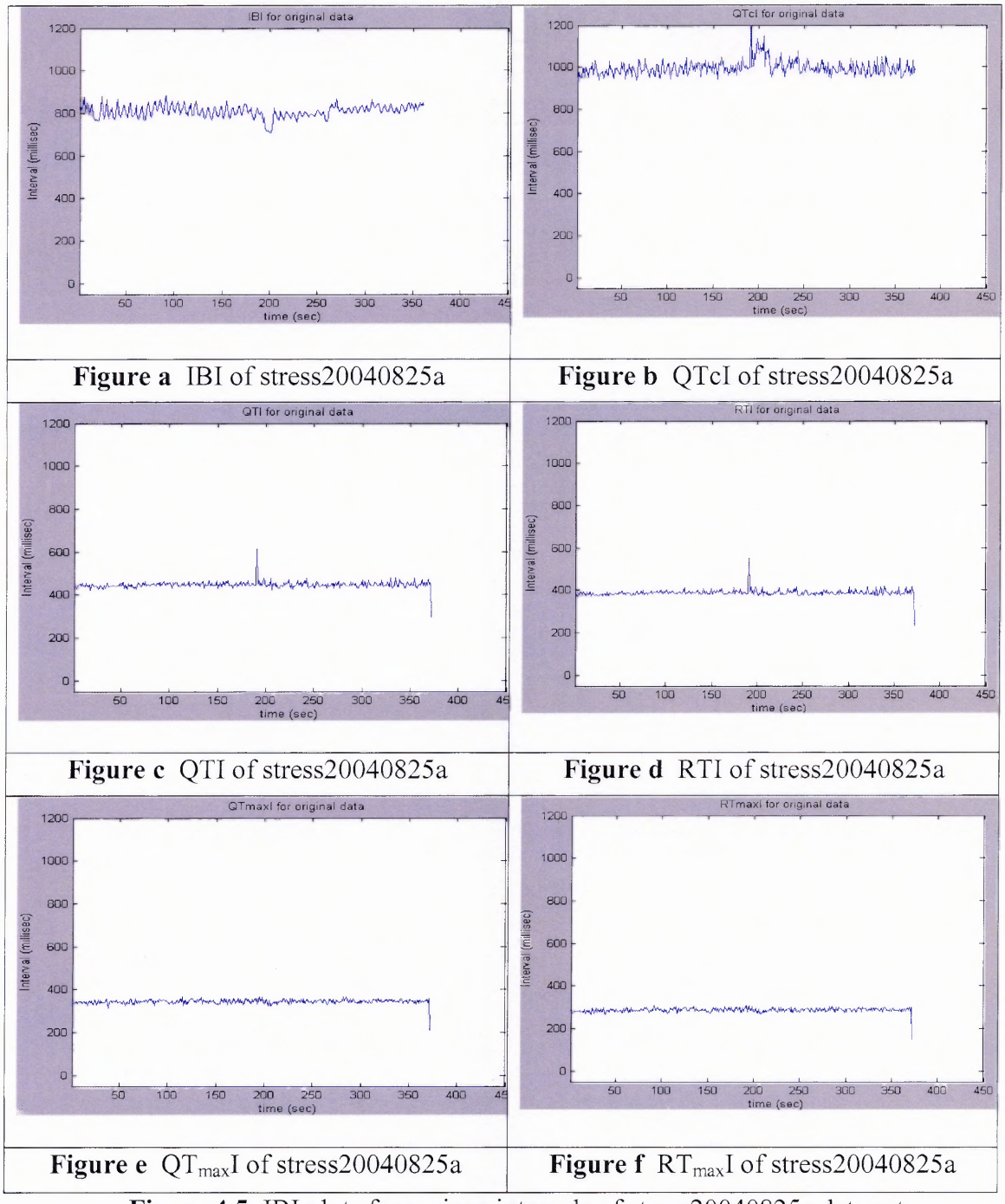

Figure a IBI of stress20040825a

Figure b QTcI of stress20040825a

Figure c QTI of stress20040825a

Figure d RTI of stress20040825a

Figure e $QT_{max}I$ of stress20040825a

Figure f $RT_{max}I$ of stress20040825a

Figure 4.5 IBI plots for various intervals of stress20040825a data set

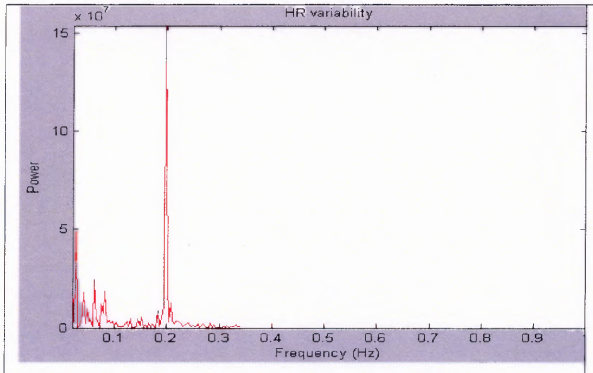

Figure a HRV of stress20040825a

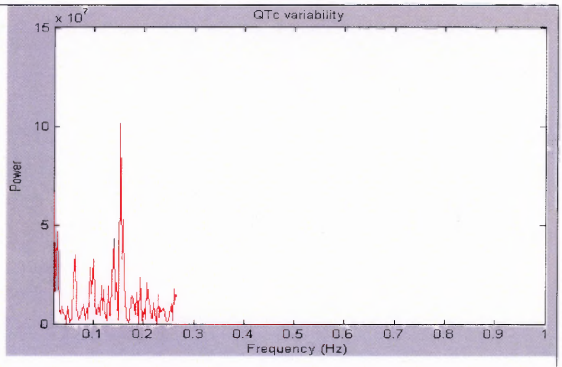

Figure b QTcV of stress20040825a

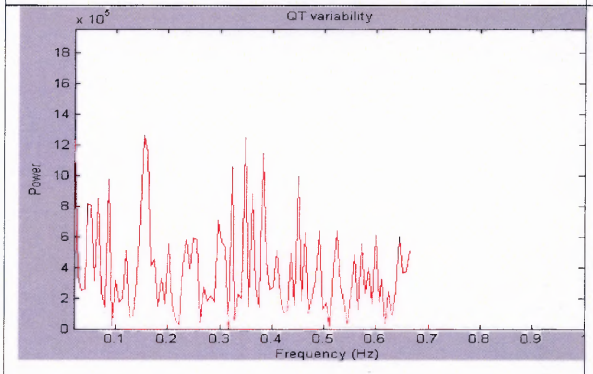

Figure c QTV of stress20040825a

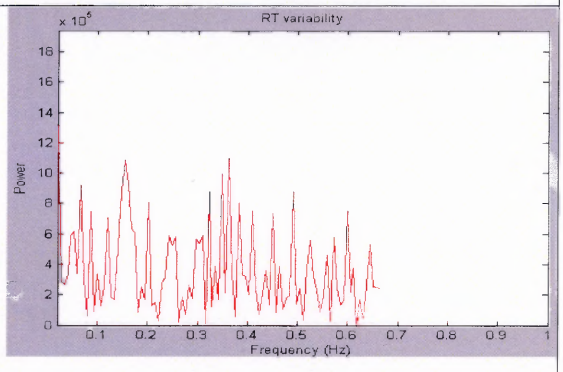

Figure d RTV of stress20040825a

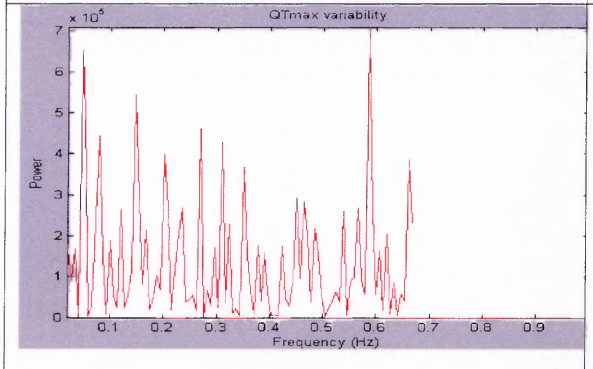

Figure e $QT_{max}V$ of stress20040825a

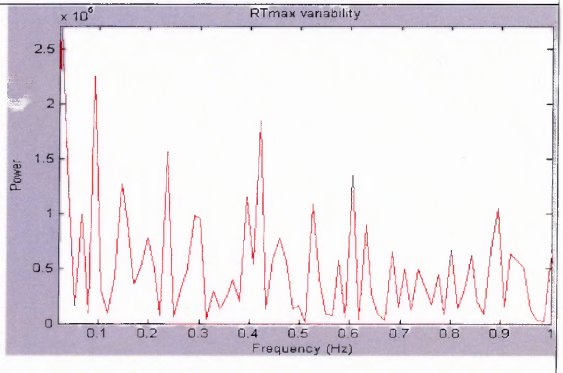

Figure f $RT_{max}V$ of stress20040825a

Figure 4.6 Variability plots of different intervals for stress20040825a data set.

Recent studies have shown that QT corrected variability shows similarity with the HR variability [32]. The increased QT variability is associated with increased sympathetic activity and a predictor of sudden cardiac death [34]. In figure 4.6 (b), the QTc variability has high peaks in the LF region when compared to HRV. Since QT interval is corrected for preceding R-to-R interval changes using Bazett's formula, the variability for corrected QT interval might be related to heart rate variability. However, the peak for the QTc is at a lower frequency (approximately 0.15 Hz), which is different from the peak of HRV, although this is still in the HF region.

The QT variability shown in figure 4.6 (c) was a result of the QTI in figure 4.5 (c). The QT variability has increased peaks both in LF and HF region; although it appears that one of the peaks occur at the same frequency (approx. 0.15 Hz) as QTc. RT variability (figure 4.6d) appears to be similar to the QT variability.

The QT_{max} variability has peaks in both LF and HF region, with a dominant peak, for this patient, at 0.6Hz. $RT_{max}V$ is different than $QT_{max}V$.

In this study, the use of controlled paced breathing at 12 breaths per minute (0.2 Hz), might have yielded RR and QT corrected spectral peaks at almost an identical frequency. In QT variability, the frequency peak at approximately 0.2 Hz was merged with other frequency components in HF and LF region. The peak was not predominant at 0.2 Hz when compared to HR variability. The same observation can be made in RT variability which looks similar to QT variability. The 0.2 Hz peak in RT variability was not clearly visible but had reduced amplitude peaks in LF and HF regions when compared to QT variability.

These observations made were similar in all the patients except for two patients in which QTc variability looked different. These differences can be seen in figure 4.7.

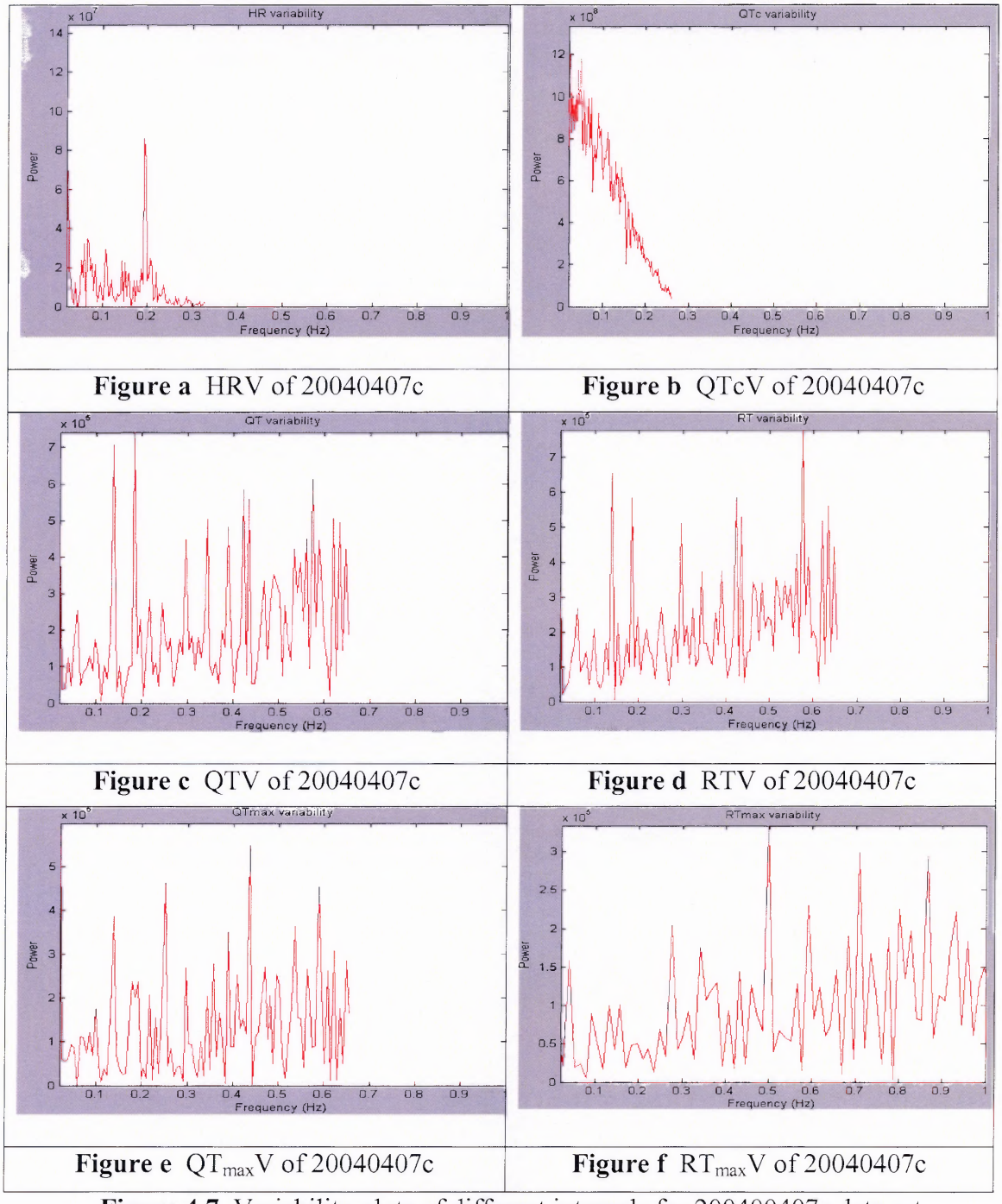

Figure a HRV of 20040407c

Figure b QTcV of 20040407c

Figure c QTV of 20040407c

Figure d RTV of 20040407c

Figure e $QT_{max}V$ of 20040407c

Figure f $RT_{max}V$ of 20040407c

Figure 4.7 Variability plots of different intervals for 200400407c data set.

In figure 4.7 (b), in QTc variability, the frequency peak at 0.2 Hz is missing, instead the frequency components are reduced in HF region. There are few high frequency components in LF region. The frequency components start reducing from the LF to the HF region. This observation can be seen in table 6. The amount of power in the HF region is less when compared to the amount of power in the LF region. However, there was not much difference in QT and RT variability because the peaks looked similar in both these variabilities. The same observation can be seen in $QT_{max}V$ and $RT_{max}V$.

4.2 LF and HF Measurement

Once the power spectrum was calculated, the total power in both the bands needs to be quantified in various intervals to measure LF and HF power. The power spectrum was calculated using Fast Fourier Transform (FFT). The code for performing FFT was written in MATLAB. The LF and HF power values were found out using power spectrum main vi in LabVIEW 7.0 Express. The values of LF and HF for heart rate, QT, QT corrected and RT variabilities for five different subjects are given in Table 6.

By analyzing the spectral power values, a quantitative analysis can be performed to look at similarities between HRV, QTV, QTcV, and RTV. Since the subjects underwent paced breathing at 12 breaths per minute, the breathing frequency peak occurred at 0.2 Hz in the HF region. Thus, the amount of power in HR-HF region was higher than the amount of power in HR-LF region except for the first (20040406a) and last (stress20040830b) patient. [27]. In this study, the results obtained for HR-HF and HR-LF power was in agreement with the other research.

The HF power in HRV can be compared to the HF power in QT and QT corrected variability. The HR-HF power is comparatively closer to QT-HF power than QT corrected HF power. Similarly, the LF power values are similar between HRV and QTV. The spectral power values used here are in normalized units. The numbers can be quantitatively compared by plotting the difference between the power values in nLF and nHF region for all the four variabilities in five different patients. Figure 4.8 shows the comparison of LF power between HRV, QT, RT and QTc variabilities in five different subjects

Table 7 Measurement of total power in LF and HF regions for four variabilities in five different subjects

Subject	**HRV**			**QTV**			**QTcV**			**RTV**		
	nLF	nHF	nLF/nHF	nLF	nHF	nLF/nHF	nLF	nHF	nLF/nHF	nLF	nHF	nLF/nHF
20040406a	0.515	0.484	1.063	0.609	0.390	1.560	0.657	0.342	1.918	0.660	0.339	1.940
20040407c	0.445	0.554	0.803	0.216	0.783	0.276	0.740	0.259	2.850	0.259	0.740	0.350
stress20040311c	0.424	0.595	0.736	0.413	0.586	0.705	0.335	0.664	0.505	0.422	0.577	0.731
stress20040825a	0.302	0.691	0.433	0.338	0.661	0.512	0.375	0.624	0.600	0.278	0.721	0.385
stress20040830b	0.535	0.464	1.153	0.325	0.674	0.481	0.393	0.606	0.649	0.338	0.661	0.512

The plots in figure 4.8 and figure 4.9 show the difference in the amount of power in LF and HF region in different variabilities for five patients. In this plot, the amount of power in the HR-LF region is comparatively closer to the amount of QT-LF power when compared to QTc-LF power in almost all patients. Quantitatively, the amount of power in QT-LF region is similar to power in RT-LF region. Figure 4.9 shows the amount of power in HF region for HRV, QT, RT and QTc variabilities. The same observation can be made in all the patients. However, the amount of the power is increased in HR-HF region when compared to the HR-LF region except for the first and last patient. Quantitatively the QTc-HF power is less than HR-HF power, and qualitatively the peaks in QTc-HF region have reduced amplitudes when compared to HR-HF region.

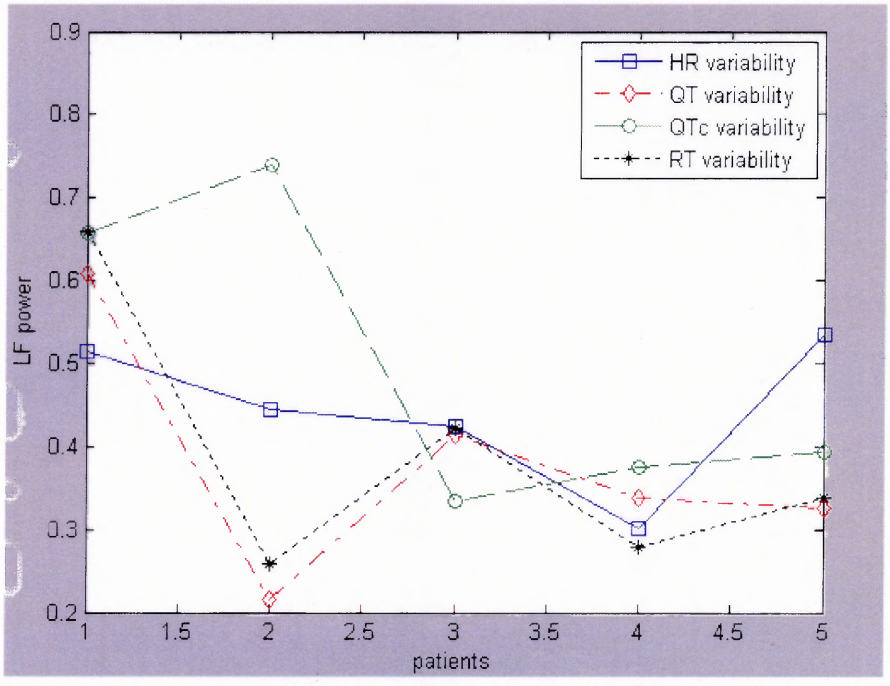

Figure 4.8 Comparison of LF powers in HR, QT, RT and QTc variabilities

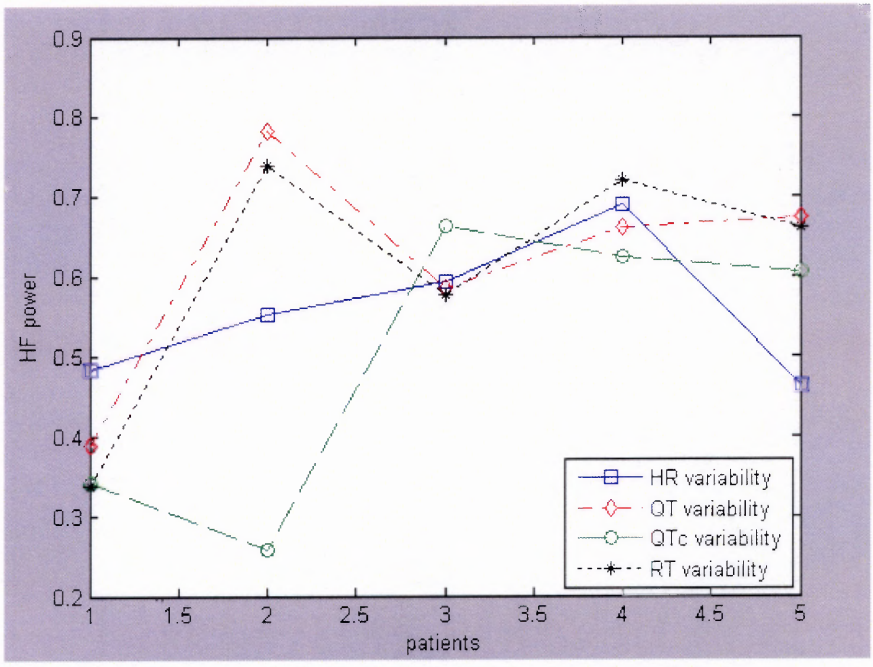

Figure 4.9 Comparison of HF powers in HR, QT, RT and QTc variabilities

CHAPTER 5

CONCLUSION

The algorithm created in this research for the detection of different points such as Q wave, T_{max} and T_{end} was validated on five minute data set segment of paced breathing at 12 breaths per minute for five different patients. It produced an overall success of 99.16% according to automatic verification of accuracy detection and 96.4% based on manual inspection.

To study the variability plots, the same five data sets mentioned above were used. From the variability plots, HR variability and QT corrected variability look similar. Since the QT interval was corrected for corresponding R-to-R changes, the variability of the HRV might be embedded in the QTc variability. However, peak changed to a lower frequency, which was still within the HF region.

A high QT variability indicates an increase in the ventricular repolarization variability. A prolonged action potential arises chiefly from an increased duration of cardiac repolarization [34]. The duration of the QT interval measured from beat to beat is the sum duration of repolarization in all the ventricular myocardial cells. An asynchrony in the duration of the repolarization could result in QT interval shortening and lengthening accompanied by larger QT variability. In this study, the duration of the QT interval was in the range of 450 to 500 milliseconds indicating normal duration of repolarization. The intervals and variabilities for other subjects could be found in Appendix E.

The variabilities of QT and RT look similar in all the patients. Qualitatively, the peaks in both the LF and HF region have similar shape. They can be analyzed quantitatively by measuring the amount of power in both LF and HF regions. Table 6 shows the comparison between the values of nLF and nHF for both QT and RT variabilities.

5.1 Future Work

In this study, ten paced breathing data sets were used with relatively noise-free ECG signals. On data sets other than these ten patients, which were used to validate the algorithm, there were several data sets for which the algorithm produced incorrect results. An example of such a data set stress20040719c is shown in figure 5.1, in which the patient has T wave amplitude that cannot be visually determined. Thus, the algorithm fails to detect the exact T_{max} and T_{end} positions. Additional work needs to be done with "non-ideal" ECG signals.

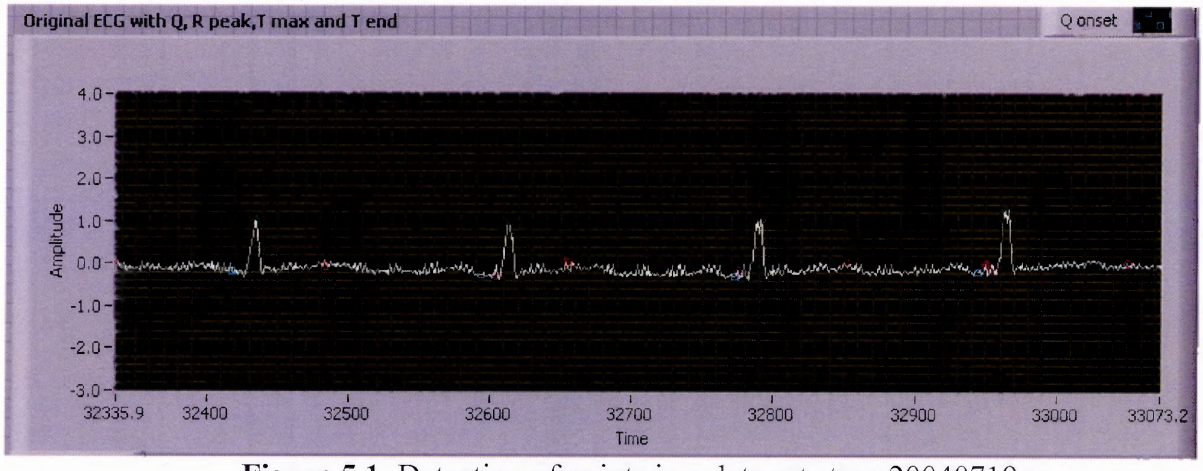

Figure 5.1 Detection of points in a data set stress20040719c

The QT detection algorithm is not robust enough to differentiate between the positive and negative T wave. Another example of data set stress20040720b is shown in figure 5.2, which shows a data set with a negative T wave. In this case, the algorithm fails to detect the negative T_{max} and T_{end}. Additional work needs to be done to look at varied T wave morphologies. In addition, while the algorithm appears to be accurate for clean ECG signals, there will be some missed or errors in positions. A manual system, similar to the R wave detection system, needs to be developed to account for these errors.

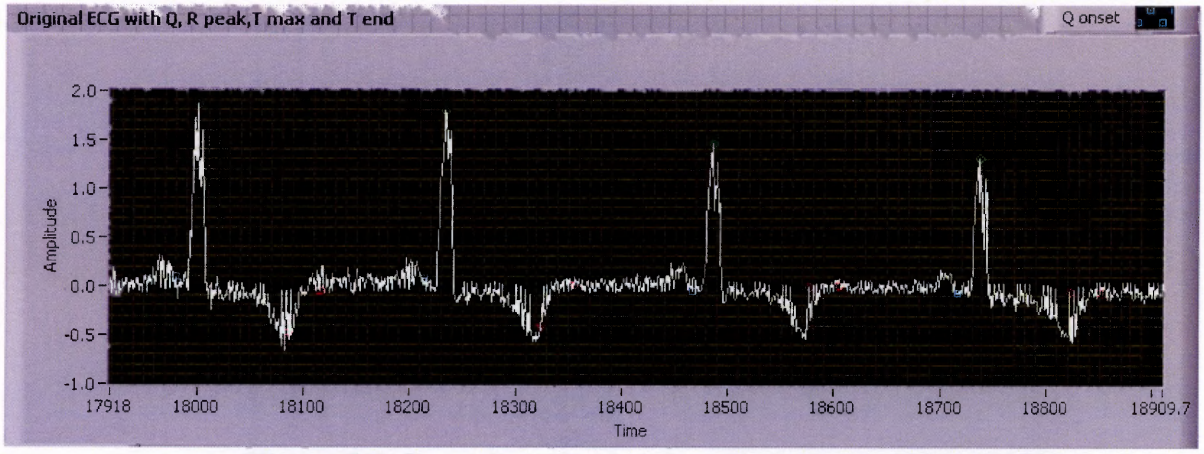

Figure 5.2 Detection of points in a data set stress20040720b.

By analyzing the variability plots in figure 4.6 (c) and figure (d) qualitatively, QT and RT variability looked similar. The peaks are visually similar in shape in both LF and HF region. Quantitatively, the amount of power in both LF and HF regions of QTV and RTV differ very little. Since, QTV and RTV do not differ much, the similarities and differences between them can be studied. If the amount of similarities is dominant over differences, RT variability can be used as a surrogate of QT variability. A more detailed study of the comparison of QT/RT variability and HRV should be performed.

The HRV, QT and other variabilities were studied using traditional frequency domain methods in this project. The Fast Fourier Transform is applied to the interpolated beat-to-beat interval of various intervals to study the spectral content of each signal. A future study can look at the behavior of HRV with respect to QT variability in the time domain and frequency domain, as well as using time-frequency analysis. These are the parameters which are not addressed in this thesis.

Using the intervals obtained from this research, one can employ them to calculate time frequency plots and see the effect of heart rate recovery after exercise on HRV, QT and QTc variabilities. The effect of the respiration and baroreceptor index on these

variabilities could be studied in time frequency analysis. The behavior and similarity of HRV with other interval variabilities can be analysed under different conditions.

One of the important parameters which could be studied in QT interval variability is the QT variability Index (QTVI). This index quantifies the relative magnitude of QT interval changes compared to heart rate variability. QTVI is the log ratio between QT interval variabilities and heart rate variabilities each normalized by the squared mean of the respective time series and is given by:

$$\mathrm{QTVI} = \log_{10}\left[\frac{QT_V/QT_m^2}{HR_V/HR_m^2}\right] \tag{5.1}$$

The QTVI index gives a non-invasive measure of beat to beat QT fluctuations and represents the relationship between QT and RR variability. Studies indicate that increased QT variability and decreased RR variability is a predictor of sudden death [33]. In other words, increased QT variance and decreased RR variance would increase QTVI. Increased QTVI can be correlated with clinical severity of heart failure. Therefore, a study of QTVI would give a better picture about the relationship between QT and RR variabilities.

APPENDIX A

LEAST SQUARES METHOD (LSI)

The Least Squares Method is a very popular technique, which is used to compute estimations of parameters and to fit data. This method is equivalent to finding a function, over a certain range, which is the "best fit" to the data points. What we mean by the "best fit" of a line to a set of points? Intuitively, a good fit is a line with little space between the line and the points it's supposed to fit. The best fitting line is the one that has the least space between itself and the data points, which represent actual measurements.

There are three ways to measure the space between a point and a line: vertically in the y direction, horizontally in the x direction, and perpendicular to the line. It is desirous to measure the space vertically, because the whole purpose in making a regression line is to use it to predict the y value for a given x value. It is nothing but measuring how far off the vertical distances of prediction points would be from the points actually measured. In general, the deviation (vertical gap) between any given point (x, y) and the line y=mx+b will be mx+b–y.

But each deviation could be positive or negative, depending on whether the line fall above or below that point. We can't simply add up deviations, because then a line would be considered good if it fell way below some points as long as it fell way above others. To prevent that, we square each deviation, and add up the squares. If we compute the deviations in the y direction, square each one, and add up the squares, we say that, the line of best fit is the line for which the sum of squares of deviations is the least. Since it's a sum of squares, the method is called the method of least squares.

The best-fit line, as stated earlier, is the line that minimizes the sum of squares of vertical deviations between itself and the measured points. We can write that sum as

$$E = \sum (y\hat{} - y)^2 \qquad \text{(A.1)}$$

Where ŷ is the predicted value on the line for a given x (namely mx+b), and the y is the actual value measured for that given x.

A line in slope-intercept form looks like $y=mx+b$, where b is the y intercept and m is the slope. The unknowns b and m needs to be found such that $y=mx+b$ is true for all the data points. There may not exist b and m that fit all these equations, but a best fit can be found. The equations can be written in the form $Xc = y$, in which the parameters X, c and y can be written as:

$$X = \begin{bmatrix} 1 & x_1 \\ 1 & x_2 \\ . & . \\ . & . \\ 1 & x_{n-1} \\ 1 & x_n \\ & \end{bmatrix} \quad c = \begin{bmatrix} m \\ b \end{bmatrix} \quad \text{and} \quad y = \begin{bmatrix} y1 \\ y2 \\ . \\ . \\ y_{n-1} \\ y_n \end{bmatrix} \qquad \text{(A.2)}$$

Where X is the array of data points of the x axes, c is the matrix of unknown parameters, that is, m slope and b intercept, and y is the matrix of data points on the y axes.

In general, this system can't be solved because the system is usually inconsistent because it is over determined. In other words, we have more equations than unknowns (the unknowns are the two variables, b and m). There is a system of equations called the

normal equations that can be used to find least squares solution to systems with more equations than unknowns.

Let X be an m by n matrix such that X^TX is invertible, then the solution to the normal equations, $X^TXc = X^Ty$, is the least squares approximation to c in $Xc = y$. Where, X and Y are array points of best-fit line on X-axis and Y-axis respectively. X^T is transpose of X array. It is important to remember that the solution to the normal equations is only an approximation to c for $Xc = y$. It is not equal to c because $Xc = y$ is inconsistent, so it has no solution. In other words, there does not exist a vector, c, that makes $Xc = y$ a true statement. Therefore, we use the normal equations to approximate c.

APPENDIX B

Q DETECTOR MODULES

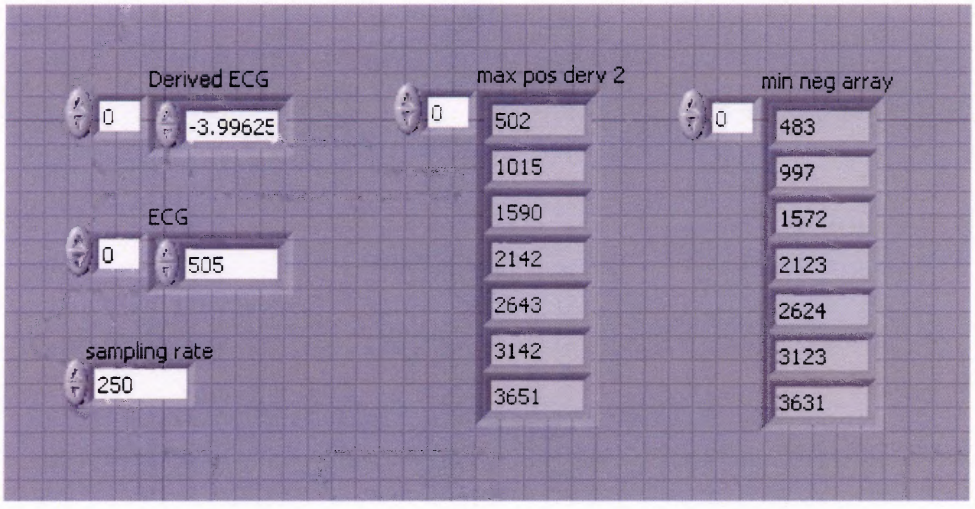

Figure B.1 Front panel of min and max points in derived ECG

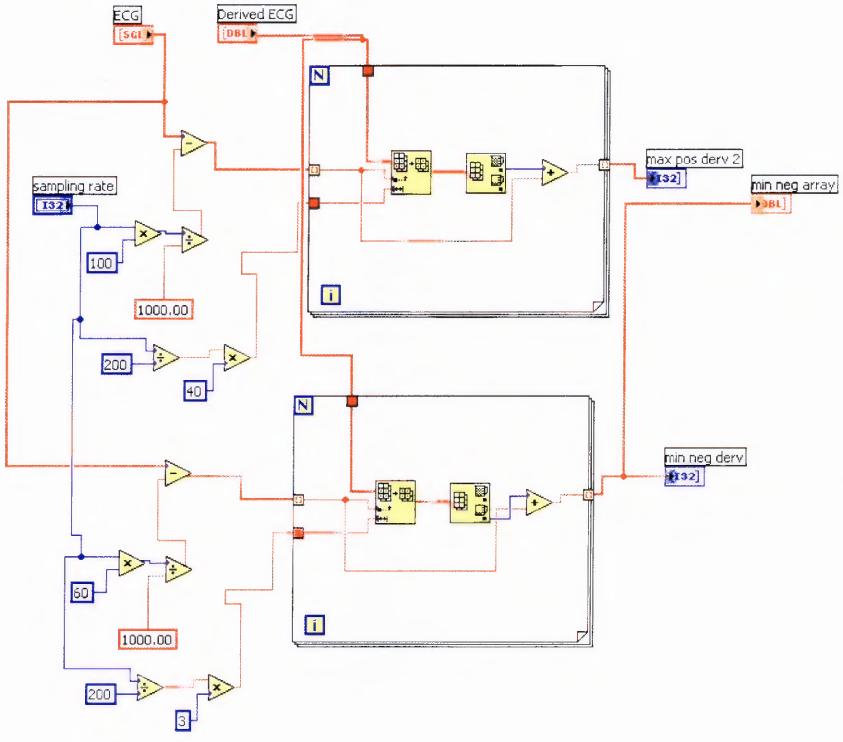

Figure B.2 Block diagram of min and max points in derived ECG

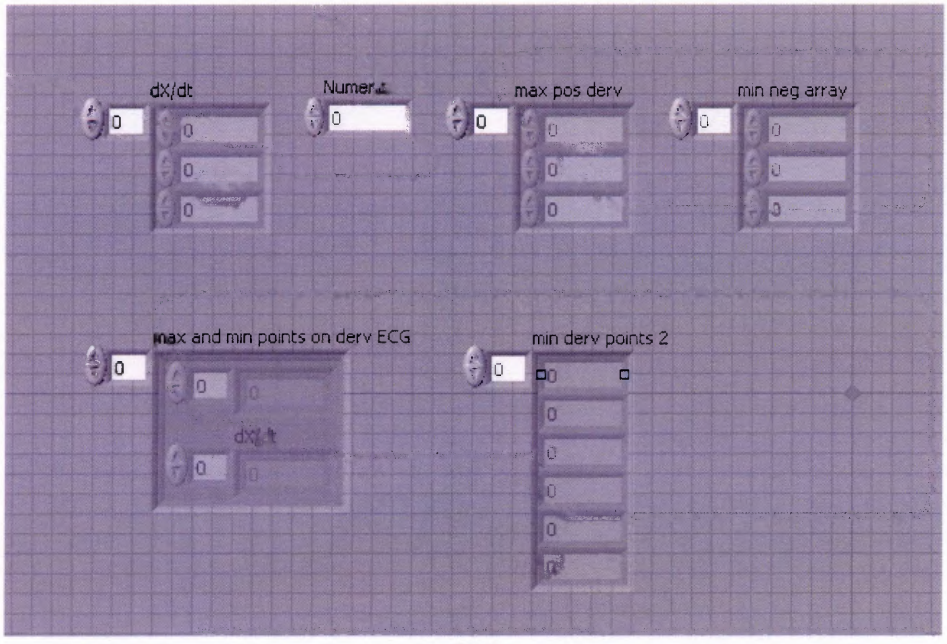

Figure B.3 Front panel of Q decision display

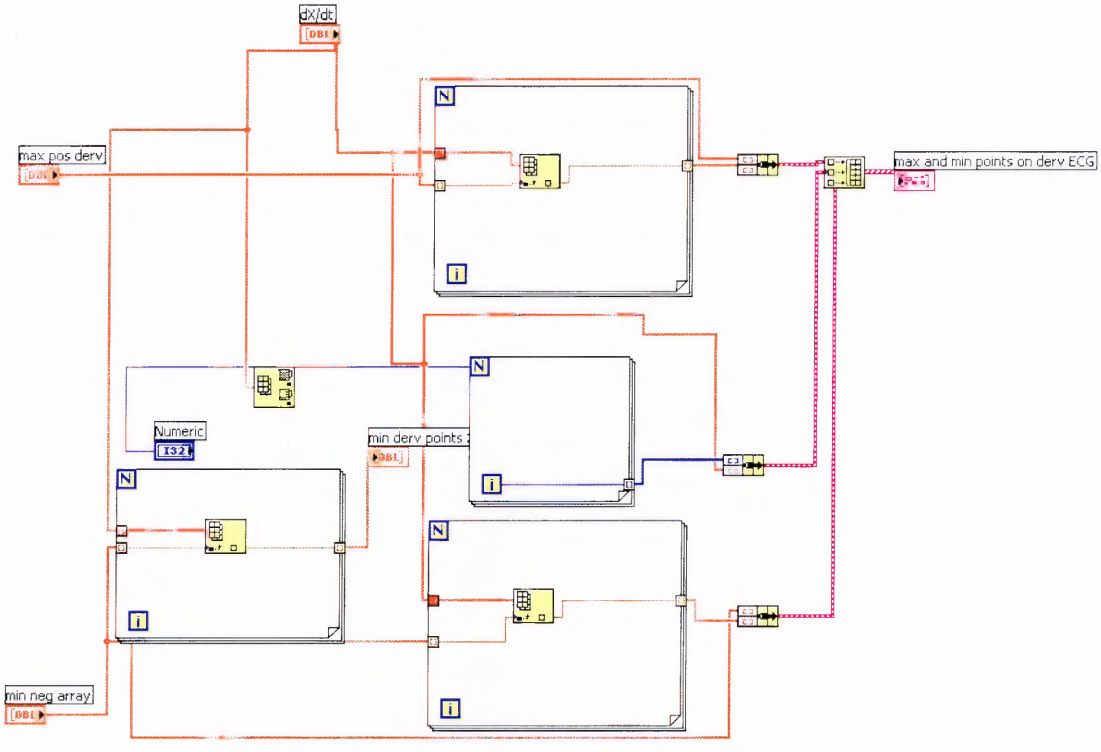

Figure B.4 Block diagram of Q decision display

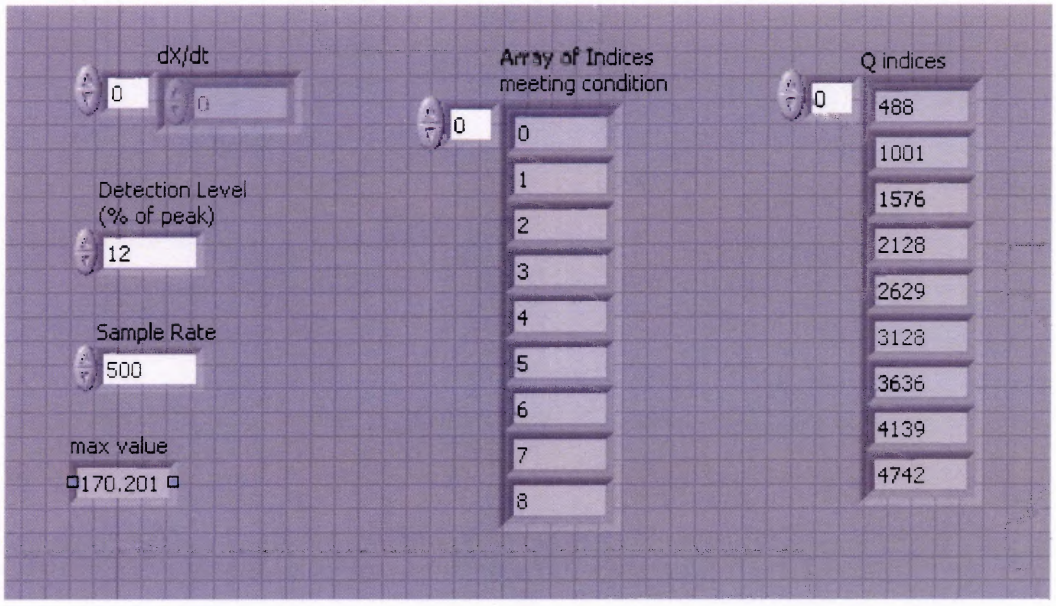

Figure B.5 Front panel of Q threshold detector

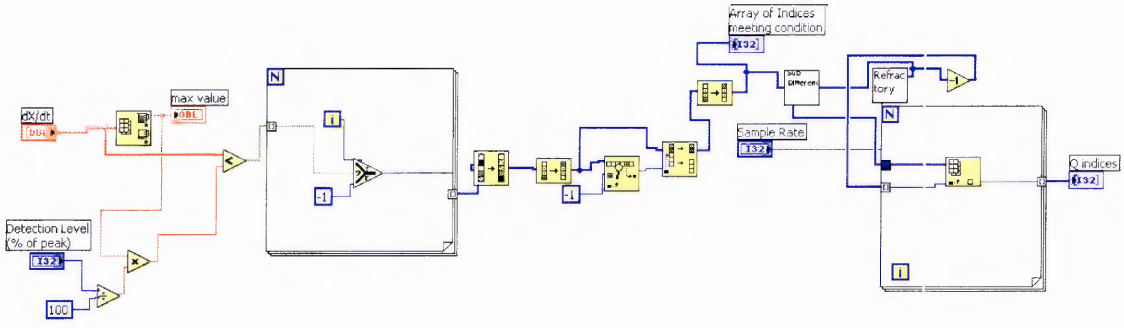

Figure B.6 Block diagram of Q threshold detector

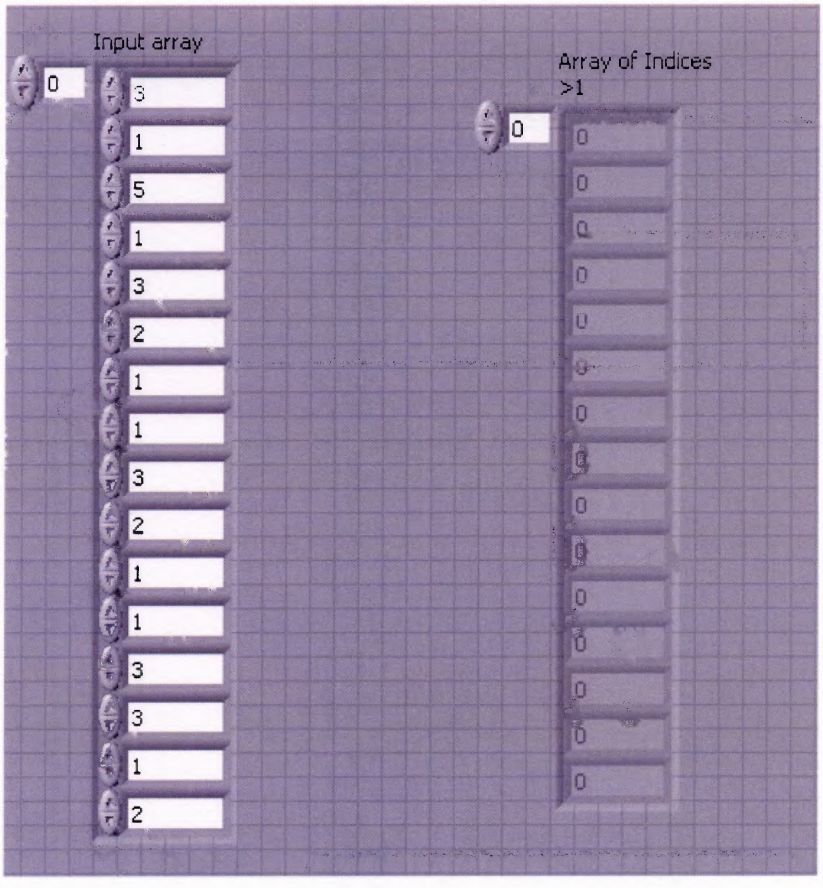

Figure B.7 Front panel of sub-indices greater than refractory

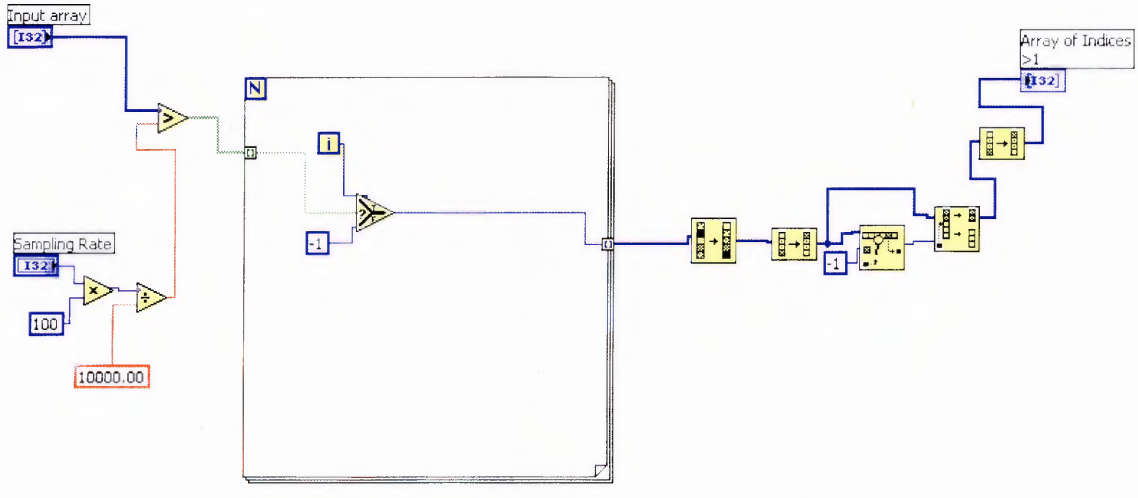

Figure B.8 Block diagram of sub-indices greater than refractory

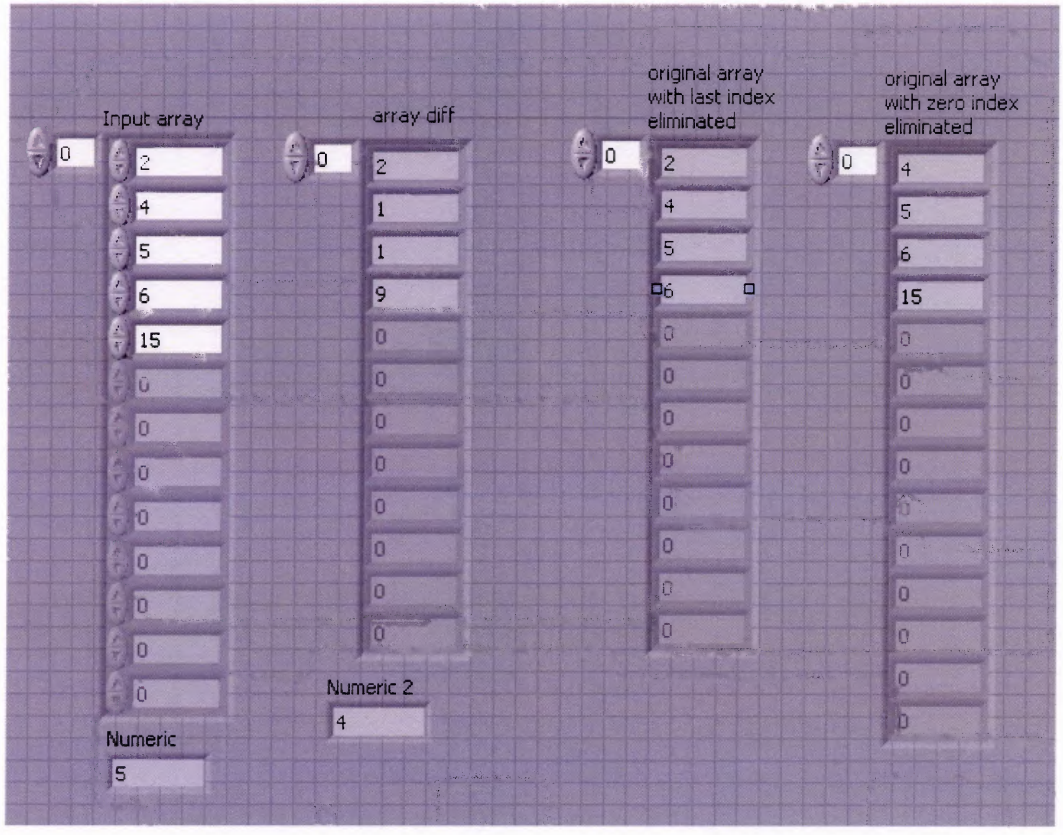

Figure B.9 Front panel of sub-difference

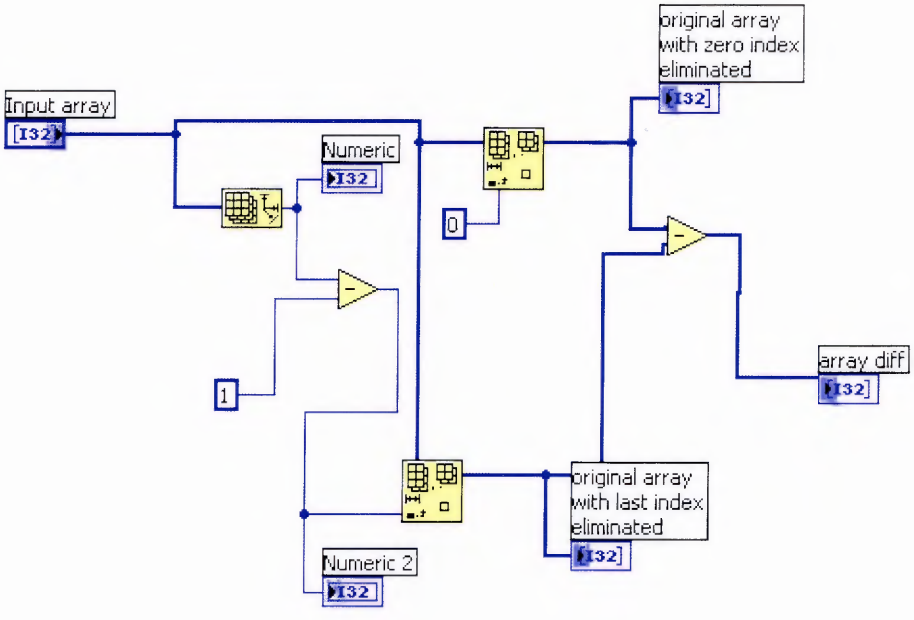

Figure B.10 Block diagram of sub-difference

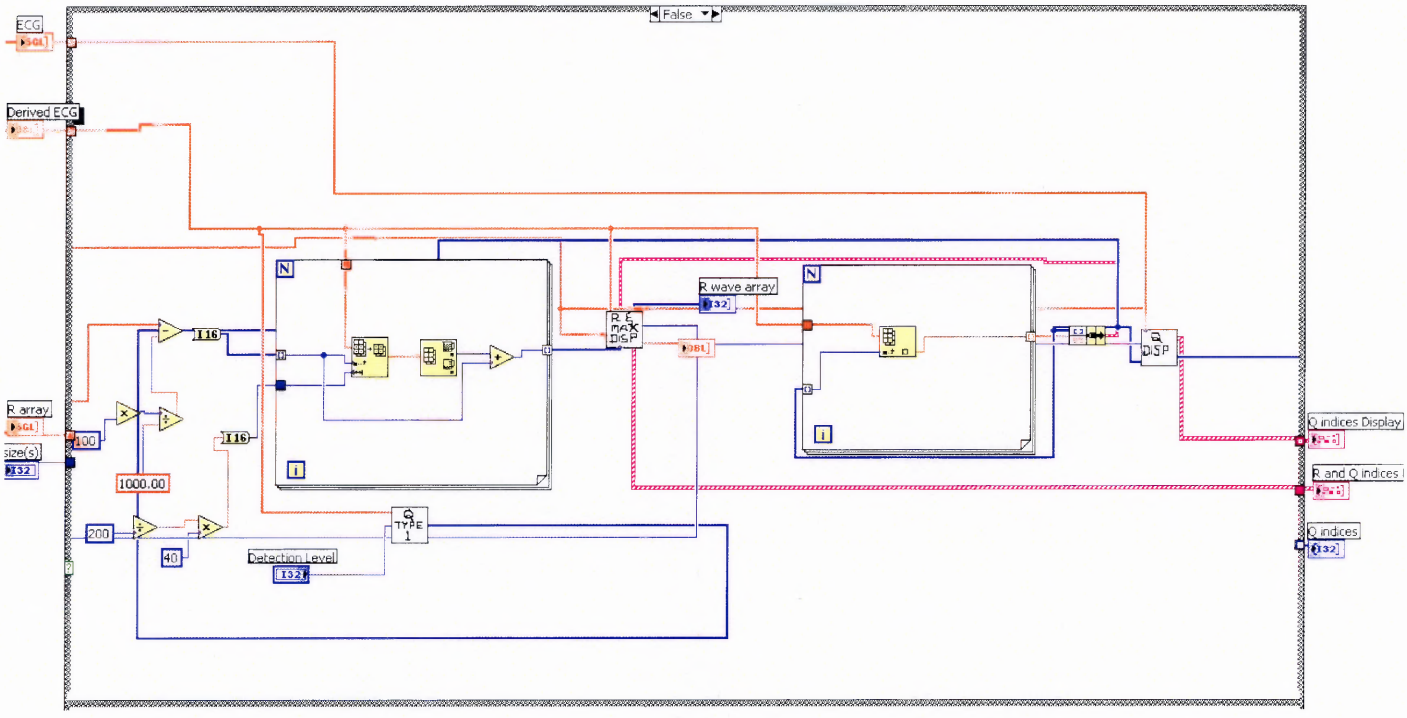

Figure B.11 Block diagram of Q type decision

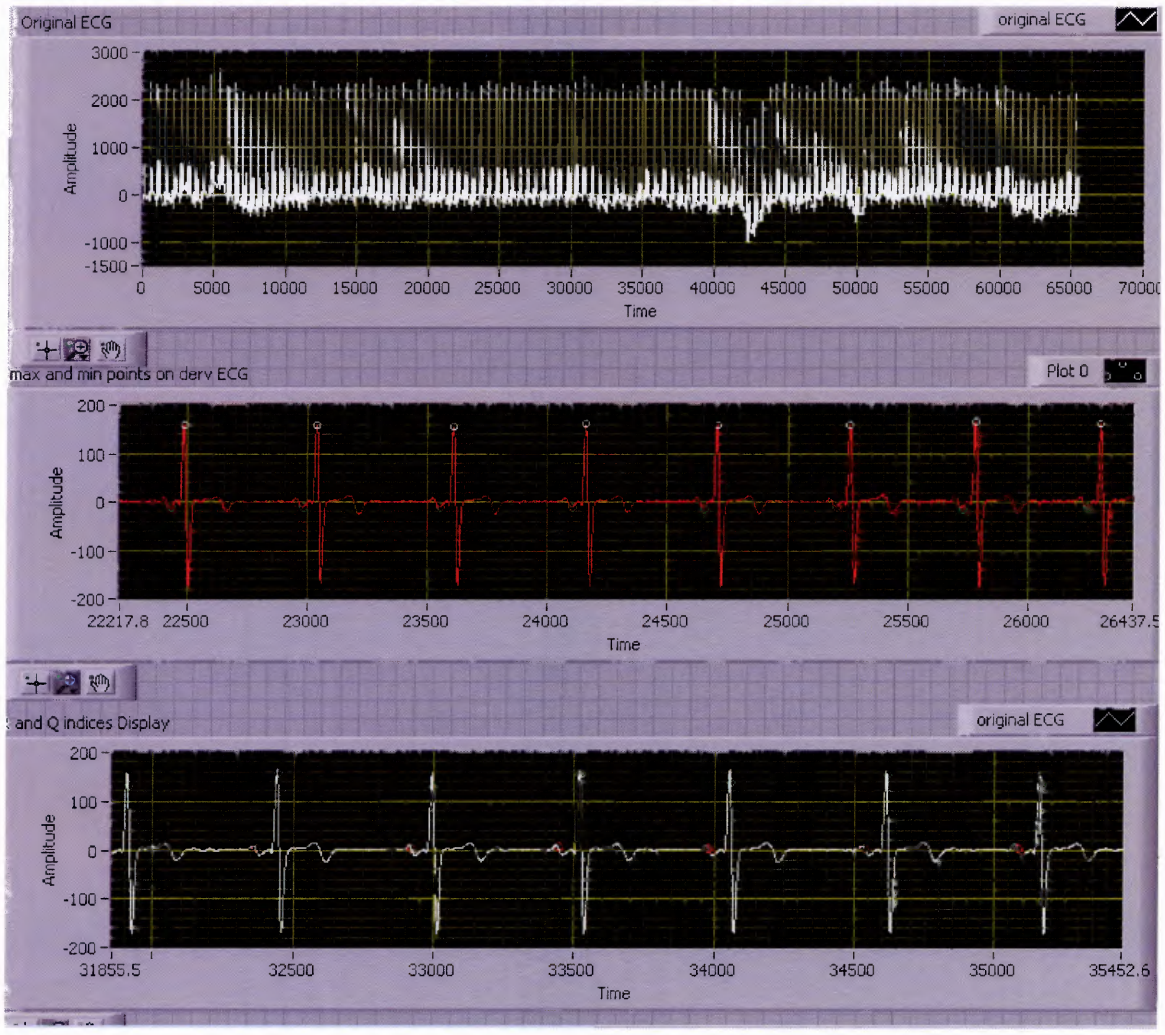

Figure B.12 Front panel of Q type decision

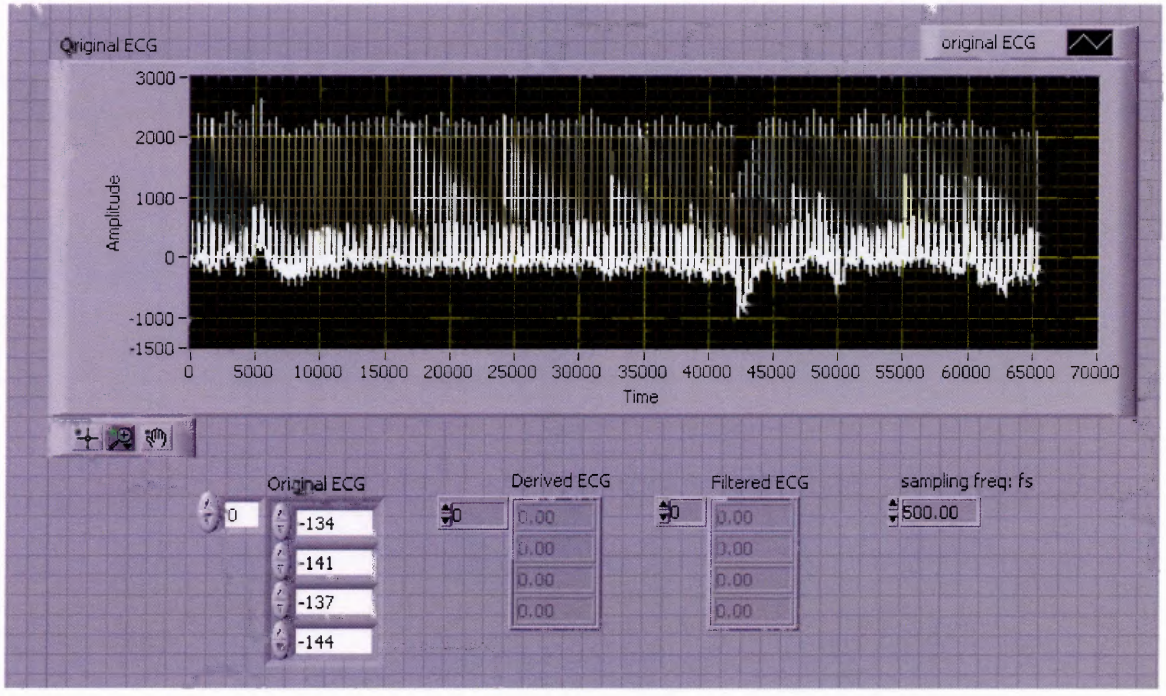

Figure B.13 Front panel of filter and differentiation module

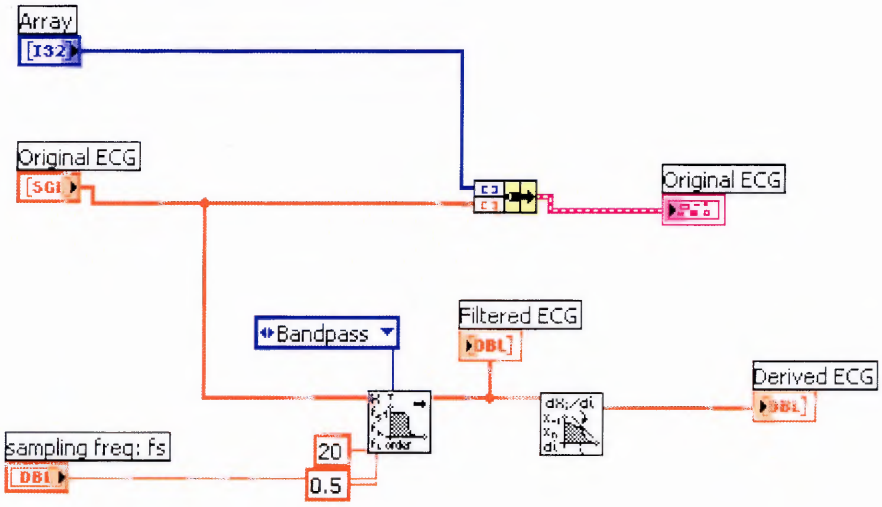

Figure B.14 Block diagram of filter and differentiation module

APPENDIX C

T DETECTOR MODULES

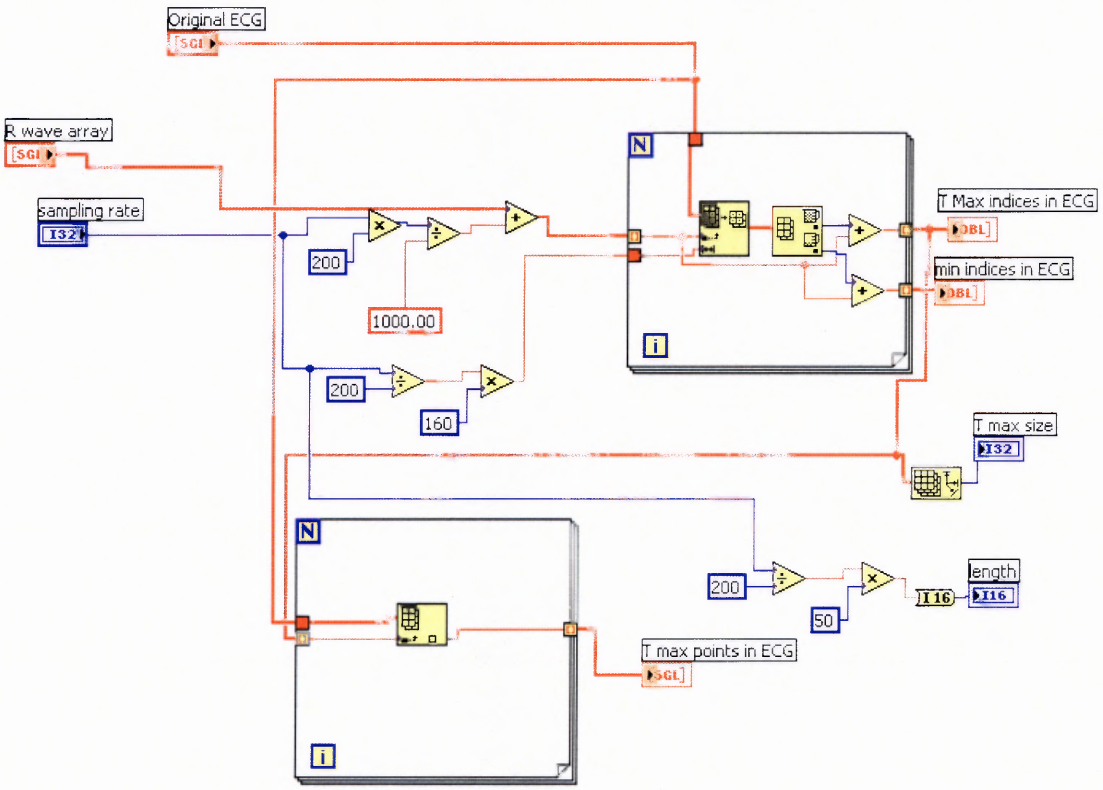

Figure C.1 Block diagram of T_{max} detector

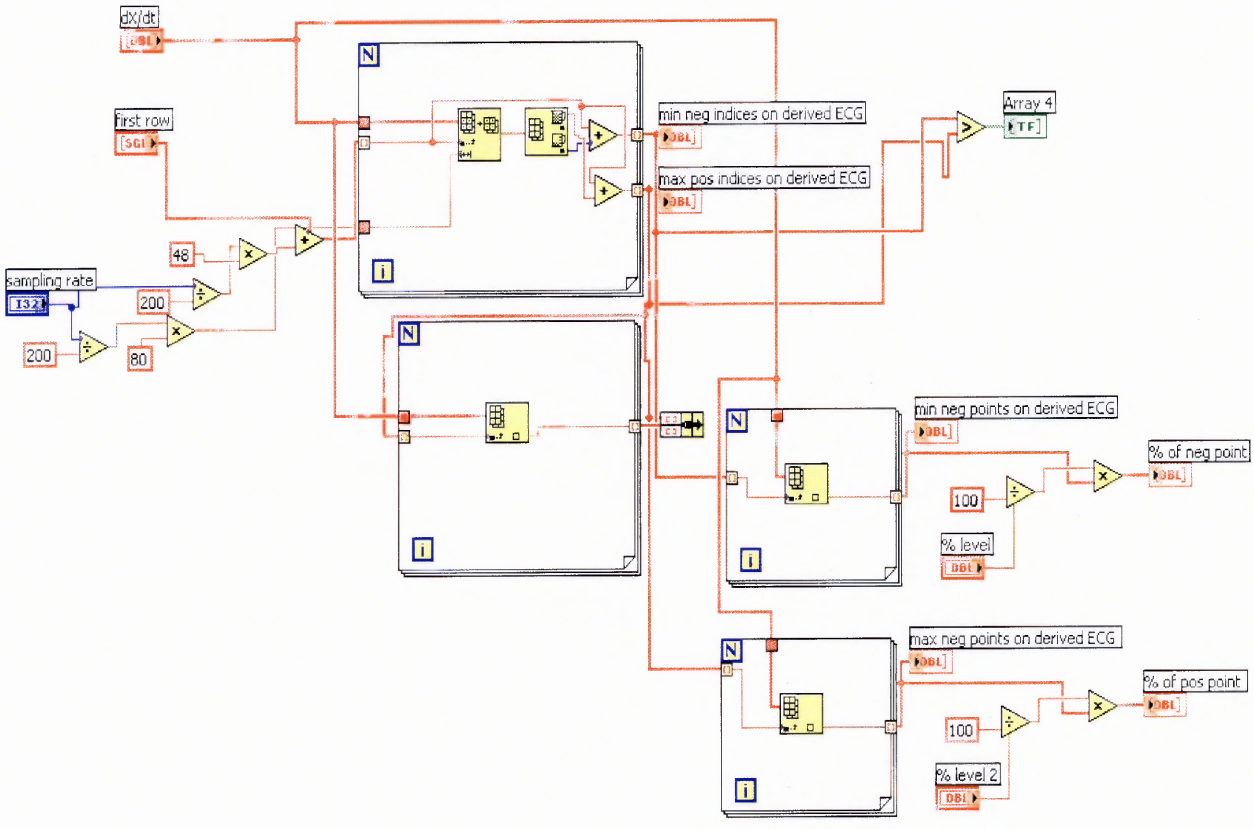

Figure C.2 Block diagram of T_{max} and T_{min} points on derived ECG

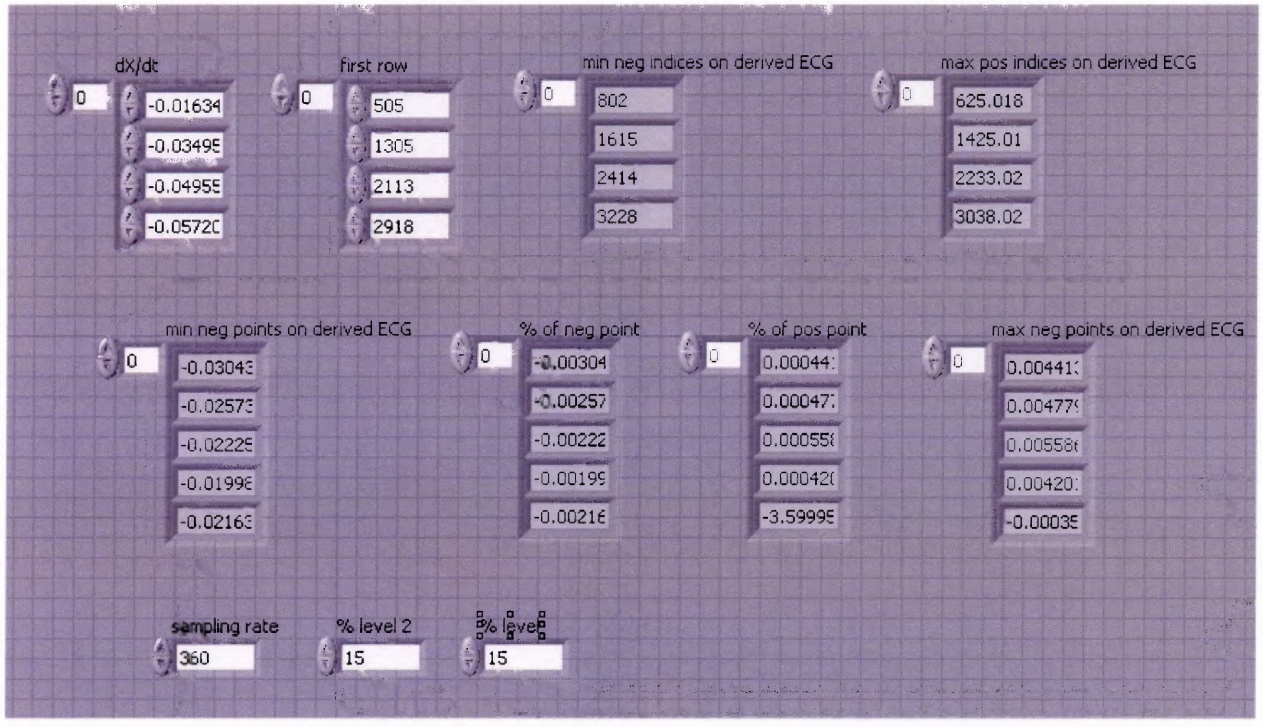

Figure C.3 Front panel of T_{max} and T_{min} points on derived ECG

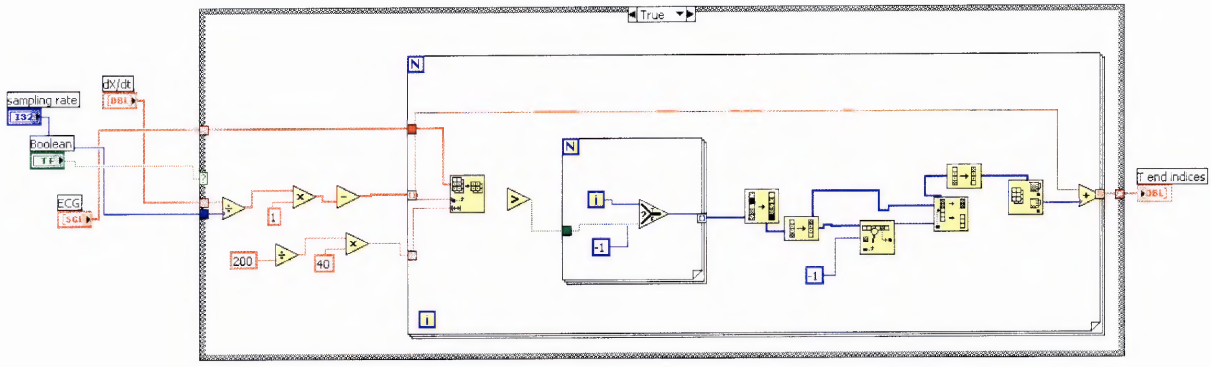

Figure C.4 Block diagram of T_{end} detector

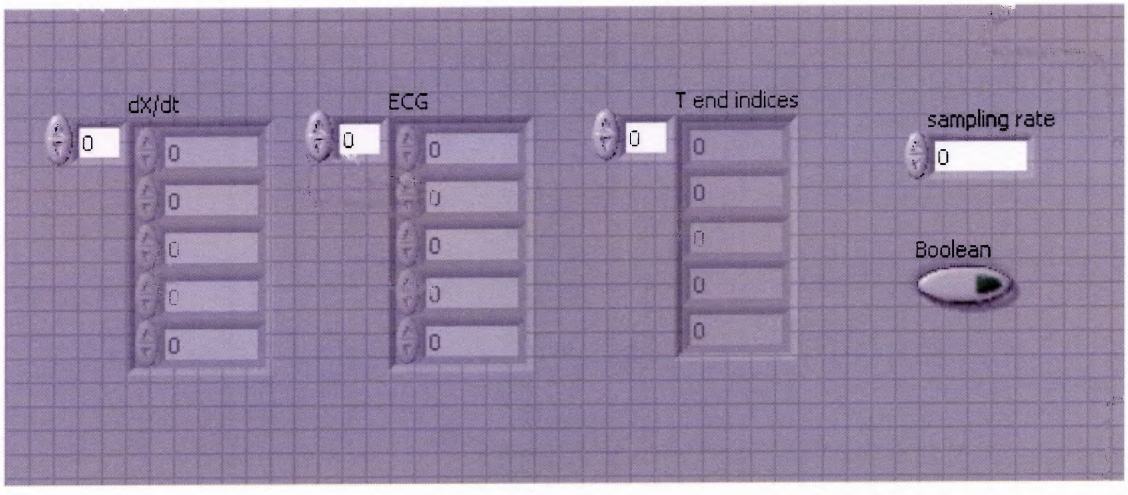

Figure C.5 Front panel of T_{end} detector

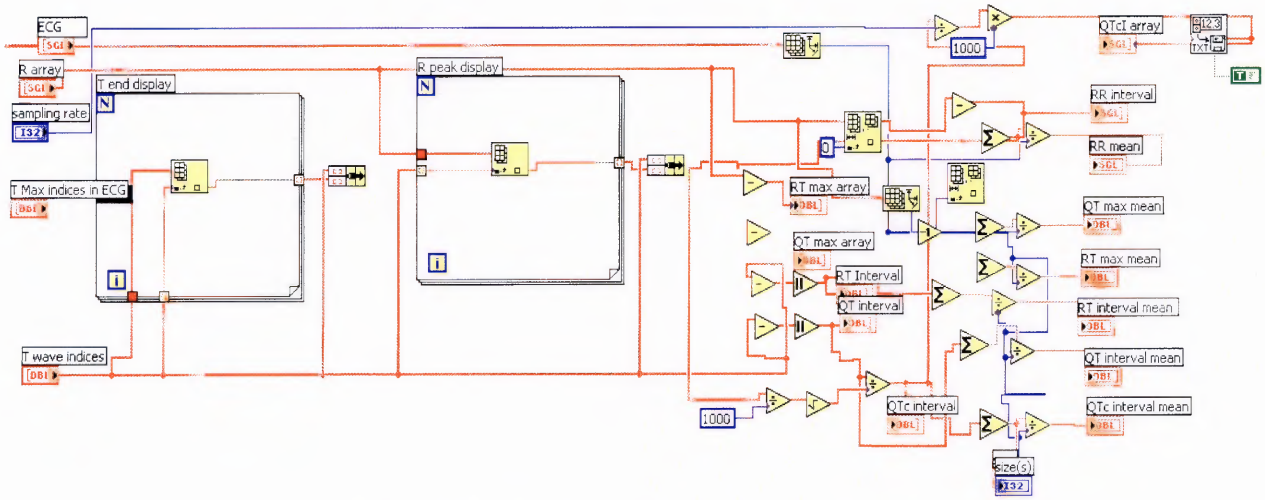

Figure C.6 Block diagram of interval calculator

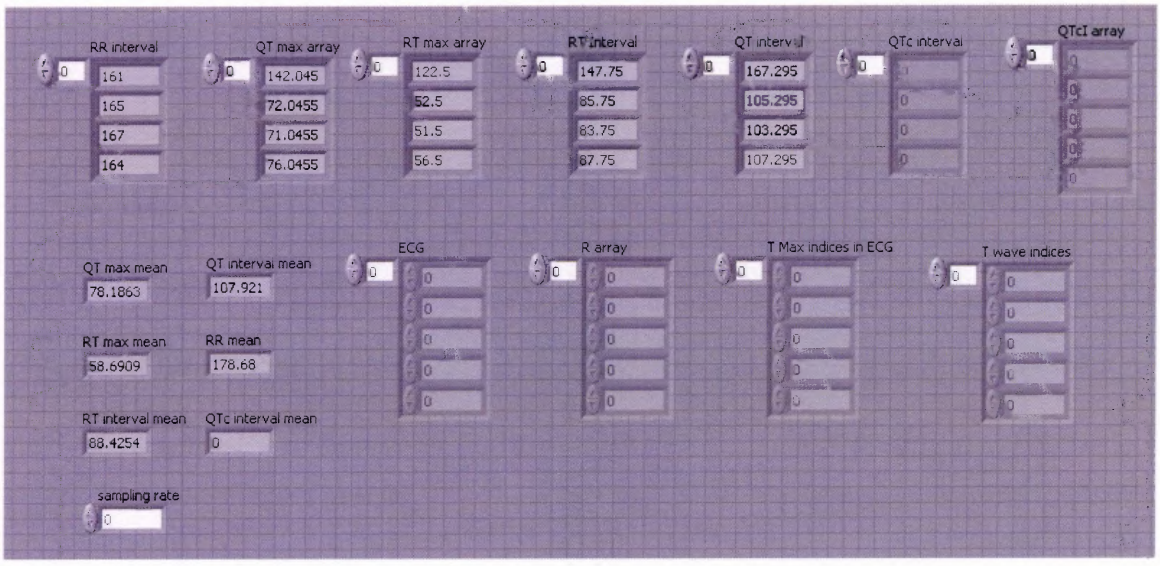

Figure C.7 Front panel of interval calculator

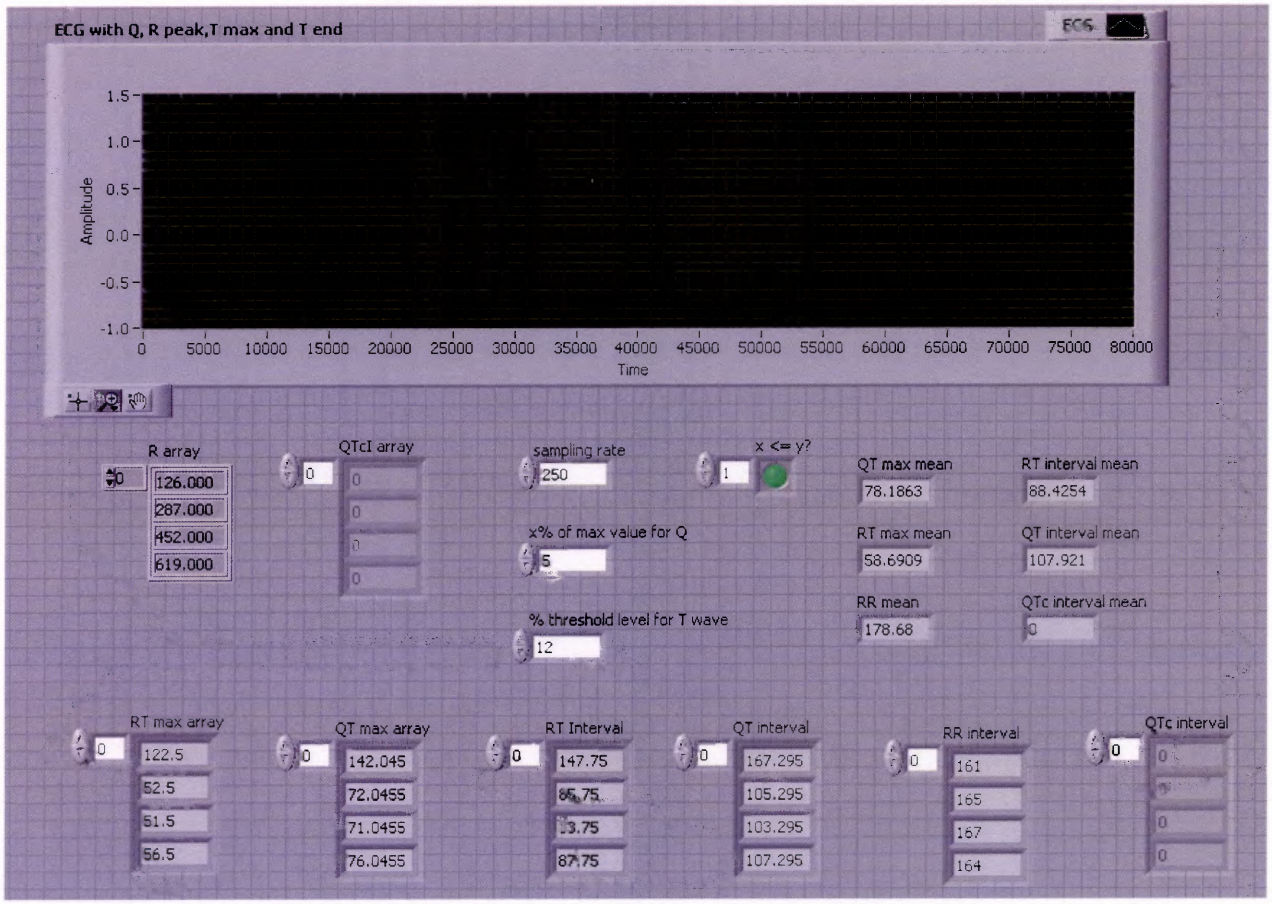

Figure C.8 Front panel of QT detector

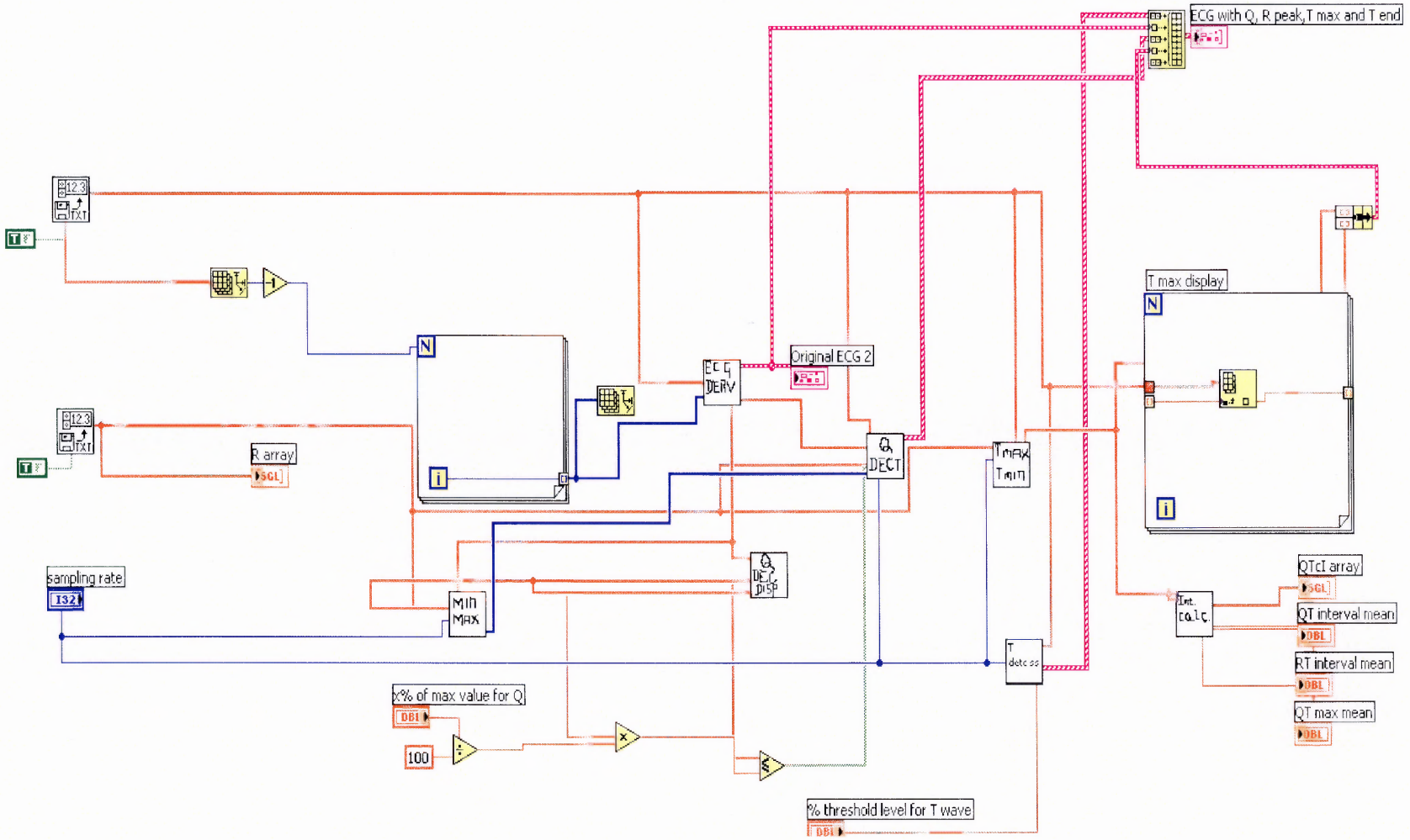

Figure C.9 Block diagram of QT detector

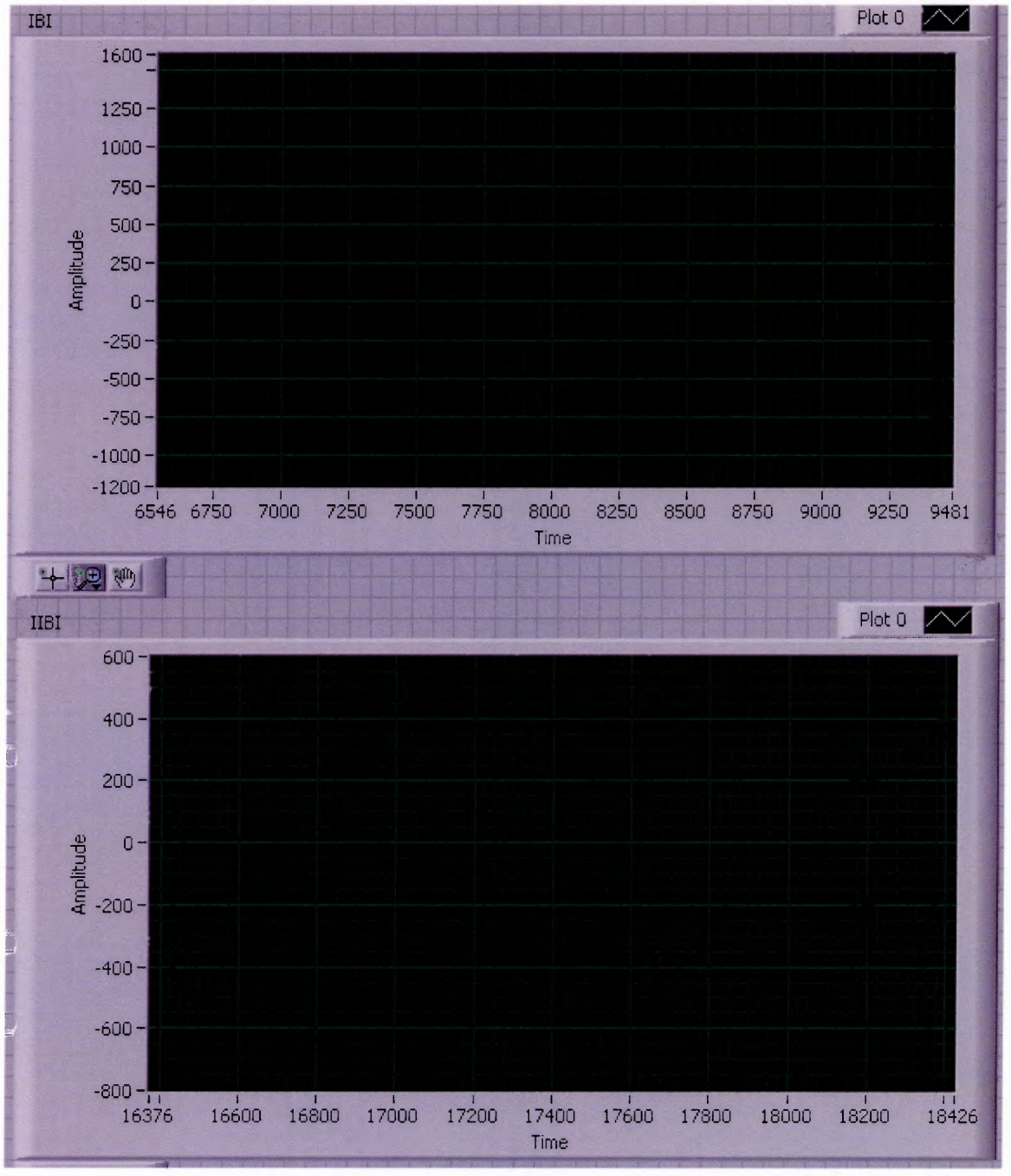

Figure C.10 Front panel of IIBI creator

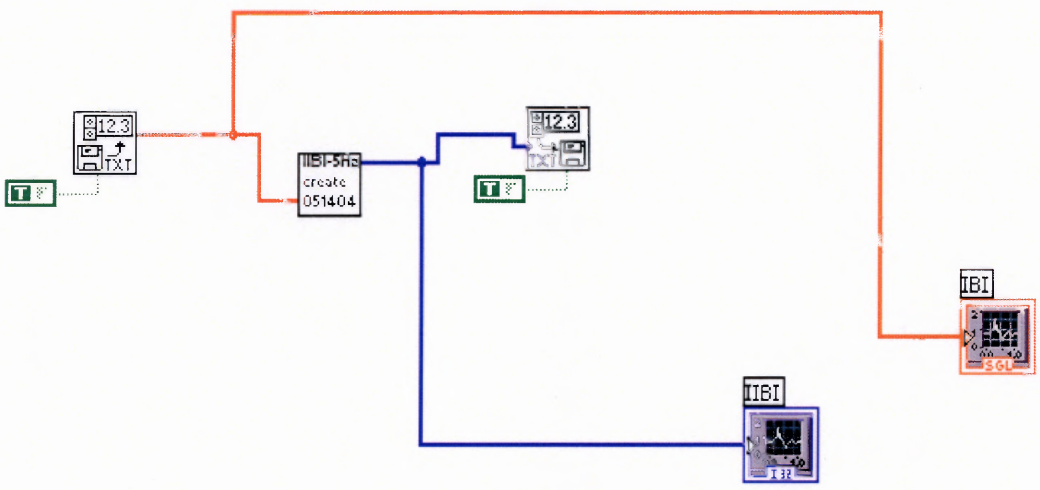

Figure C.11 Block diagram of IIBI creator

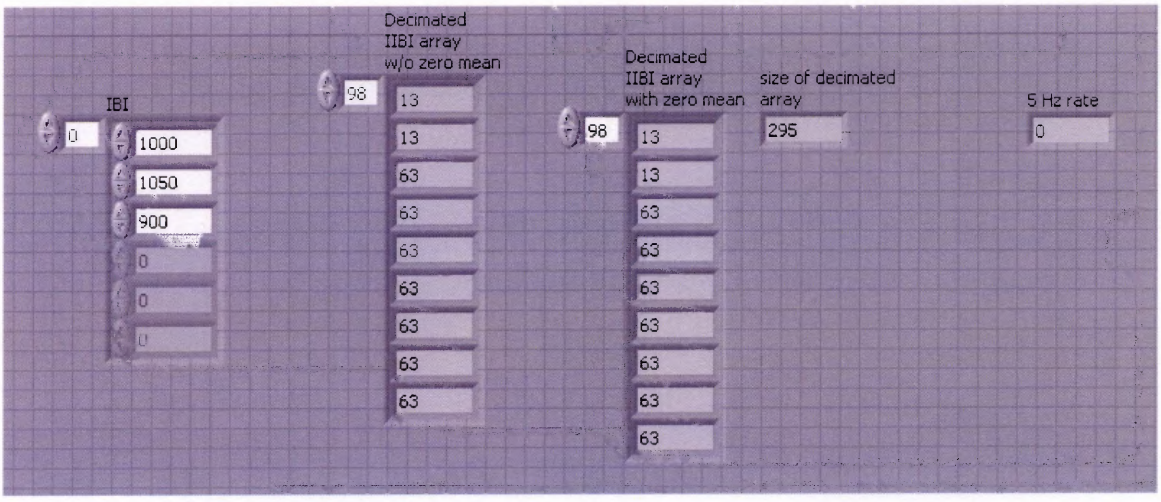

Figure C.12 Front panel of sub-vi IIBI creator

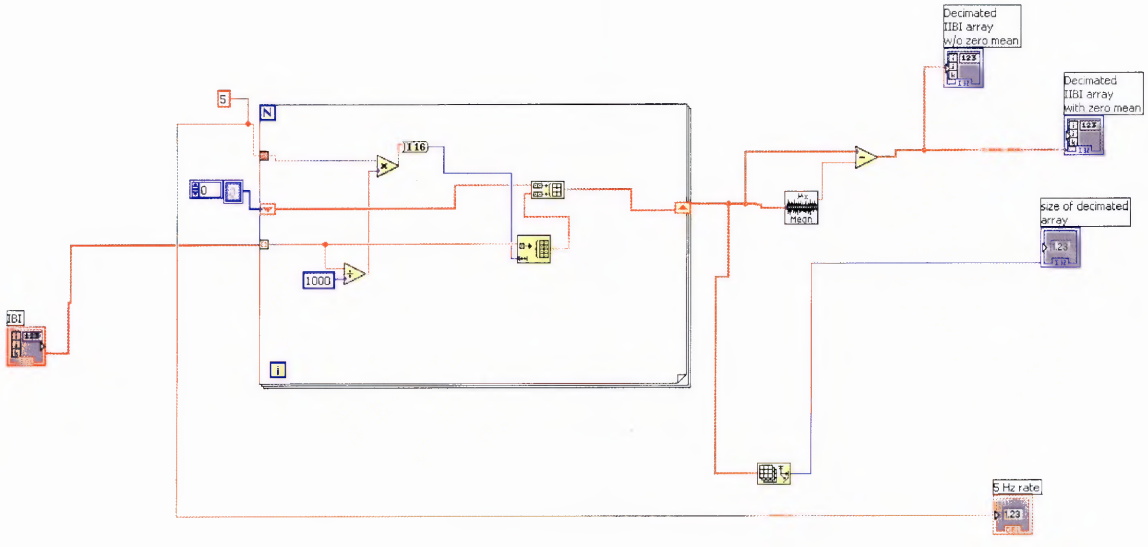

Figure C.13 Block diagram of sub-vi IIBI creator

APPENDIX D

MATLAB CODES

%MATLAB code for IBI interval plotting%

```
[File, Path, FILTERINDEX] = uigetfile('*.*', 'Choose the clean
IIBI data file you wish to process');
original_rawdata=load ([Path File])';
rawdata=original_rawdata(:);

[row,col]=size (rawdata);
I=1:row;
I=I(:);
n=10;
% x=hann(n);
% x=hann(n,'symmetric');

figure

plot (I,rawdata);
axis ([0.03 450 200 1300]);
title ('    QTcI for original data');
xlabel ('time (sec)');
ylabel ('Interval (millisec)');
```

%MATLAB code for IIBI variability plotting%

```
[File, Path, FILTERINDEX] = uigetfile('*.*', 'Choose the clean
IIBI data file you wish to process');
original_rawdata=load([Path File])';
rawdata=original_rawdata(:);

x = rawdata;
%N = length(x);

%order=5;
%freq=0.03;
sf=5;
%nfreq=freq/sample;

[row,col]=size(x);
I=1:row;
I=I(:);
A=(I/sf);        % Time axis in sec

fftsize=length(x);
x=x-mean(x);
fftx=fft(x,fftsize);
p=fftx.*conj(fftx);
%f=sf*(0:(fftsize/2-1))/fftsize;
f=sf*(0:(fftsize-1))/fftsize;
%clear fftx
n=64;
fftx=hann(n);
fftx=hann(n,'symmetric');

%figure

% plot (I,x);
% title('      IBI for original data');
% xlabel('time (sec)');
% ylabel('amplitude');

figure
plot(f(1:100),p(1:100),'r');
%plot(f(1:150),p(1:150)/max(p),'r');
axis([0.02 1 0 max(p)]);
xlabel('Frequency (Hz)');
ylabel('Power');
title('HR variability');
```

APPENDIX E

INTERVAL AND VARIABILITY PLOTS

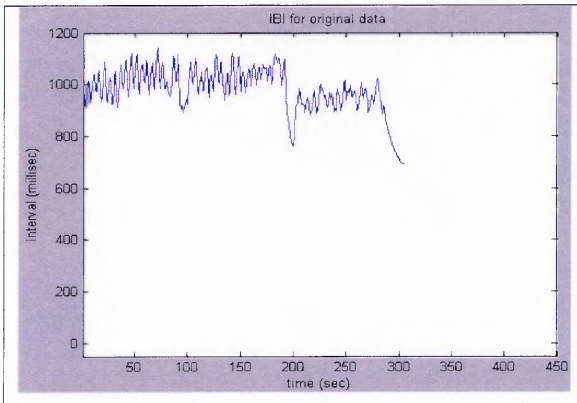

Figure a IBI of 20040406a

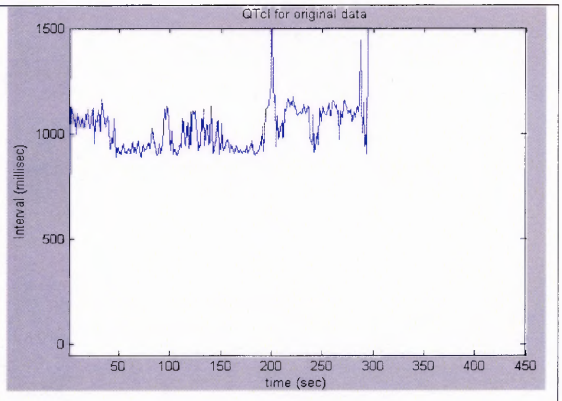

Figure b QTcI of 20040406a

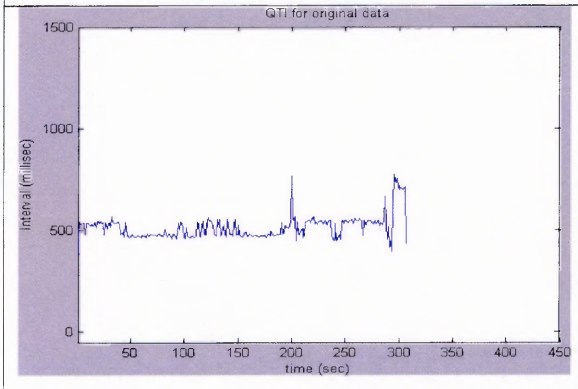

Figure c QTI of 20040406a

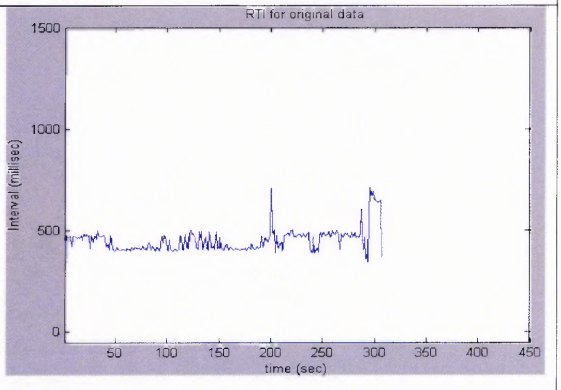

Figure d RTI of 20040406a

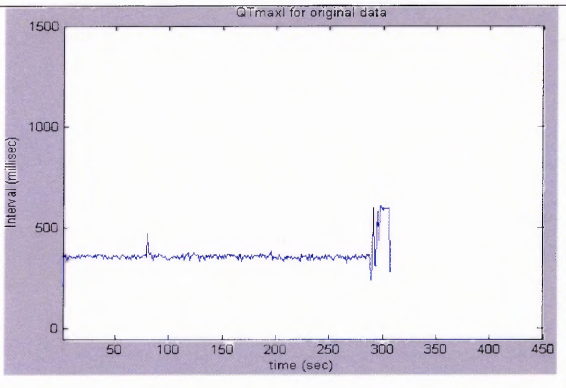

Figure e $QT_{max}I$ of 20040406a

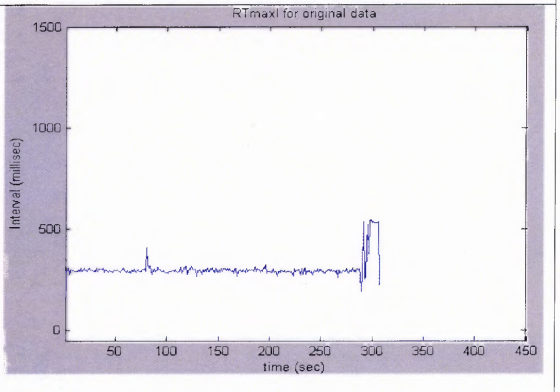

Figure f $RT_{max}I$ of 20040406a

Figure E.1 Interval plots of 20040406a data set

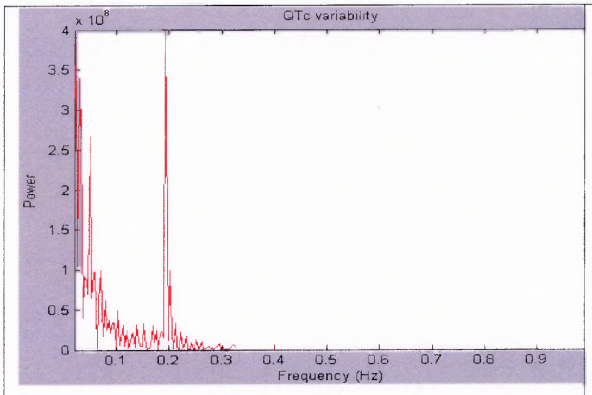

Figure a HRV of 20040406a

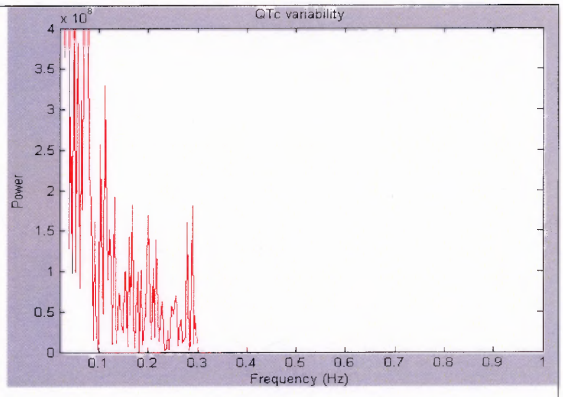

Figure b QTcV of 20040406a

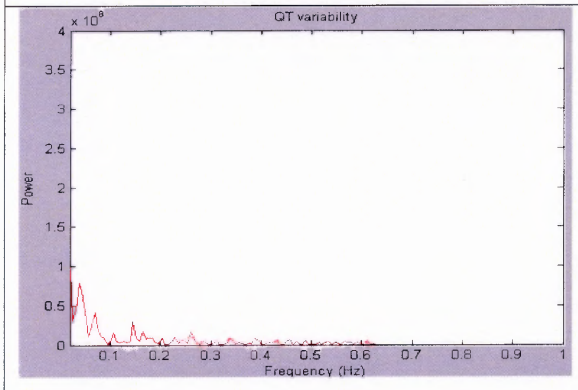

Figure c QTV of 20040406a

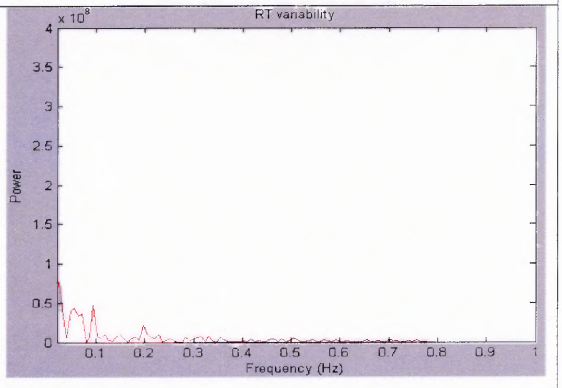

Figure d RTV of 20040406a

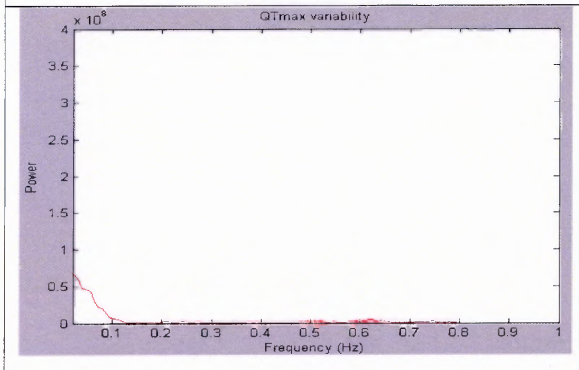

Figure e $QT_{max}V$ of 20040406a

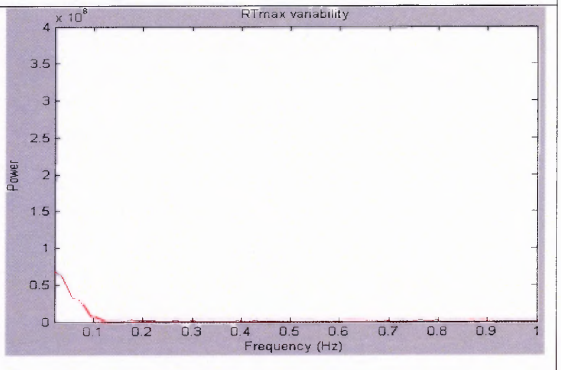

Figure f $RT_{max}V$ of 20040406a

Figure E.2 Variability plots of 20040406a data set

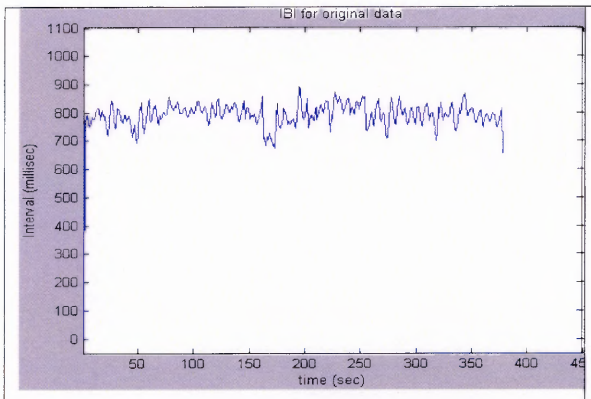

Figure a IBI of 20040407c

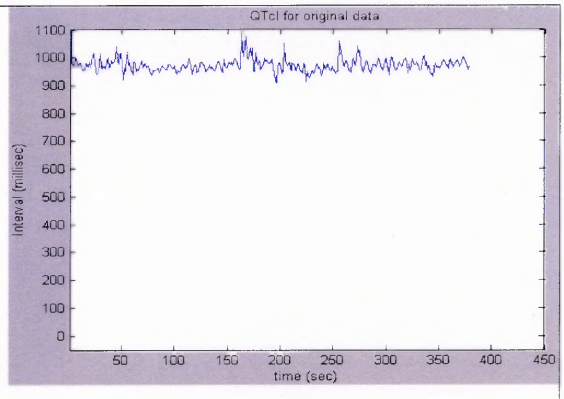

Figure b QTcI of 20040407c

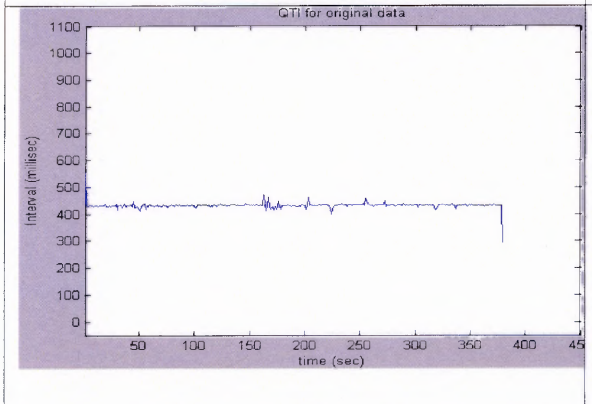

Figure c QTI of 20040407c

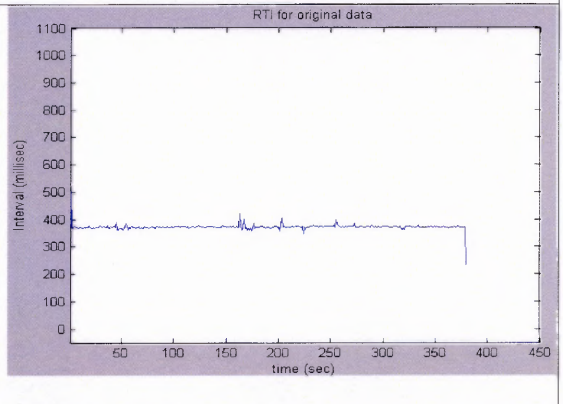

Figure d RTI of 20040407c

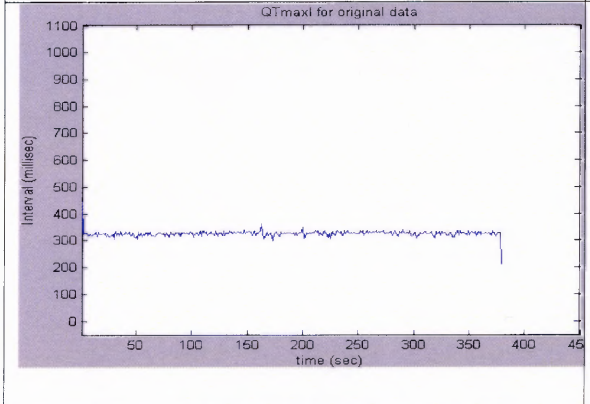

Figure e $QT_{max}I$ of 20040407c

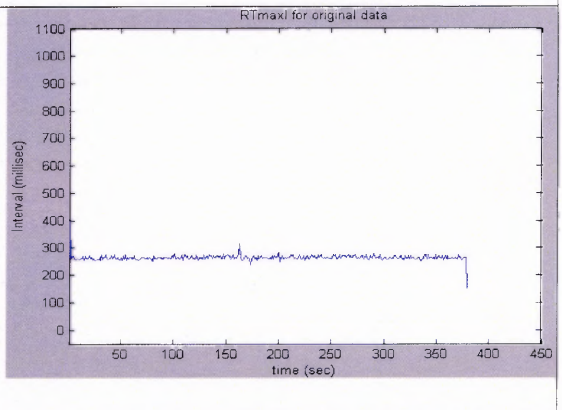

Figure f $RT_{max}I$ of 20040407c

Figure E.3 Interval plots of 20040407c data set

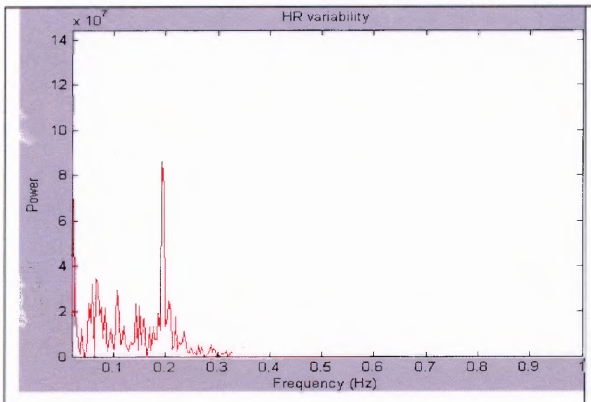

Figure a HRV of 20040407c

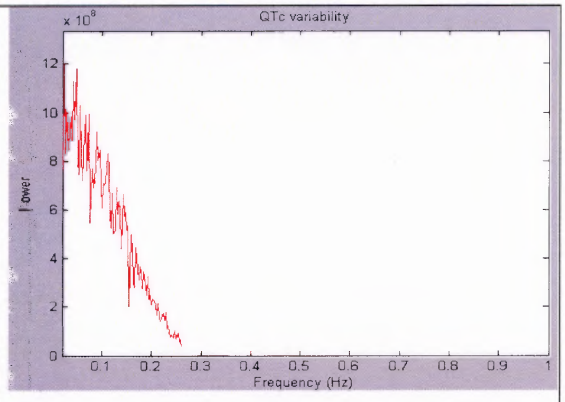

Figure b QTcV of 20040407c

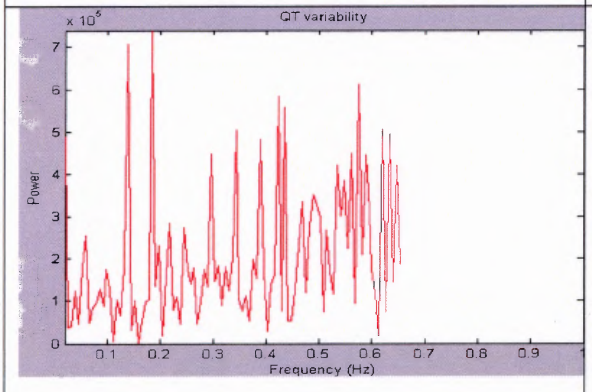

Figure c QTV of 20040407c

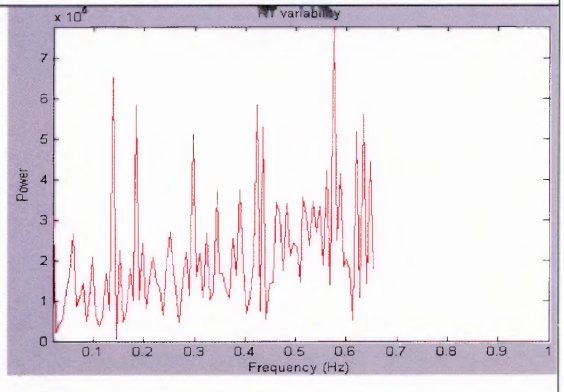

Figure d RTV of 20040407c

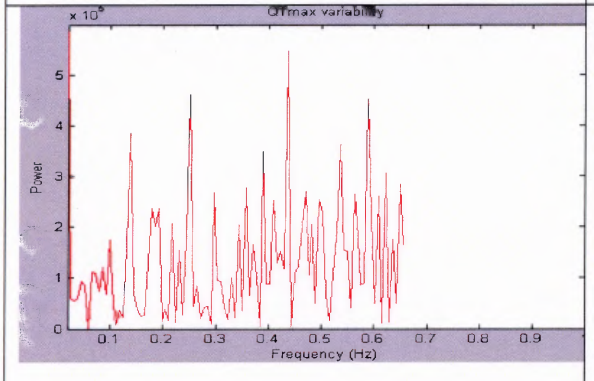

Figure e $QT_{max}V$ of 20040407c

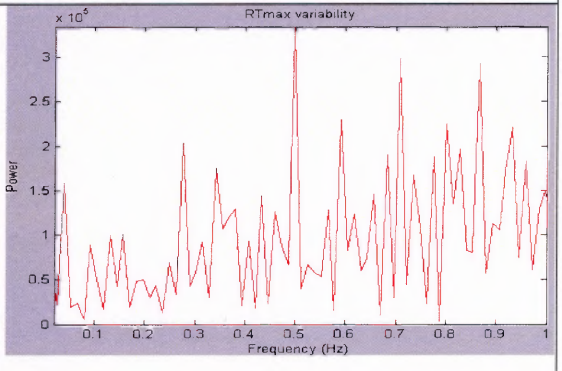

Figure f $RT_{max}V$ of 20040407c

Figure E.4 Variability plots of 20040407c data set

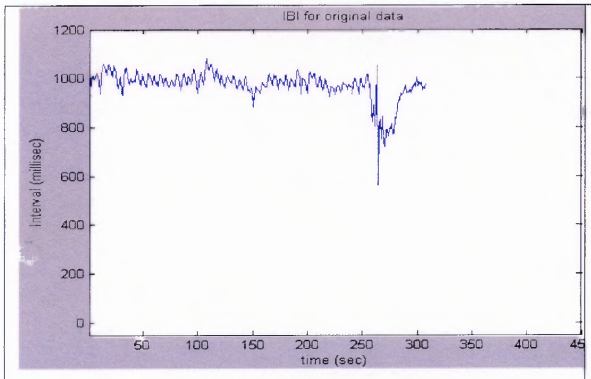

Figure a IBI of stress20040311c

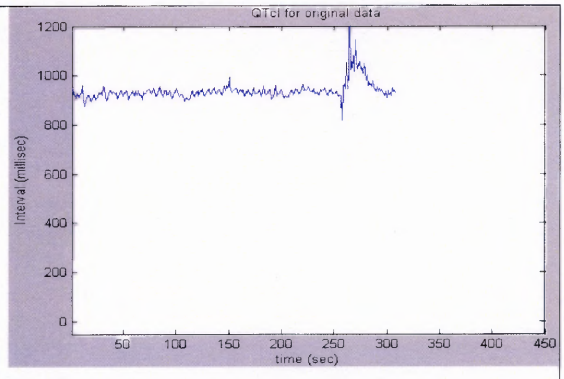

Figure b QTcI of stress20040311c

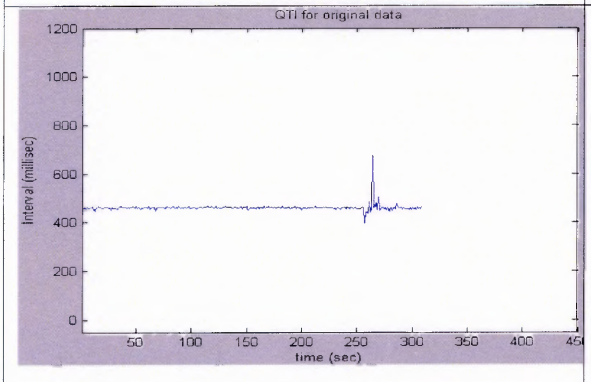

Figure c QTI of stress20040311c

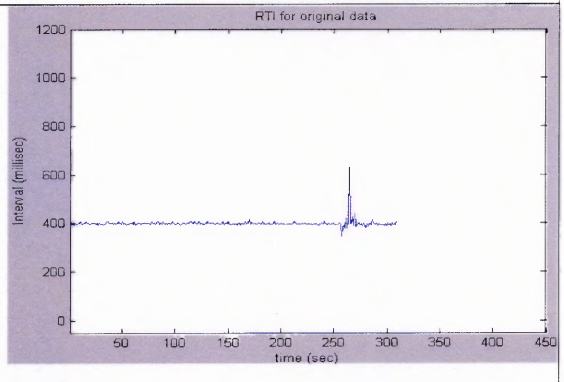

Figure d RTI of stress20040311c

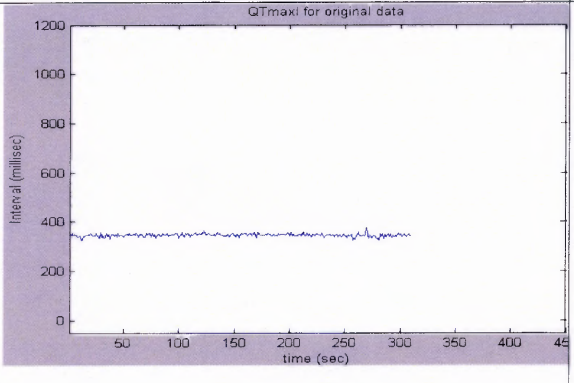

Figure e $QT_{max}I$ of stress20040311c

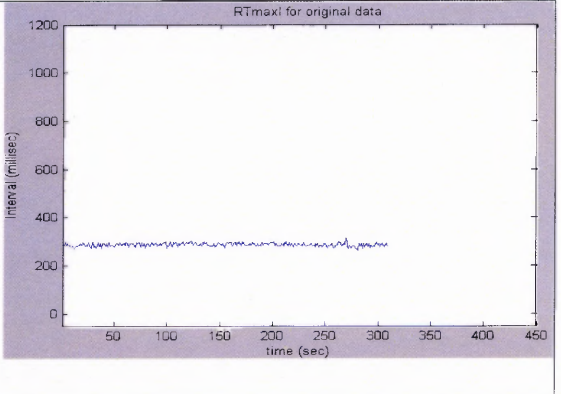

Figure f $RT_{max}I$ of stress20040311c

Figure E.5 Interval plots of stress20040311c data set

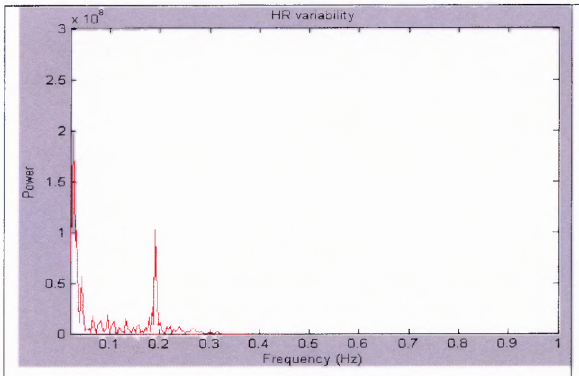

Figure a HRV of stress20040311c

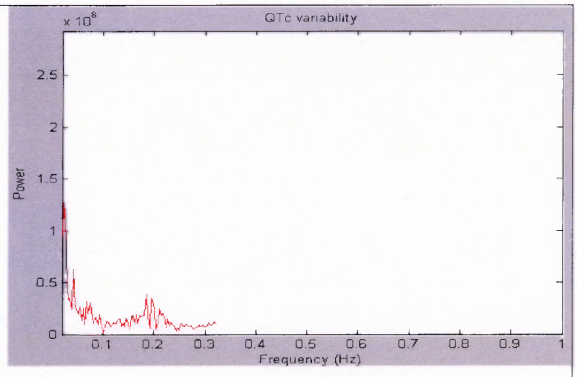

Figure b QTcV of stress20040311c

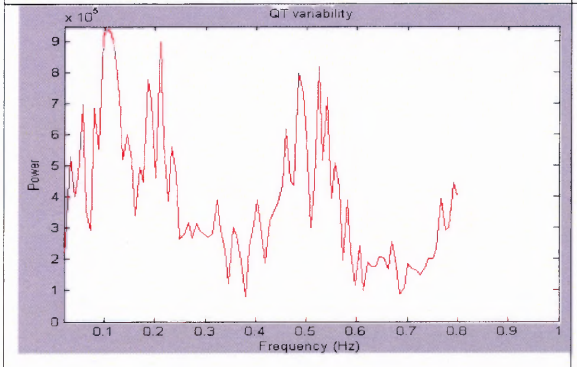

Figure c QTV of stress20040311c

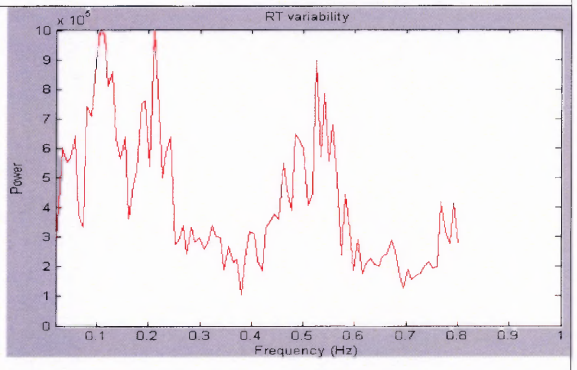

Figure d RTV of stress20040311c

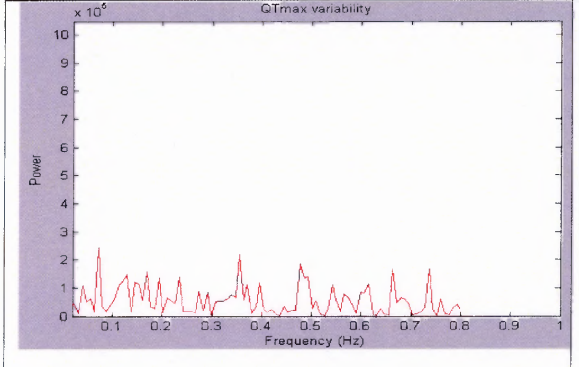

Figure e $QT_{max}V$ of stress20040311c

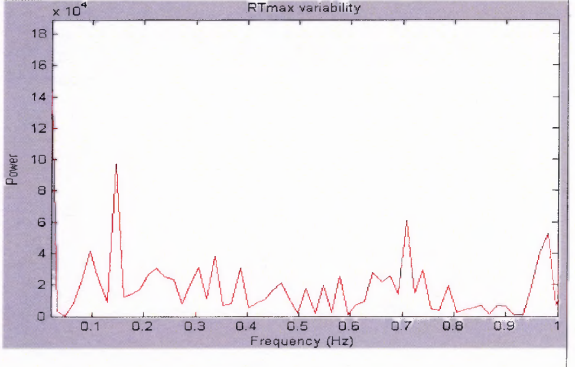

Figure f $RT_{max}V$ of stress20040311c

Figure E.6 Variability plots of stress20040311c data set

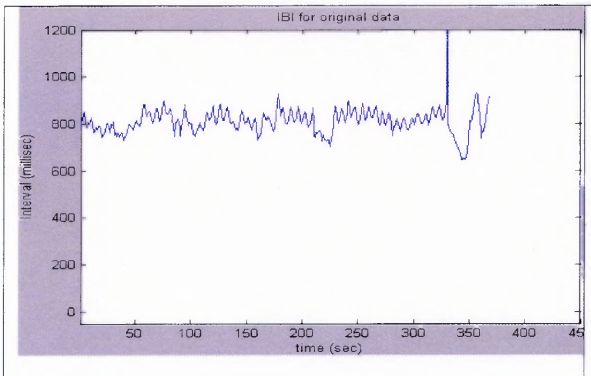

Figure a IBI of stress20040830b

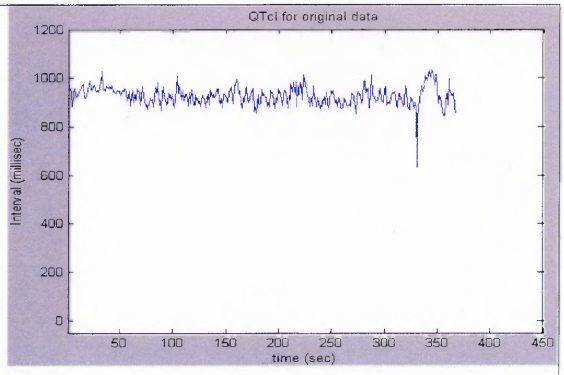

Figure b QTcI of stress20040830b

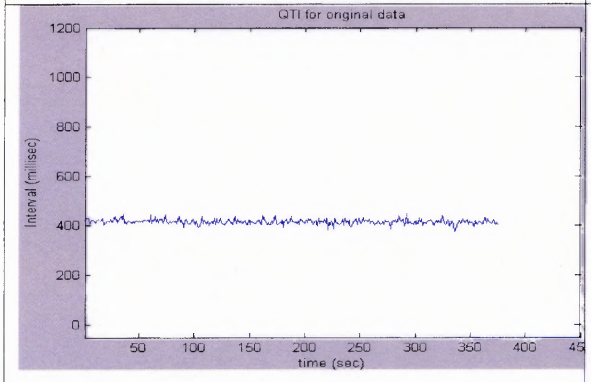

Figure c QTI of stress20040830b

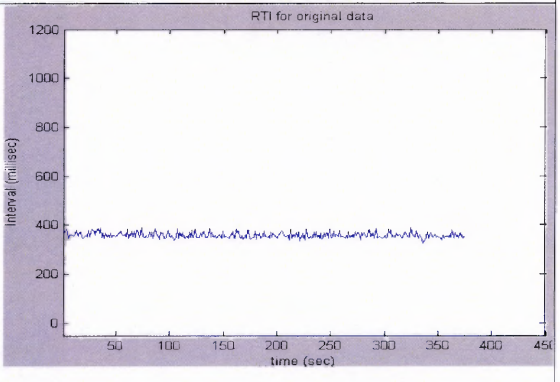

Figure d RTI of stress20040830b

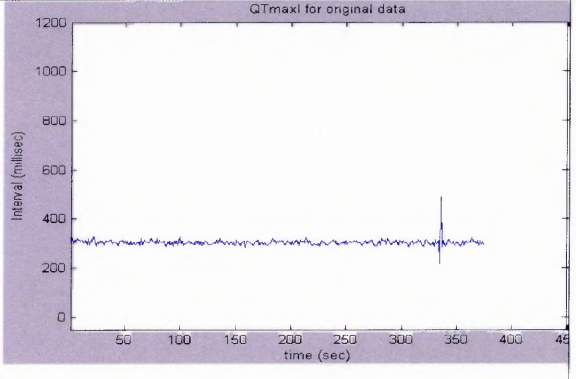

Figure e $QT_{max}I$ of stress20040830b

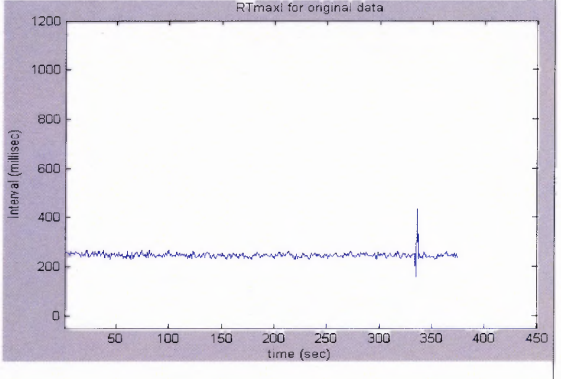

Figure f $RT_{max}I$ of stress20040830b

Figure E.7 Interval plots of stress20040830b data set

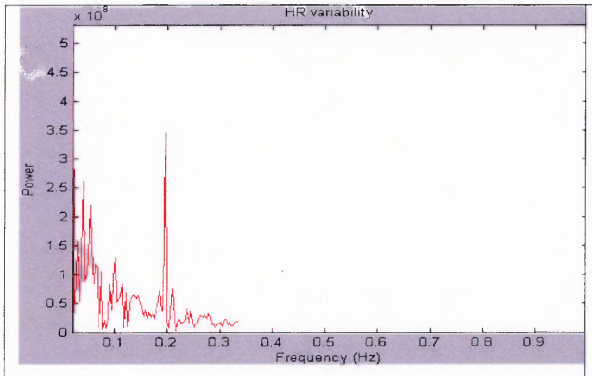

Figure a HRV of stress20040830b

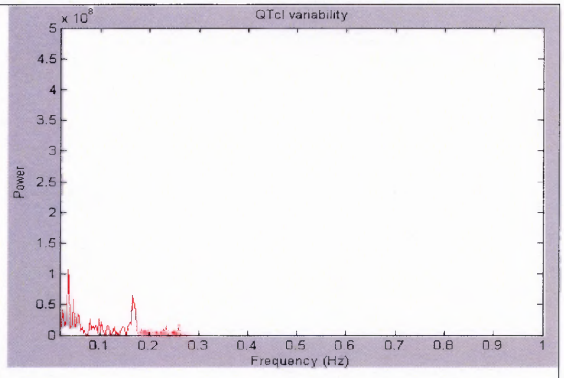

Figure b QTcV of stress20040830b

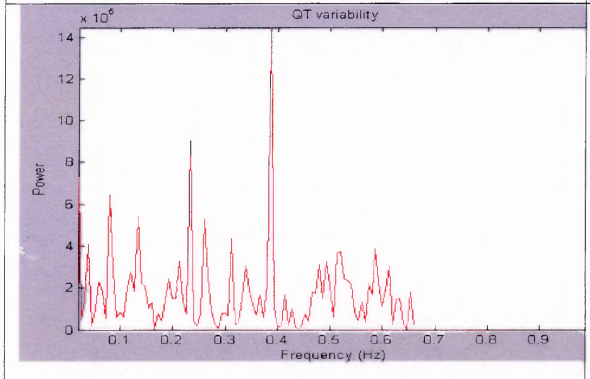

Figure c QTV of stress20040830b

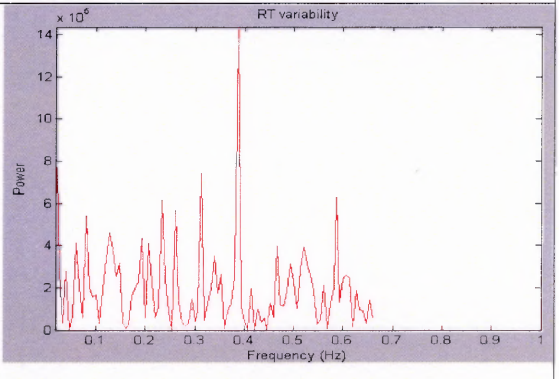

Figure d RTV of stress20040830b

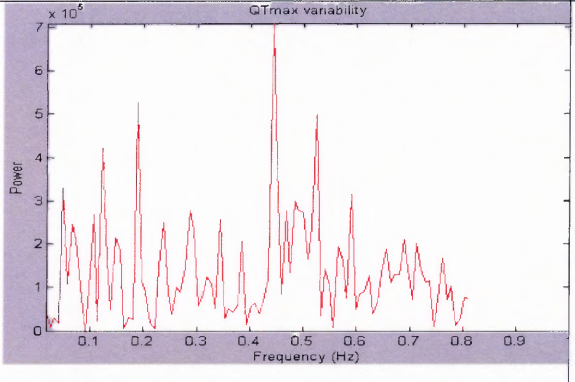

Figure e $QT_{max}V$ of stress20040830b

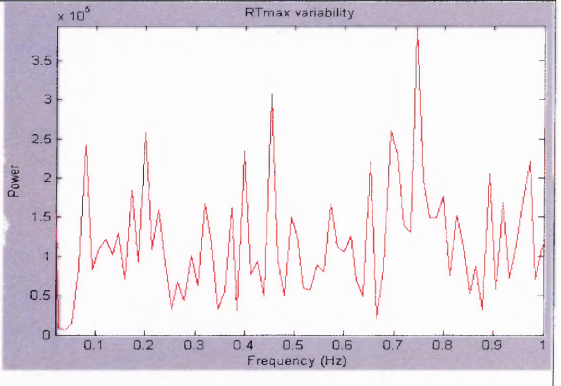

Figure f $RT_{max}V$ of stress20040830b

Figure E.8 Variability plots of stress20040830b data set

REFERENCES

1. L. Cromwell, F. Weibell, E. Pfeiffer, "*Biomedical Instrumentation and Measurements*", Prentice Hall, 1996.

2. A. Guyton, J. Hall, "*Textbook of Medical Physiology*", Philadelphia: W.B. Saunders, c1996.

3. http://www.cvphysiology.com/Arrhythmias/A013.htm

4. Q. Xue, S. Reddy, "Algorithms for Computerized QT Analysis", *Journal of Electrocardiology*, Vol. 30 Suppl.

5. A. Hunt, "Accuracy of popular automatic QT interval algorithms assessed by 'Gold Standard' and comparison with novel method: computer simulation study", *BMC Cardiovascular Disorders*, September 2005.

6. Q. Xue, S. Reddy, "New Algorithms for QT Dispersion Analysis", *IEEE Computers in Cardiology*, 1996.

7. P. Lanjewar, V. Pathak, Y. Lokhandwala, "Issues in QT interval Measurement", *Indian Pacing and Electrophysiology Journal*, vol. 4(4), 2004, pg. 156-161.

8. J. Sahambi, S.N. Tandon, R.K.P. Bhatt, "An Automated Approach to beat-by-beat QT Interval Analysis", *IEEE Engineering in Medicine and Biology*, May/June, 2000, Pg. 97-101

9. N. B. McLaughlin, R. Campbell, A. Murray, "Comparison of automatic QT measurement techniques in the normal 12 lead electrocardiogram", *British Heart Journal*, 74 Vol. 2, 1995, pg. 84-89.

10. P. Laguna, N.V. Thakor, P. Caminal, R. Jane, H. Yoon, "New algorithm for QT interval analysis in 24-hour Holter ECG: performance and applications", *Medical & Biological Engineering & Computing*, January 1990.

11. I.K. Daskalov, I.I. Christov, "Automatic detection of the electrocardiogram T-wave end", *Medical & Biological Engineering & Computing*, vol. 37, 1997.

12. R. Berger, "QT Variability", *Journal of Electrocardiology*, vol 36. Supplement, 2003.

13. J. Kautzner, "QT interval Measurements", *Cardiac Electrophysiology Review*, 2002; 6:273-277.

14. A. Krahn, G. Klein, R. Yee, "Hysteresis of the RT Interval with Exercise: A new marker for the Long-QT Syndrome?" *Circulation*, 1997; 96:1551-1556.

15. V. Batchvarov et. al., "QT-RR relationship in healthy subjects exhibits substantial intersubject variability and high intrasubject stability", *The American J Physiology Heart Circulation* 282: H2356-H2363, 2002

16. http://www.long-qt-syndrome.com/long_qt_syndrome_intro.html

17. M. Nakagawa et. al., "Dynamics of QT interval in a patient with long QT syndrome and a normal QT interval", *Japanese Circulation Journal* Vol. 62, March 1998.

18. http://patients.uptodate.com/topic.asp?file=carrhyth/49133

19. http://patients.uptodate.com/topic.asp?file=carrhyth/49415&title=Ventricular+premature+beats

20. K. Lund, H. Nygaard, A. Pedersen, "Weighing the QT intervals with the slope or the amplitude of the T wave", *Annals of Noninvasive Electrocardiology* 2002 Jan; 7(1):4-9.

21. J. Erdulfo et. al., "Comparative Usefulness of Beat-to-Beat QT Dispersion and QT interval Fluctuations for identifying Patients With Organic Heart Disease at Risk for Ventricular Arrhythmias", *Circulation Journal* Vol. 67, Feb 2003; pg 125-128

22. P. Camina et. al., "New Algorithm for QT Dispersion Analysis in XYZ-Lead Holter ECG. Performance and Applications", *IEEE Computers in Cardiology* Vol. 25, 1998; 709-712.

23. V. Batchvarov et. al., "QT interval and QT Dispersion Measured with the Threshold Method depend on Threshold Level", *Pacing Clinical Electrophysiology* 1998 Nov; 21; 2372-2375.

24. K. Lund, B' Lund, C. Brohet, H. Nygaard, "Evaluation of Electrocardiogram T-wave dispersion measurement methods", *Medical & Biological Engineering & Computing* 2003, vol 41; 410-415.

25. Q. Xue, S. Reddy, "New Algorithms for QT Dispersion Analysis", *IEEE Computers in Cardiology* 1996, 293-296.

26. N. Velislav et. al., "QT-RR Relationship in Healthy Subjects exhibits Substantial Intersubject Variability and High Intrasubject Stability", *American Journal of Physiological Heart Circulation Society*, 2002, 282; H2356-H2363.

27. P. Asselin, "Relationship between Autonomic Nervous System and the Recovering Heart Post Exercise Using Heart Rate Variability", *NJIT, MS Thesis*, May 2005.
28. T. Oza, "An Automated Approach for Comparative Analysis of QT interval and Heart Rate Variability", *NJIT MS Thesis*, January 2001.

29. Y. Murakawa et. al., "Is the QT Interval an Indicator of Autonomic State?" *Japan Heart Journal* Dec 2000; 713-720.

30. G. Schreier, D. Hayn, S. Lobodzinski, "Development of a New QT algorithm with Heterogeneous ECG Databases", *Journal of Electrocardiology*, 2003 vol 36; 145-150

31. Z. Sahinoglu, "Analysis of Multi lead QT Dispersion by means of an Algorithm implemented in LabVIEW", *NJIT MS Thesis*, January 1998.

32. V.K. Yeragani, R. Berger, R. Pohl, R. Balon, "Effect of age on Diurnal Changes of 24-hour QT Interval Variability", *Springer Verlag 2004*

33. G. Piccirillo et. al., "Influence of age, Autonomic Nervous System and Anxiety on QT Interval Variability", *Clinical Science* 2001, 101; 429-438.

34. M.L. Migaux, F. Marciano, L. De Caprio, "Spontaneous Variability of the QTc Interval in Healthy Subjects", *IEEE Computers in Cardiology* 1996, 529-532.